A Lamb wave-based liquid sensor for biomedical applications

Master Thesis

Widesh Gahar

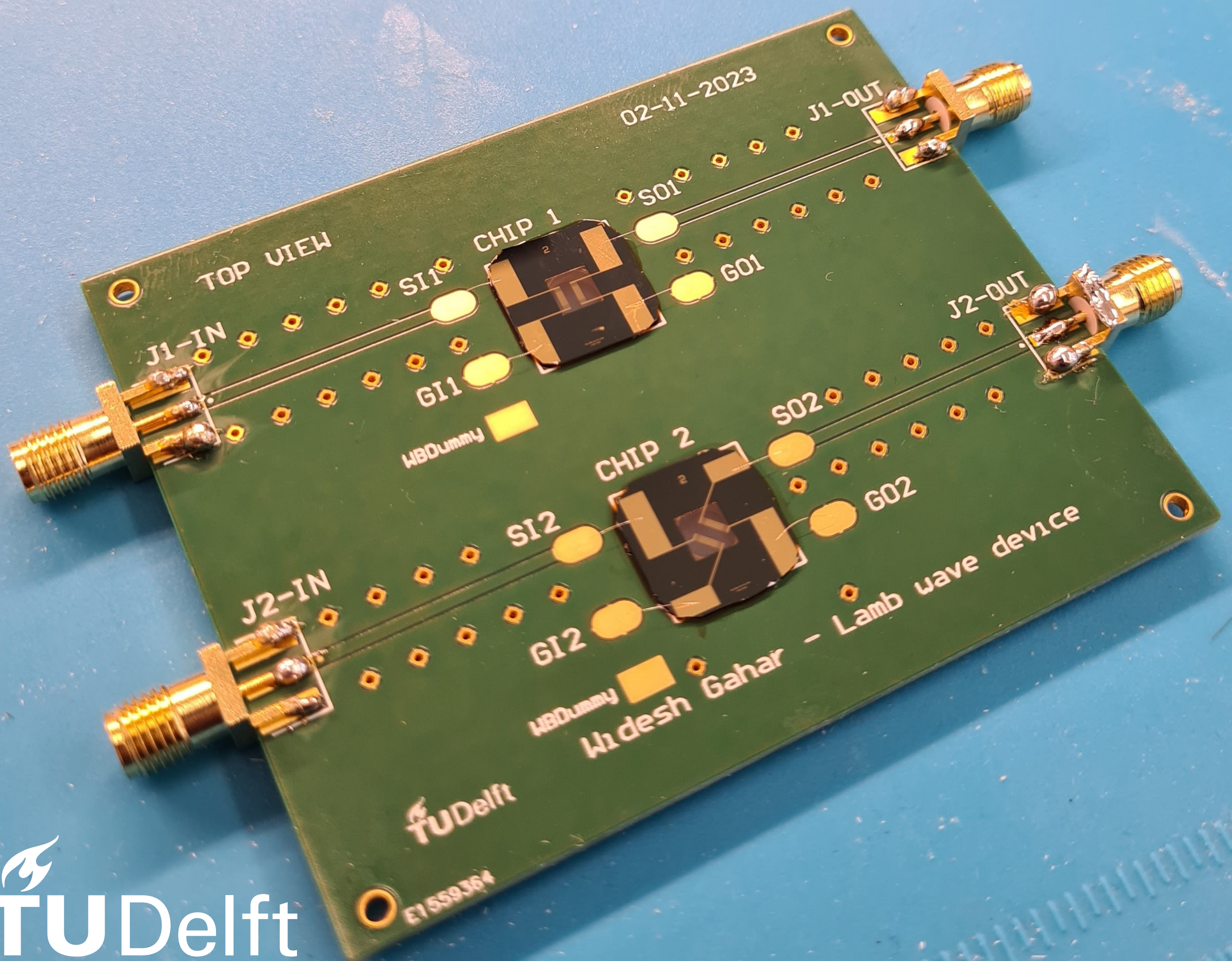

Delft University of Technology

TU Delft

A Lamb wave-based liquid sensor for biomedical applications

by

Widesh Gahar

Student number: 4521641
Project Duration: November 2022 - March 2024
Thesis committee:

Thesis committee:	Prof. dr. P.J. French	TU Delft
	dr. T. Manzaneque	TU Delft
	dr. ir. E. Korkmaz	The Hague University of Applied Sciences
	dr. A.S. Sisman	TU Delft, daily supervisor

TU Delft

Summary

This study presents an AlN-based Lamb wave (A0 mode) liquid sensing device designed for biomedical applications. The Lamb wave device features a 1.5 µm composite membrane consisting of a 500 nm LPCVD SiN and a 1 µm of a c-axis oriented AlN film. Additionally, an innovative 45° rotated IDT design was explored to minimize edge reflections towards the output IDT. Liquid testing experiments, involving IPA, DI water, and D-PBS, were conducted to see if the devices were able to differentiate between these liquids.
Results demonstrate that the fabricated Lamb wave devices exhibit sensitivity to mass loading and can distinguish between liquids based on phase, frequency, and gain characteristics. Devices with the rotated IDT design have shown a significant increase in resonance by 15 dB, as well as enhanced sensitivity compared to those with the normal design. Furthermore, devices with the rotated design demonstrated a higher Q factor of 680, indicating superior performance over the normal design (Q factor of 450). These findings suggest that a Lamb wave device with the 45° rotated IDT design holds considerable potential for applications that demand accurate liquid characterization and detection.

Acknowledgements

This project would not have been possible without the people who supported me every step of the way. First, I would like to express my gratitude to my supervisor Paddy French and my daily-supervisors: Alper Sisman and Erdal Korkmaz, who introduced me to the MEMS industry with this interesting thesis project. Their guidance and constructive feedback has been very useful during the whole project. The thesis project provided ample opportunities for in-depth discussions with the supervisors. I greatly appreciated Alper's commitment to being available beyond office hours, as it allowed us to address various topics and find effective solutions for any obstacles encountered. I extend my appreciation to Tomás Manzaneque for his willingness to serve as a member of the thesis committee and enabling me to graduate.

I would like to express my sincere thanks to the dedicated staff at Else Kooi Lab, specifically Silvana Milosavljevic, Mario Laros, Johannes van Wingerden, and Daniel van der Plaats, for their invaluable support in providing the necessary trainings on various equipment essential for my project. I am particularly grateful for the insightful discussions I had with Johannes, which greatly contributed to achieving the desired output. Furthermore, Johannes' assistance with deposition recipes and measurements played a pivotal role in obtaining the desired results.

I am grateful to the Kavli Nanolab staff, namely Eugene Straver, Charles de Boer, Roald van der Kolk, Bas van Asten, Marinus Fischer, Brian van den Bulk, Hozanna Miro, Lodi Schriek, and Marc Zuiddam, for their invaluable assistance in providing me with the necessary equipment training within a limited timeframe. Their availability for discussions regarding various issues I encountered during the fabrication process was greatly appreciated. I would like to specifically acknowledge Hozanna for conducting the XRD measurements on my behalf, saving me the need for additional training. Furthermore, I extend my thanks to Eugene for his efforts in looking for alternative products and methods that could resolve the problems I faced during fabrication.

I would like to express my gratitude to Johan Meyer for generously sharing his project experiences and lending his nano VNA equipment for the final measurements. His valuable advice not only saved time but also offered a new approach to overcoming different obstacles.

I would like to express my deepest gratitude to my parents, Anandprakash Gahar and Tidjmala Ganpat Gahar, for their unwavering love and support throughout my studies. Additionally, I am immensely grateful to my siblings, Prawesh, Amisha, Rishaya, and Samairaa, as well as my niece, Shanvi, for always being there for me. I am also indebted to my uncle Joy Chabile, my girlfriend and friends, whose unconditional support has been invaluable. Their understanding and encouragement have been instrumental in helping me overcome challenges.

Widesh Gahar
Delft, March 2024

Contents

Summary i

Acknowledgements ii

Nomenclature ix

1 Introduction 1
1.1 Thesis objective 2
1.2 Outline of the thesis 2

2 Background 3
2.1 Lamb Waves 4
2.2 Resonator parameters 6
2.2.1 Sensitivity 6
2.2.2 Insertion Loss 6
2.2.3 Electromechanical coupling coefficient (k^2) 6
2.2.4 Quality factor (Q) 7
2.2.5 Signal-to-noise ratio (SNR) 7
2.2.6 Temperature effects 7

3 Design of the Lamb wave device 9
3.1 Design criteria 9
3.1.1 Basic requirements for thin film structures 9
3.1.2 Ability to excite A0 mode Lamb waves 10
3.1.3 High quality (002) oriented piezoelectric layer 10
3.1.4 Sensitivity 10
3.1.5 Withstand mass loading 10
3.2 Material selection 10
3.2.1 Base substrate 11
3.2.2 Piezoelectric layer 11
3.2.3 IDT 14
3.2.4 Silicon Nitride 15
3.3 Sensor design 16
3.3.1 Membrane layers 16
3.3.2 Membrane dimension 16
3.3.3 IDT Design parameters 17

4 COMSOL simulation 19
4.1 Determining the resonant frequency 19
4.2 Propagation of the signal 20
4.3 Performance of the Lamb wave device 23

5 Device fabrication 26
5.1 Test fabrication 27
5.1.1 Sputtering of 1um AlN 28
5.1.2 Maskless lithography 31
5.1.3 RIE 32
5.1.4 KOH wet etching 32

5.2 Final device fabrication process . . . 34
5.2.1 Fabrication Result . . . 36
5.3 Problems encountered during fabrication process . . . 37
5.3.1 Finding suitable resist and developer for AlN layer . . . 37
5.3.2 KOH wet etching . . . 38

6 Experimental setup **40**
6.1 Fabricated Lamb wave devices . . . 40
6.2 PCB design . . . 40
6.3 Vector Network Analyzer . . . 41
6.4 Liquid tests . . . 42

7 (Experimental) Results and Discussions **43**
7.1 VNA measurements . . . 43
7.1.1 Liquid test . . . 43
7.1.2 Phase shift vs density . . . 49
7.1.3 Frequency shift vs density . . . 50
7.1.4 Impact of different liquid volume on the sensing area . . . 53
7.1.5 Evaluation of reproducibility . . . 54
7.1.6 Analyzing performance parameters for devices with Normal and Rotated designs. 55

8 Conclusions and Future work **57**
8.1 Conclusions . . . 57
8.2 Future research and recommendations . . . 57
8.2.1 Lamb wave device as biosensor . . . 58

References **60**

A Flow chart **63**

B FABRICATION RESULTS **70**

C MASK DESIGNS **77**

D DEPOSITION MEASUREMENTS **79**

E EXTRA MEASUREMENT RESULTS **81**

List of Figures

1.1 Acoustic waves can be classified into two groups based on their propagation modes: Bulk Acoustic Waves (BAW) which travel freely through the entire volume of the piezoelectric substrate, and Surface Generated Acoustic Waves (SGAW) which are produced and detected on the surface of the substrate. BAWs can be classified into longitudinal BAW (L-BAW); shear BAW (S-BAW), thickness shear modes (TSM)- quartz crystal microbalance (QCM); film bulk acoustic wave (FBAR), thickness extensional mode (TEM), lateral field excitation (LFE) mode; Lamb waves, acoustic plate wave (APW). SGAWs can be classified into Rayleigh SAW (R-SAW), Sezawa mode waves; shear-horizontal SAWs (SH-SAWs); Love mode wave; pseudo-surface acoustic waves (PSAW) or Leaky SAWs (LSAW), Lamb wave mode; flexural plate wave (FPW). 1

2.1 Four types of seismic waves [12]. 3
2.2 Antisymmetric Lamb wave mode. 4
2.3 Symmetric Lamb wave mode. 4
2.4 Displacement fields of different Lamb wave modes from COMSOL simulation[16]. . . . 4

3.1 3D Cross-section of a Lamb wave device. 11
3.2 Al–N bonds formed distorted tetrahedron [24]. 12
3.3 Geometry of crystallographic planes for (100), (002), (101) and (110) in hexagonal AlN lattice [24]. 12
3.4 The phase velocities of the first two Lamb wave modes compared to the phase velocities of longitudinal wave, Rayleigh wave and shear wave propagation in AlN membrane [16]. 13
3.5 Anisotropic etching of (100) silicon. 16
3.6 IDT design. 17
3.7 Top-side design view of the Lamb wave device. 18
3.8 Back-side design view of the Lamb wave device. 18
3.9 Design 1 - Normal. 18
3.10 Design 2 - Rotated. 18

4.1 Unit cell representation of the Lamb wave device. 19
4.2 Eigenfrequency study. 20
4.3 Normal IDT design. 21
4.4 Rotated IDT design. 21
4.5 Output voltage (normal vs rotated design). 22
4.6 Edge reflections towards the output IDTs (normal vs rotated design). 22
4.7 Gain in dB (normal vs rotated design). 23
4.8 2D Lamb wave device design with the added load. 23
4.9 2D propagation of the Lamb wave device with added load. 24
4.10 Output voltage of different densities. 24
4.11 Phase vs Frequency. 25
4.12 Phase shift vs liquid density at 62.25 MHz. 25

5.1 XRD pattern of the two different AlN film recipes. 31
5.2 Design of the test membrane. 32
5.3 RIE result. 32

5.4 Top-side view of wafer with SiN/AlN/SiN membranes. 33
5.5 Back-side view of wafer with SiN/AlN/SiN membranes. 33
5.6 After the completion of KOH wet etching process Design 1. 37
5.7 After the completion of KOH wet etching process Design 2). 37
5.8 Lamb wave device - Design 1. 37
5.9 Lamb wave device - Design 2. 37
5.10 AR-P 5350 Lift-off resist structure after metal evaporation [36]. 38

6.1 Top-side view of the PCB design. 41
6.2 Back-side view of the PCB design. 41
6.3 Lamb wave devices attached and wirebonded on a PCB with the SMA connectors. . . . 41
6.4 Measurement setup for the liquid tests. 42

7.1 Device 1 Gain comparison - NORMAL design. 44
7.2 Device 2 Gain comparison - NORMAL design. 44
7.3 Device 3 Gain comparison - NORMAL design. 45
7.4 Device 1 Gain comparison - ROTATED design. 45
7.5 Device 2 Gain comparison - ROTATED design. 46
7.6 Device 3 Gain comparison - ROTATED design. 46
7.7 Device 1 Phase comparison - NORMAL design. 47
7.8 Device 2 Phase comparison - NORMAL design. 47
7.9 Device 3 Phase comparison - NORMAL design. 48
7.10 Device 1 Phase comparison - ROTATED design. The D-PBS liquid test could not be performed on Device 1 - rotated design as the membrane was broken. 48
7.11 Device 2 Phase comparison - ROTATED design. 49
7.12 Device 3 Phase comparison - ROTATED design. 49
7.13 Phase shift vs liquid density of devices with NORMAL design. 50
7.14 Phase shift vs liquid density of devices with ROTATED design. 50
7.15 Frequency shift vs liquid density of devices with NORMAL design. 51
7.16 Frequency shift vs liquid density of devices with ROTATED design. 51
7.17 Frequency shift vs liquid density between liquids for devices with NORMAL design. . . . 52
7.18 Frequency shift vs liquid density between liquids for devices with ROTATED design. . . 52
7.19 Gain of various volume levels of DI water - NORMAL design. 53
7.20 Gain of various volume levels of DI water - ROTATED design. 53
7.21 Gain of various volume levels of D-PBS - NORMAL design. 54
7.22 Gain of various volume levels of D-PBS - ROTATED design. 54
7.23 Repeating of dry test - NORMAL design. 55
7.24 Repeating of dry test - ROTATED design. 55
7.25 Gain comparison between Normal and Rotated design for Device 2. 56

B.1 After deposition of 500 nm LPCVD SiN on a bare DSP wafer 70
B.2 After deposition of 1 um AlN 71
B.3 Bad AlN deposition due to contamination. Therefore it is essential to include a cleaning step after each wafer deposition. 71
B.4 Exposure result Design 1 (Normal Design) 72
B.5 Exposure result Design 2 (Rotated Design) 73
B.6 Post Lift-off process normal design 74
B.7 Post Lift-off process rotated design 74
B.8 After the completion of KOH wet etching process Design 1 (Front-side) 75
B.9 After the completion of KOH wet etching process Design 1 (Back-side) 75
B.10 After the completion of KOH wet etching process Design 2 (Front-side) 76
B.11 After the completion of KOH wet etching process Design 2 (Back-side) 76

C.1 Mask design of the normal structure 77
C.2 Mask design of the rotated structure 78
C.3 Mask design of the backside pattern 78

E.1 Device 1 Gain comparison - NORMAL design. 81
E.2 Device 2 Gain comparison - NORMAL design. 82
E.3 Device 3 Gain comparison - NORMAL design. 82
E.4 Device 1 Gain comparison - ROTATED design. 83
E.5 Device 2 Gain comparison - ROTATED design. 83
E.6 Device 3 Gain comparison - ROTATED design. 84

List of Tables

3.1 Basic requirements for bio-sensing and microfluidic applications [2]. 9
3.2 AlN physical properties [8]. 13
3.3 Key properties of commonly used electrode materials [2]. 15
3.4 IDT design parameters. 17

5.1 Process conditions 1 um AlN (recipe 1 and 2). 29
5.2 Stress measurement results. 30

6.1 Overview of the fabricated Lamb wave devices. 40

D.1 Results of SiN thickness measurement - Batch 2 79
D.2 Results of AlN stress and thickness measurement - Batch 3 79
D.3 Results of SiN thickness measurement - Batch 3 79
D.4 Results of AlN stress and thickness measurement - Batch 3 80

Nomenclature

Abbreviations

Abbreviation	Definition
Al	Aluminium
AlN	Aluminium Nitride
Au	Gold
CD9	Cluster-of-Differentiation 9
Cr	Chromium
D(RIE)	Deep reactive-ion etching
DSP	Doubble side polished
EKL	Else Kooi Laboratory
EWI	Elektrotechniek, Wiskunde en Informatica
FPW	Flexural plate wave
IDT	Interdigital Transducer
KN	Kavli Nanolab Delft
KOH	Potassium hydroxide
LOC	Lab on chip
LPCVD	Low pressure chemical vapor deposition
N-VNA	Nano Vector Network Analyzer
PCB	Printed circuit board
PECVD	Plasma-enhanced chemical vapor deposition
PZT	Lead zirconate titanate
RIE	Reactive-ion etching
SAW	Surface acoustic wave
Si	Silicon
SiN	Silicon Nitride
SMA	SubMiniature version A
TMAH	Tetramethylammonium Hydroxide
ZnO	Zinc oxide

Symbols

Symbol	Definition	Unit
f_0	Resonant frequency	$[Hz]$
th	Thickness	$[m]$
W	Width	$[m]$
k	wavenumber	$[1/m]$
ω	angular frequency k^2	Electromechanical coupling coefficient

Symbol	Definition	Unit
Q	Quality factor	
C	Stiffness constant	$[N/m^2]$
ε	Dielectric constant	$[F/N]$
e	Piezo constant	$[C/m^2]$
ρ	Density	$[kg/m^3]$
λ	Wavelength	$[m]$
N	Number of fingerpairs	
V_p	Phase velocity	$[m/s]$

Chapter 1

Introduction

The demand for compact, reliable, disposable, and affordable sensors is on the rise in industrial, medical, and various other scientific and engineering sectors. The sensor market is experiencing rapid growth, with an annual increase of approximately 18% [1]. In particular, the biosensor market holds great promise due to its applications in advancing areas of healthcare, biotechnology, and medicine. Areas of immense medical significance include the utilization of biosensors in personal glucose testing, HIV, and early cancer detection. Furthermore, the capability to detect pathogenic and physiologically relevant molecules in the body with remarkable sensitivity and selectivity makes the biosensor a potent tool for the early diagnosis and treatment of diseases [1].

Acoustic wave devices have become an important area of research due to their high sensitivity, compact size and real-time response, which are the main factors for their widespread use. Acoustic waves are created by applying an alternating current or radio frequency excitation to electrodes on a piezoelectric layer. The piezoelectric structure will demonstrate a tendency to vibrate near its resonant frequency or one of its harmonics. The generated acoustic wave travels perpendicular to the surface, into the bulk media (Bulk Acoustic Wave, BAW), or along the surface (Surface Acoustic Wave, SAW). The different types of modes are illustrated in figure 1.1 [2]. An acoustic wave sensor can detect the presence of a specific phenomenon by detecting changes in the amplitude, phase or frequency of the input electrical signal, or by measuring the time-delay between the input and the output electrical signal [3].

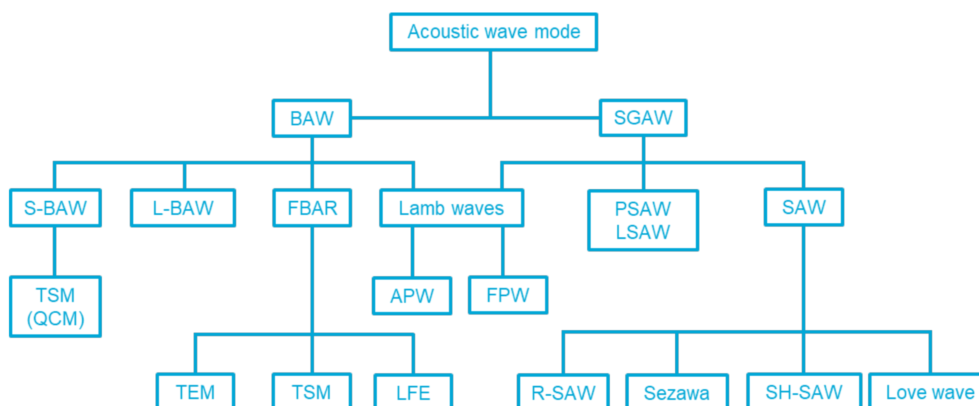

Figure 1.1: Acoustic waves can be classified into two groups based on their propagation modes: Bulk Acoustic Waves (BAW) which travel freely through the entire volume of the piezoelectric substrate, and Surface Generated Acoustic Waves (SGAW) which are produced and detected on the surface of the substrate. BAWs can be classified into longitudinal BAW (L-BAW); shear BAW (S-BAW), thickness shear modes (TSM)- quartz crystal microbalance (QCM); film bulk acoustic wave (FBAR), thickness extensional mode (TEM), lateral field excitation (LFE) mode; Lamb waves, acoustic plate wave (APW). SGAWs can be classified into Rayleigh SAW (R-SAW), Sezawa mode waves; shear-horizontal SAWs (SH-SAWs); Love mode wave; pseudo-surface acoustic waves (PSAW) or Leaky SAWs (LSAW), Lamb wave mode; flexural plate wave (FPW).

Acoustic wave based biosensors have been widely acknowledged as a reliable technique for detecting a range of chemical or biological analytes, making them an invaluable tool in medical diagnosis.

A notable example is the work of [4], who employed an acoustic microsensor to detect insulin, which then enabled the use of glycine-HCL to remove insulin for further examination. In [5], a glucose biosensor was successfully created by utilizing a multilayer Love-mode surface acoustic wave. Additionally, acoustic sensors have proven to be effective in detecting various DNA [6] and cancer cells [7]. Another noteworthy contribution in this area comes from [7], who developed a surface acoustic wave (SAW) device incorporating a gold layer to immobilize specific antibodies. This device enables the detection of a specific antigen, serving as a cancer biomarker [8].
Among all the acoustic wave modes, Lamb wave mode is chosen for this project. Lamb waves propagate on both side of the plate due to the thin plate structure, enabling both sides to serve as the sensing area. Furthermore, by using the opposite side of the plate (membrane) as the sensing area, the electrodes of the Lamb wave devices can be protected as they will be isolated from the surrounding environment [9].

Although Lamb wave sensors were extensively studied in the late 1990s, they have not been widely published. This is due to the following reasons:

- Lamb wave sensors are not as sensitive as other devices due to their low operation frequency.
- The membrane structures are thin and fragile.
- The fragility limits the minimum film thickness.
- The thin film structure has high temperature sensitivity [2].

In recent years, however, there have been a number of advances in thin film-based Lamb wave devices, including new structural configurations, electrode configurations, high-frequencies-wave configurations, and even the implementation of Lamb wave on Flexible SAW devices [2]. With these developments, it will be tried to successfully fabricate a functional Lamb wave device that can be used for biomedical applications.

1.1 Thesis objective

The objective of this thesis is to fabricate a two-port Lamb wave liquid sensing device that can be used for biomedical applications. The fabricated device should be able to distinguish between different type of liquids.

1.2 Outline of the thesis

This thesis will begin with a chapter exploring the background of this subject, delving deeper into the concept of Lamb wave devices. Chapter 3 will outline the design criteria that the sensor will need to meet, followed by the material selection and the design of the Lamb wave device. The simulation design and results are described in Chapter 4. Chapter 5 will describe the fabrication of the resulting sensor design, followed by the test setup in Chapter 6. In Chapter 7, the results and discussions obtained from the experimental measurements that validate the functionality of the fabricated Lamb wave device will be presented. Finally, Chapter 8 will cover the conclusion of the thesis, along with recommendations for future work.

Chapter 2

Background

Wave propagation in a guided surface was first explained by Lord Rayleigh in 1889, and these waves are now referred to as "Rayleigh waves". The Rayleigh waves are surface waves that are elliptical in shape and cause both vertical and horizontal motion along the wave path [10]. Rayleigh waves are a subclass of seismic waves, which also includes S-waves, P-waves and Love waves. Seismic waves occur when materials inside the Earth suddenly move due to causes such as an earthquake, volcanic eruptions, explosive events, landslide, avalanche and even fast-flowing rivers. The four types of seismic waves are presented in figure 2.1 [11]. Following Rayleigh, the British applied mathematician Horace Lamb reported the waves found in plates in 1917 in one of his historical publications "On waves in an elastic plate". The waves were subsequently named after Lamb, who also established the theoretical basis for such waves. Initially, Lamb waves did not receive much attention because of the complex equations needed to explain them. However, this topic was revisited in 1945 by Osborne and Hart to investigate Lamb waves activated by structures in underwater explosions. Their study revealed a great deal of potential applications for Lamb waves. Mindlin provided a complete Lamb wave solution in 1950, and Gazis and Victorov provided further details in 1958 and 1967, respectively, by evaluating the dispersive properties of the Lamb waves. Firestone and Ling introduced Lamb wave based damage detection during the 1940-1951 period, and after this, Lamb waves found niches in Seismology and Non-Destructive Evaluation (NDE) in the 1950s and 1960s. In addition to theoretical development, Worlton (1961) and Frederick (1962) conducted intensive experimental investigations to gain a better understanding of the fundamental of the Lamb waves. With the development of computing devices in the 1980s and 1990s, Lamb wave engineering applications have seen unprecedented growth, particularly in Lamb wave based damage identification techniques of recent years [10].

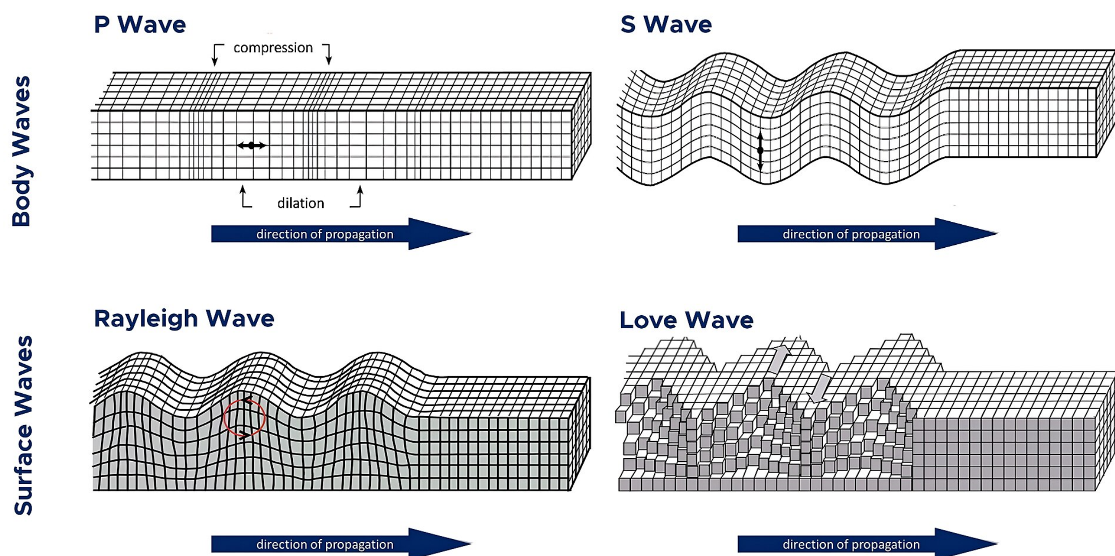

Figure 2.1: Four types of seismic waves [12].

2.1 Lamb Waves

Lamb waves are elastic waves with longitudinal and shear vertical displacements. They are excited by the interdigital transducers (IDTs) when the thickness of the substrate is less than or equal to the wavelength of the wave. There are two types of Lamb waves, namely passive and positive. Passive Lamb waves are generated by a remote acoustic wave source without the usage of a piezoelectric substrate, while positive Lamb waves are generated by a thin piezoelectric layer itself [2]. This project will focus on positive Lamb waves.

Rayleigh waves are turned into Lamb waves when the thickness of membrane is smaller than the acoustic wavelength. These Rayleigh waves travel on both sides of the membranes, which allows sensing on both sides of the plate. This is what makes Lamb waves different from other acoustic waves. The overlapping of the wave on the upper and lower surfaces results in the generation of an antisymmetric (A_n) mode with a lower velocity (frequency) and a symmetric mode (S_n) with a higher velocity (frequency) [13]. The terms S_n or A_n are typically used to refer to the nth order symmetric or asymmetric Lamb wave modes, respectively, where "n" is an integer between 0 and infinity and indicates the amount of standing waves along the plate thickness [14]. These modes with its particle's motion around the membrane's median are illustrated in figure 2.3 and figure 2.2 respectively [2][15]. Figure 2.4 illustrates the displacement fields of various Lamb wave modes obtained through COMSOL [16].

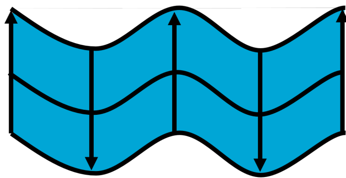

Figure 2.2: Antisymmetric Lamb wave mode.

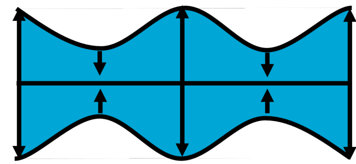

Figure 2.3: Symmetric Lamb wave mode.

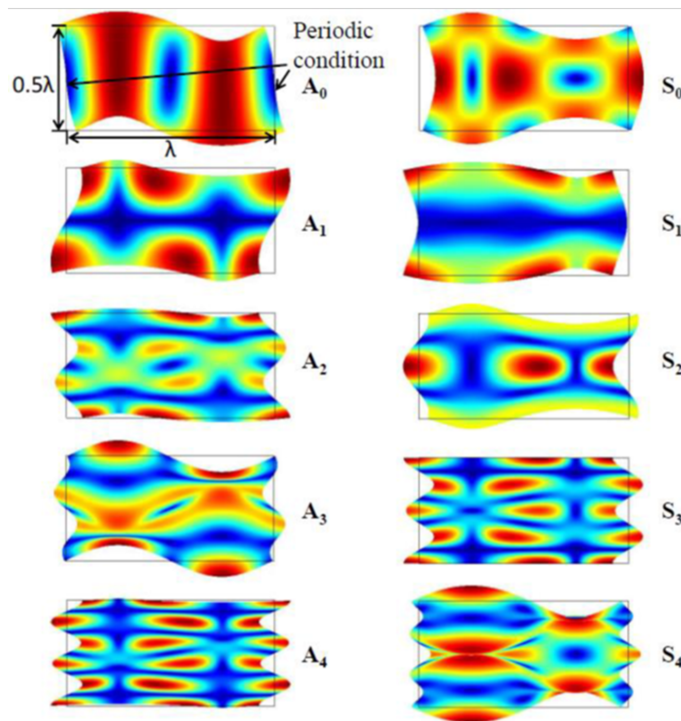

Figure 2.4: Displacement fields of different Lamb wave modes from COMSOL simulation[16].

The equations for the symmetric and antisymmetric modes, also known as the Rayleigh-Lamb frequency equations, can be expressed as follows:

$$\frac{tan(qh)}{tan(ph)} = -\frac{4k^2pq}{(q^2-k^2)^2} \quad \text{symmetric modes} \tag{2.1}$$

$$\frac{tan(qh)}{tan(ph)} = -\frac{(q^2-k^2)^2}{4k^2pq} \quad \text{antisymmetric modes} \tag{2.2}$$

With the help of equation 2.1 and equation 2.2, the velocities and the operation frequency of the device can be determined. In these equations, h stands for half of the plate thickness. p and q are given by:

$$p = \left(\frac{\omega}{c_L}\right)^2 - k^2 \tag{2.3}$$

$$q = \left(\frac{\omega}{c_T}\right) - k^2 \tag{2.4}$$

Additionally, k is the wavenumber and is equal to:

$$k = \frac{\omega}{c_p} \tag{2.5}$$

Here, c_p is the phase velocity of the Lamb wave mode and ω is the angular frequency.

$$\omega = 2\pi f \tag{2.6}$$

Substituting the above equations, the relationship between the phase velocity and the wavelength can be observed.

$$c_p = \left(\frac{\omega}{2\pi}\right)\lambda \tag{2.7}$$

For Lamb wave devices, the two most useful modes are the lowest order antisymmetric mode A0 and the symmetric mode S0 in plates with a low thickness-to-wave ratio. In this case, the thin plate can be roughly described as a homogeneous isotropic plate. Lamb wave velocities of A0 and S0 modes can be determined with the following equations:

$$V_{A0} = \frac{2\pi h}{\lambda}\sqrt{\frac{E}{12(1-v^2)p}}\frac{1}{\sqrt{\frac{\pi^2h^2}{3\lambda^2}+1}} \tag{2.8}$$

$$V_{S0} = \sqrt{\frac{E}{(1-v^2)p}} \tag{2.9}$$

,where E = Young's modulus, v = Poisson's ratio, ρ = density, h = thickness, and λ = wavelength of Lamb wave. On ultra-thin plates, the Lamb wave velocity in S0 mode is dispersionless and does not depend on the plate thickness, whereas the wave velocity in A0 mode does depend on the plate thickness [9]. The resonant frequency of a Lamb wave device is determined by:

$$f_0 = \frac{V_p}{\lambda} \tag{2.10}$$

,where $V_p = V_{A0}$ or $V_p = V_{S0}$.

Therefore, according to Equation 2.8, 2.9 and 2.10, depending on the device's center frequency, the interdigital sensor structure and plate thickness can be specified.

The A0 mode, also referred to as flexural plate wave (FPW), exhibits a high sensitivity to mass loading and can effectively be employed in liquid environments with minimal attenuation [17]. Therefore, the A0 Lamb wave mode will be employed in this study.

2.2 Resonator parameters

The essential parameters of an acoustic wave sensor consist of sensitivity, responsiveness, stability, reproducibility, reversibility, dynamic testing range, sensing limit, reliability, flexibility, cost, and environmental factors including temperature and humidity [2].

The acoustic phase velocity (v) is defined as $f_r = v/\lambda$, with λ being the wavelength. When the acoustic velocity changes, the corresponding resonant frequency changes. The following relation describes the various sources that can influence the acoustic phase velocity change, Δv [2]:

$$\frac{\Delta f}{f_0} = \frac{\Delta v}{v_{acoustic}} = \frac{1}{v}\left(\frac{\delta v}{\delta m}\Delta m + \frac{\delta v}{\delta \sigma}\Delta \sigma + \frac{\delta v}{\delta c}\Delta c + \frac{\delta v}{\delta \varepsilon}\Delta \varepsilon + \frac{\delta v}{\delta T}\Delta T + \frac{\delta v}{\delta P}\Delta P + \frac{\delta v}{\delta \eta}\Delta \eta + \frac{\delta v}{\delta \rho}\Delta \rho ...\right) \tag{2.13}$$

The equation above makes the assumption that any external disturbances mentioned below are of a small. Δm represents the alteration in mass load, $\Delta \sigma$ denotes the modification in conductivity, Δc signifies the change in mechanical constant, $\delta \varepsilon$ represents the variation in dielectric constant, ΔT denotes the shift in temperature, ΔP signifies the alteration in pressure, $\delta \eta$ represents the change in viscosity, and $\delta \rho$ denotes the variation in density [2].

2.2.1 Sensitivity

The mass sensitivity of the device can be expressed as:

$$S_r = \lim_{\Delta x \to 0} \frac{\Delta f}{f_0\ \Delta x} = \frac{df}{f_0\ dx} \tag{2.14}$$

,where Δf represents the frequency shift caused by Δx. The Δx is the change or alteration of variables such as temperature, pressure, mass, density, viscosity and conductivity. For gravimetric and mass sensors, this frequency change is expressed as [2]:

$$\Delta f = \frac{2\Delta m {f_0}^2}{A\sqrt{\rho \mu}} \tag{2.15}$$

,where μ = mass/area ratio, ρ = density of materials, and A = surface area. The majority of acoustic wave devices exhibit a mass sensitivity that is proportional to the mass per area and the square of operating frequency. According to equation 2.15, increasing the resonant frequency and decreasing the basic mass and surface area of the device increases the sensitivity of gravimetric acoustic sensors.

2.2.2 Insertion Loss

The propagation of a signal through a medium results in the loss of energy, which is referred to as insertion loss. This loss is quantified in decibels. A lower insertion loss indicates superior performance, as it signifies minimal energy loss during signal transmission. Conversely, when the insertion loss is excessively high, it can hinder the proper receiving of the signal at the other end of the medium. Additionally, the insertion loss will rise when the travel path of the signal is increased [18].

2.2.3 Electromechanical coupling coefficient (k^2)

The electromagnetic coupling coefficient (k^2) is a measure of the electrical to acoustic conversion efficiency in piezo-electric materials. The k^2 can be determined by the following equations [2]:

$$k^2 = \frac{e_{31}^2}{C_{11}\varepsilon_{33}} \tag{2.16}$$

,where, e_{31} is the electric field, C_{11} the material elastic constant and ε_{33} the permittivity.

$$k^2 = 2\frac{v_{free} - v_{metal}}{v_{free}} \tag{2.17}$$

$$k^2 = \frac{\pi}{2}\frac{f_s}{f_p}\left[tan\left(\frac{\pi}{2}\frac{f_s}{f_p}\right)\right]^{-1} \tag{2.18}$$

$$k^2 = \frac{\pi}{4N}\left(\frac{G}{B}\right)_{f=f_0} \tag{2.19}$$

In the above equations, v_{free} and v_{metal} represent the velocities of the free surface and metalized (or short-circuited) surface phases, respectively. Moreover, the frequency f_s respresents the resonance frequencies in series , while f_p represent the parallel configurations. N refers to the number of finger pairs present. G represents the conductance (real part), while B symbolizes the susceptance (imaginary part) [2].

In order to encompass the impact of material properties, as well as the structure and geometry of the resonator, on the acoustic device, the effective electromechanical coupling coefficient, k^2_{eff}, is introduced[2].

$$k^2_{eff} = \frac{\pi^2}{4}\left(\frac{f_p - f_s}{f_p}\right) \tag{2.20}$$

$$k^2_{eff} = \frac{f_p^2 - f_s^2}{f_p^2} \tag{2.21}$$

2.2.4 Quality factor (Q)

The quality factor Q is often used as a measure to describe acoustic wave resonator performance. Increased quality factor (Q) value enhances the stability of the output frequency and phase, while simultaneously decreasing insertion loss and narrowing the bandwidth [19]. Factors that influence the quality factor include dielectric loss of piezo-electrical materials/film, ohmic loss in contacts and electrodes, the limited lateral size of resonators, acoustic leakage into the substrate, roughness of the surface and interface, internal friction in piezo-electric thin film material at defects or grain boundaries, columnar structure, cracks and voids [2].

The Q factor can be determined with the S parameter measurements using the following equations:

$$Q = \frac{f_s/f_p}{1-(f_s/f_p)^2}\sqrt{\frac{(1-|S_{12max}|)}{|S_{12max}|}\frac{(1-|S_{11min}|)}{|S_{11min}|}} \tag{2.22}$$

$$Q = \frac{f_0}{\Delta f_{-3dB}} \tag{2.23}$$

S_{11} represents the reflection signal, while S_{12} corresponds to the transmission signal of the device [2].

2.2.5 Signal-to-noise ratio (SNR)

The comparison between the level of a desired signal and the level of background noise is quantified using the Signal-to-noise ratio (SNR) [20].

2.2.6 Temperature effects

Temperature effects play a significant role in acoustic wave-based sensing. The dependence on temperature is due to a range of parameters, including temperature coefficient of frequency (TCF), temperature coefficient of delay (TCD), and temperature coefficient of velocity (TCV), which are associated with the thermal coefficient of expansion (TCE,α) of the device materials [2].

$$TCF = -TCD = \frac{1}{f_0}\frac{df}{dT} = \frac{1}{v}\frac{dv}{dT} - \frac{1}{L}\frac{dL}{dT} = \frac{1}{v}\frac{dv}{dT} - \alpha \tag{2.24}$$

$$TCD = \frac{1}{\tau_0}\frac{\tau - \tau_0}{T - T_0} \tag{2.25}$$

The time delays at temperatures T and T_0 are represented by τ and τ_0, respectively. The determination of the temperature coefficient of frequency (TCF) typically involves experimental measurements, where the changes in frequency values are recorded as a function of temperature [2].

Chapter 3

Design of the Lamb wave device

3.1 Design criteria

3.1.1 Basic requirements for thin film structures

In order to effectively integrate piezoelectric films for mass sensing that can be used for bio-sensing and microfluidic applications, the basic requirements for thin film structures should be met. Some of the requirements are listed in table 3.1.

Table 3.1: Basic requirements for bio-sensing and microfluidic applications [2].

Microstructure consideration	Dense structure and low porosity High crystalline quality Strong texture Uniformity Smooth surface Good stoichiometry
Piezoelectric properties	High electromechanical coupling coefficient (k^2) High acoustic wave velocity High frequency Good thermal stability (low thermal coeffcient) High quality factor (Q) Low acoustic loss Low damping
Fabrication requirements	Low film stress Good adhesion to substrates Easy deposition Cost effective High deposition rate Easy etching/patterning Reproducible
Biosensing	High sensitivity High resolution Good selectivity Rapid response Low power requirement Biocompatible Easy to immobilize antibodies on surfaces
Microfluidics	Flexible film Not reactive (chemically) Easy surface adjustment Ability to control hydrophobic properties of a surface

3.1.2 Ability to excite A0 mode Lamb waves

The main focus of this project is the design of an A0 Lamb wave device, the requirements to produce this type of Lamb wave mode should be considered first. In order to accomplish this, it is necessary to determine the frequency at which this specific Lamb wave mode is generated. To simplify the process, it is more efficient to begin with a fixed wavelength and membrane thickness for this device. Once the values of these parameters have been chosen, the phase velocity and frequency can be determined by utilizing equation 2.8 and equation 2.10, respectively. A finite element method (FEM) analysis of this design can also help find the expected resonant frequency of the device. Additionally, the FEM analysis can provide a visual representation of the specific wave type that is being excited by the IDTs. This analysis can be instrumental in assessing whether the desired mode is successfully generated.

3.1.3 High quality (002) oriented piezoelectric layer

In order to ensure an optimal performance of a piezoelectric layer, a high quality (002) orientation, also known as c-axis orientation, is preferred for the piezoelectric layer. To achieve this, it is important to find the ideal recipe that can produce the desired orientation for the chosen piezoelectric material. The orientation of the produced piezoelectric layer will be determined by using the Bruker XRD equipment.

3.1.4 Sensitivity

As with other acoustic wave devices, the applicability of Lamb wave devices in liquid sensing primarily relies on the frequency and phase shift of the devices. These sensors are equipped with high frequency (MHz – GHz) acoustic waves that travel through or on the surface of a piezoelectric medium. The travelling acoustic waves should be sensitive to changes on the surface of the sensor and in the piezoelectric material. Changes such as mass loading or viscosity in the propagation path cause the velocity and amplitude of the waves to change. For this project, it is important for the device to be able to detect a frequency and phase shift when different types of liquid are applied to the sensing area. This allows the device to distinguish liquids of different densities.

3.1.5 Withstand mass loading

The functionality of the fabricated Lamb wave device will be tested by adding fluids with different densities to determine whether the Lamb wave device is able to sense the density variation of the mass load. Therefore, it is essential to have a solid membrane structure that can withstand various liquid drops. By ensuring that the overall stress in the deposited layers is (low) tensile stress instead of compressive stress, a reliable membrane structure can be achieved. Furthermore, it is important to keep the size of the membrane small to prevent potential breakage.

3.2 Material selection

The correct selection of materials plays a fundamental role in the development of a high-performance Lamb wave device. A Lamb wave device consists of a base substrate, a thin piezoelectric layer in the middle and an electrode layer (IDTs) on top of the piezoelectric layer. The piezoelectric layer which is formed on the base substrate will be suspended with etching to create the membrane. Figure 3.1 illustrates the cross-sectional view of a basic Lamb wave device.

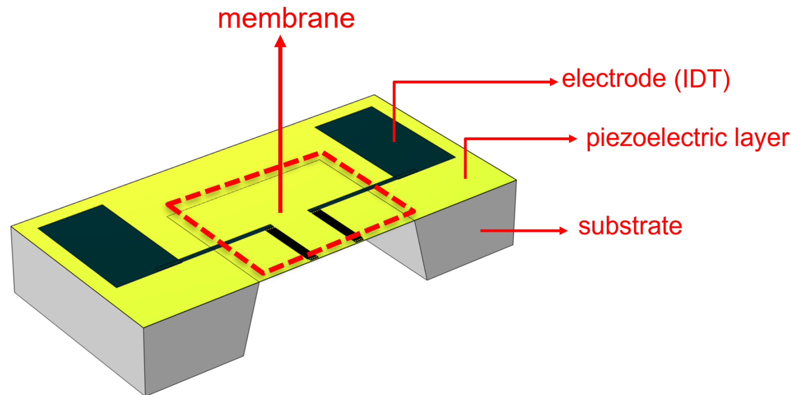

Figure 3.1: 3D Cross-section of a Lamb wave device.

3.2.1 Base substrate

For this project, the base substrate will be a 4" p-type Double Side Polished (DSP) Si wafer with (100) orientation. The (100) orientation was preferred as this will give a nice anisotropic etching during the KOH wet etching process at the end.

3.2.2 Piezoelectric layer

Piezoelectric materials have the ability to convert mechanical stress into an electric potential, making them energy transducing materials. This occurrence is also known as direct piezoelectric effect. Piezoelectric materials can also produce the converse piezoelectric effect, where mechanical stress is created when exposed to an electrical field [21]. In order to display piezoelectric behavior, a material must possess dielectric characteristics, implying that it should not conduct electricity, and its structure should not have a center of symmetry [22].

Thin film acoustic waves

Acoustic wave devices based on piezoelectric thin film materials such as zinc oxide (ZnO), aluminum oxide (AlN) and Lead zirconate titanate (PZT) have been identified as one of the key technologies for future Acoustofluids and Lab On Chip (LOC) devices. Since these applications are based on thin films instead of expensive and brittle bulk materials or substrates, Microelectronics, Sensors and Microfluidics can easily be integrated into one LOC device at low cost. Piezoelectric thin film also allows for the integration of multiple functionalities onto different substrates (silicon, glass, metal or polymer). Polymers are of particular importance for the development of Flexible and Wearable Sensing Devices based on these piezoelectric films. Piezoelectric thin films find extensive application in MEMS due to their ability to efficiently convert voltage-deflection, have high energy densities, exhibit low noise, operate at high frequencies, and require low power [2]. For this project, AlN is chosen as the piezoelectric layer.

Aluminum nitride (AlN)

Aluminium nitride (AlN) thin film is a III-V semiconductor material that has been frequently used in electronic devices, acoustic wave devices, optoelectronic devices, and piezoelectric transducers. AlN has interesting characteristics that make it attractive among nitride-based materials, including a wide bandgap energy of 6.2 eV, strong thermal conductivity, and a high wave velocity. The crystalline AlN has a hexagonal natural structure also known as wurtzite structure. This structure is mechanically strong, can withstand high temperatures, and is chemically stable [23].

AlN has a lattice parameter of 3.110 to 3.113 Å on the a-axis and 4.978 to 4.982 Å on the c-axis, with a c/a ratio of 1.600 to 1.602. In Figure 3.2 and in Figure 3.3, the Al-N bond formation and the crystallographic planes of the different planes of AlN are shown [24]. Each Al atom has four N atoms, forming a tetrahedron structure with three B_1 bonds between Al-$N_{(i=1,2,3)}$ atoms and one B_2 bond between Al-N_0 bond. The bond lengths are 0.1885 and 0.1917 nm of the B_1 and B_2, respectively. Furthermore, the bond angles are $107.7°$ for N_0-Al-N_1 and $110.5°$ for N_1-Al-N_2. The (100) plane is made up of B_1 bonds, and the (002) and (101) planes are made up of B_1 and B_2 bonds [25].

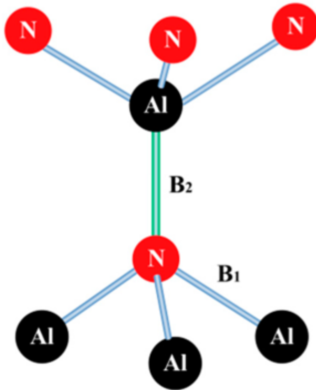

Figure 3.2: Al–N bonds formed distorted tetrahedron [24].

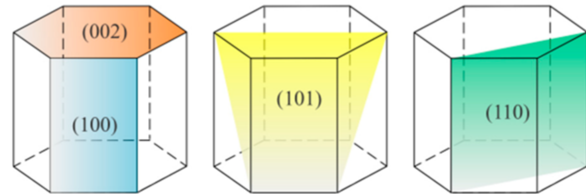

Figure 3.3: Geometry of crystallographic planes for (100), (002), (101) and (110) in hexagonal AlN lattice [24].

AlN films can be deposited using a variety of methods, such as pulsed laser deposition (PLD), molecular beam epitaxy, metal-organic chemical vapour deposition (MOCVD) and sputtering. Sputtering has advantages in the deposition of AlN due to its low processing temperature, ease of control over the film deposition, lack of toxic material production, and widespread use in thin-film industrial applications. The sputtering technique relies on ion bombardment towards the target that forms a coating on a substrate. Most reports on AlN indicate that its preferred orientations for potential applications are (100) and (002). Both the orientations have their benefits for applications [23].

A few of the AlN film properties such as the thermo-optic coefficient, oxidation resistance and thermal conductivity, are known to be significantly influenced by the microstructure and crystal phase. Controlling the AlN films preferred orientation and microstructure is therefore crucial. There have been studies done on the preferential orientation of AlN films using the sputtering technique. It has been reported that by including hydrogen gas during the deposition, it was possible to switch between the preferential orientations of (100) and (002) oriented. The preferential orientation of (100) and (002) of AlN using sputtering can be obtained by altering the vacuum chamber's overall pressure, applying a bias voltage to the substrate holder, raising the substrate's temperature, and altering the target to substrate distance [23].

The electromechanical coupling coefficient has the highest value along the (002) orientation, which leads piezoelectric researchers to focus more on the formation of a high quality (002) oriented AlN film [25]. Therefore, the aim of this project is to produce a high quality (002) oriented 1 um of AlN layer to serve as the piezoelectric layer for the Lamb wave device. The physical properties of AlN is given in table 3.2 [8].

Table 3.2: AlN physical properties [8].

	Symbol	Value	Unit
Stiffness constants	C11	345	$10^9[N/m^2]$
	C12	125	
	C13	120	
	C33	395	
	C44	118	
	C66	110	
Dielectric constants	ε_{11}	8	$10^-11[F/N]$
	ε_{33}	9.5	
Piezo constants	e_{15}	-0.48	$[C/m^2]$
	e_{31}	-0.58	
	e_{33}	1.55	
Mass density	ρ	3260	$[kg/m^3]$

Figure 3.4 shows the phase velocity dispersion of the zero order Lamb wave modes (S_0 and A_0) propagating in AlN, compared to the phase velocity of longitudinal wave, Rayleigh wave and shear wave modes in AlN. The S0 Lamb wave mode displays a phase velocity of approximately 10000 m/s, which is comparable to that of Bayesian Wave Wave (BAW). However, it exhibits a much lower phase velocity dispersion compared to the A0 Lamb wave mode. As a result, the high phase velocity of S0 mode in AlN membrane is appropriate for high frequency devices, and the low phase velocity dispersion of the S0 Lamb wave mode is preferred for fabrication stability. As the plate is thickening, both the phase velocity of the A0 Lamb and S0 Lamb wave modes approach the Rayleigh mode phase velocity [26].

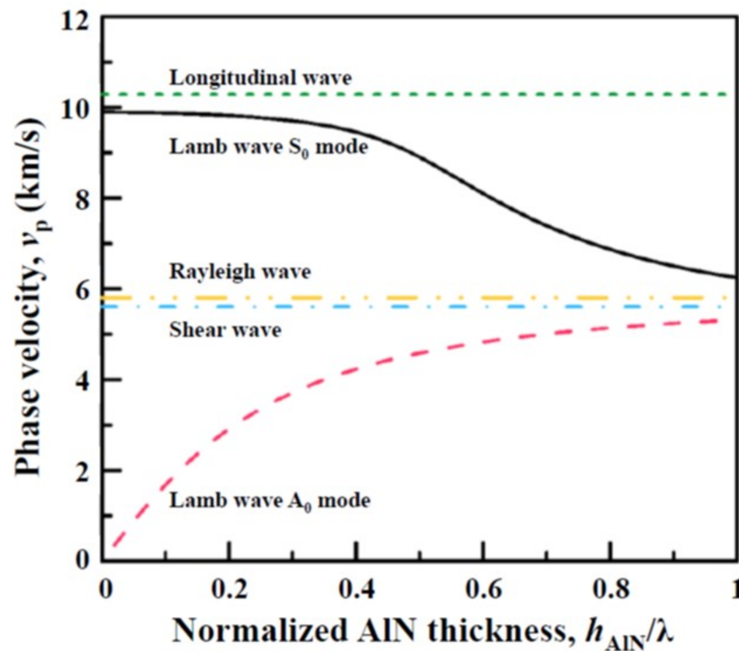

Figure 3.4: The phase velocities of the first two Lamb wave modes compared to the phase velocities of longitudinal wave, Rayleigh wave and shear wave propagation in AlN membrane [16].

Film stress

When AlN films are deposited through sputtering, large intrinsic stress can be introduced. The deposition process may also introduce thermal stresses. Intrinsic stresses are the result of a combination of film defects (such as voids and dislocations), interfacial structures (such as lattice mismatches) of the film and substrate, and/or the bombardment of ions/electrons during the sputtering and re-stalling process. In multilayer structures such as SAWs or FBARs, intrinsic stresses occur due to the constant

mismatches between layers of materials whose lattice structures differ, and are commonly referred to as epitaxial stresses. Structural relaxation reduces intrinsic stress once the film thickness reaches a critical value.

The extrinsic film stress is caused by external factors arising from the interaction of deposited material with the surrounding environment. These external factors are primarily related to the parameters of the film process (temperature, pressure, gas partial pressure, power, bias voltage) which play a significant role in the formation of film stress. The magnitude and characteristics (tensile or compressive film stress) of the film stress depend largely on the deposition method.

Typically, a low gas pressure will lead to a high compressive stress because of the long average free path, during which the ions and radicals are exposed to a greater amount of energy from the electrical field. This high energy bombardment, combined with the dense film structure, results in a high compressive pressure. On the other hand, a high deposition pressure results in the opposite effect, namely the formation of tensile stress, as the film structure becomes more porous.

The intrinsic stress of the film can be lowered by increasing the temperature of the deposition. This is due to the high migration rate of atoms/ions at high temperatures. The high deposition temperature may also significantly reduce defects, resulting in a decrease in intrinsic stress within the film. However, the thermal stress component may be more significant.

Post-deposition thermal annealing is often used to reduce the film stress as well as the defect density. It also improves the crystal quality, which in turn improves the device performance.

Generally speaking, film stress depends on the thickness of the film. Initially, film stress increases as the thickness increases. After reaching a critical value, film stress decreases as the thickness increases, mainly due to intrinsic stress relaxation once the critical value is reached. The critical thickness of the film depends on the evolution of the lattice mismatch of the film with the substrate, the porosity/density of the substrate, and the stiffness of the substrate. All of these parameters are closely related to deposition parameters.

Sputtered AlN films are more susceptible to stress than other thin film films such as ZnO, as they typically have much higher film stresses. AlN films often display signs of delamination and cracking, as well as significant warping of the coated structures. Furthermore, a high film stress can alter the mechanical, thermal, and piezo-electrical properties of the various layers, thus altering the elastic constant of thin films and the deformation of structures. This is commonly referred to as the Acoustoelectric Effect (AE). High film stress alters both the mechanical and electric properties of the films, resulting in long-term instability and unreliable acoustic wave devices.

The film stress is of greater importance for the Lamb wave devices as these devices typically have thin membrane multi-layered structures and are susceptible to bending or cracking when subjected to excessive stress. Therefore, it is essential to consider methods to minimize the stress of deposited thin films in order to achieve a consistent membrane and a dependable Lamb wave device [2].

3.2.3 IDT

The use of Interdigital Transducers (IDT) is the most direct and effective method of exciting surface acoustic waves on a piezoelectric substrate. When an alternating current (AC) or radio frequency (RF) signal is applied to the input IDT (which is on the piezoelectric layer), the piezoelectric material will convert the electrical signal into mechanical wave that will travel through the substrate. The output IDT will reconvert this mechanical wave into electrical signal. This signal will have a phase difference depending on the distance traveled and the physical characteristics of the medium. The phase difference between input and output signals will change proportionally to any mass that is added to the piezoelectric sensing area between the input and output IDT [8].

Aside from the quality of the piezoelectric film, the electromechanical coupling coefficient is also affected by the type of materials, patterns, and dimensions that are chosen for the electrodes. For mass sensing applications, the electrodes should be thin to reduce mass damping, have a high acoustic impedance to keep the acoustics inside the piezo-electric layer, and also have high conductivity to reduce the series resistance when sending out the excitation signal. The main characteristics of commonly used materials for electrodes are listed in table 3.3 [2].

Table 3.3: Key properties of commonly used electrode materials [2].

Material	Resistivity ξ $(10^{-8}\Omega m)$	Phase velocity longitudinal and shear (m/s)	Poisson ratio	Density $(10^3 kg/m^3)$	Young's Modulus (Gpa)	Acoustic impedance Z $(10^6 kg/m^2 s)$	Acoustic performance: $X = Z/\xi$ $(10^{14} kg/m^3\ s\ ohm)$
Al	2.82	6350-6500 (3040-3120)	0.33	2.695	76	17.65	6.26
Au	2.44	2650-3210 (1200)	0.42	19.32	78	51.2	20.98
Mo	5.3	6290-6700 (3400)	0.307	10.28	230	63.74	12.03
Pt	10.5	3260 (170)	0.38	21.14	170	63.42	6.04
Cu	1.7	5010-5200 (2270)	0.355	8.96	128	44.89	26.41
Ir	4.7	5350-5560	0.21	22.3	525	118.19	25.15
Ag	1.59	3600 (1600)	0.37	10.6	100	38.16	24
Ru	7.1	1260	0.3	12.2	220	27.57	3.88
W	5.6	5200-5500 (2900)	0.28	19.25	410	92.4	16.5
Ni	6.99	5600 (3000)	0.31	8.84	200	44.2	6.32
Ti	42	6100 (3100)	0.32	4.48	110	27.33	0.65
Hf	33	3010	0.37	13.3	110	40.03	1.21
Ta	13.2	4100 (2900)	0.34	16.6	200	68.06	5.16
Cr	12.5	6650 (4030)	0.21	7.19	140	46.74	3.74
CNT	1.5	12000 (6000)	0.22	1.5	1300	57.2	38.13

In order to create the IDTs, the metal film that will be employed must be both thick enough to offer low electrical resistance and also thin enough not put too much mechanical stress on the acoustic wave. While there are several materials suitable for electrodes, the key challenge is to select a material that can easily be deposited on wafers through evaporation with a thickness of 100 nm. Additionally, the selected material should also be not be etched by KOH during the wet etching process, which is essential for suspending the membrane in the final stages of fabrication.

Aluminum while also being the most common used material for electrodes, can easily be deposited through evaporation with good thicknesses. However, a significant drawback arises from the fact that aluminum is susceptible to etching by KOH. This vulnerability can potentially lead to the complete destruction of the IDT structure. To overcome this issue, a more suitable alternative is to utilize gold as the electrode material. Gold exhibits excellent resistance to the KOH wet etching process over an extended period of time. To ensure proper adhesion of the gold layer onto the piezoelectric layer, a thin layer of chromium needs to be deposited first.

3.2.4 Silicon Nitride

With the presence of the LPCVD (Low pressure chemical vapor deposition) SiN layer, the transmission gain will be improved [8]. LPCVD SiN is made from a mix of DCS, SiH2C2, and ammonia, or NH3, at temperatures between 700 to 900 °C. At low pressures (less than 1 Torr), SiN thin films have outstanding uniformity in terms of film thickness, composition, and conformal steps coverage [27].

LPCVD SiN

LPCVD technique will be used to have 500 nm of SiN on both sides of the wafer. With this method, a low stress film can be obtained which is highly recommended for the fabrication of membrane devices. The LPCVD SiN layer on the backside of the wafer will be needed to create the patterned etch mask for the wet etching process. The LPCVD SiN layer on the front side of the wafer will not only enhance the device's performance, but it will also serve as an etch stop layer when the bulk silicon is etched from the backside through the KOH wet etching.

PECVD SiN

In sensors, the active surface of the semiconductor needs to be protected from the outside world. To do this, the passivation layers should be chemically inert, resistant to corrosion, act as a barrier to water diffusion, and have a good adhesion. They should also have a wide bandgap and strong electrical breakdown strength, depending on the environment. The most used materials as passivation layers are SiO2 and SiN [28].

Due to the fact that the electrodes that require protection during the fabrication process are unable to tolerate the high temperature of LPCVD, the appropriate deposition technique to employ is PECVD

(Plasma-enhanced chemical vapor deposition). This technique has the capability to deposit SiN even at a temperature as low as 300°C. Nevertheless, it is important to acknowledge that the quality of the deposited material is not as favorable as that achieved through LPCVD, as the latter's higher deposition temperature guarantees a superior quality.

3.3 Sensor design

3.3.1 Membrane layers

As mentioned in section 2.1, Lamb waves are only generated when the thickness of the plate is less than the wavelength of the wave. Based on the chosen materials for the A0 Lamb wave device design, the membrane plate will be composed of 500 nm LPCVD SiN and 1 μm AlN stacked on top of one another. The total thickness of the composit membrane plate is thus 1.5 μm, which complies with the criterion of the plate being thinner than the wavelength of the Lamb wave.

3.3.2 Membrane dimension

Wet etching with a KOH solution is the most common method of removing the bulk silicon of the wafer or dies to create the membranes. This method is the simplest but also the most complex part of the manufacturing process. KOH is a type of etchant that selectively attacks silicon in (100) planes, resulting in a typical anisotropic v-etch with side walls that intersect the surface at an angle of 54.7 degrees.

Due to anistropic wet etching process, the membrane size will be smaller than the designed mask opening as illustrated in figure 3.5. Therefore, it is essential to understand the relation between the designed mask opening and the actual membrane dimension.

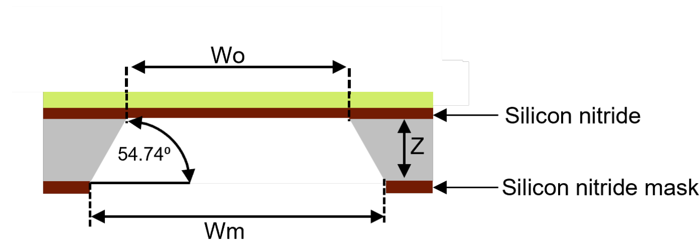

Figure 3.5: Anisotropic etching of (100) silicon.

The actual width of the membrane can be calculated with equation:

$$W_o = W_m - 2 \cdot \frac{z}{tan(54.74°)} \tag{3.1}$$

This equation can be simplified as

$$\begin{aligned} W_o &= W_m - \frac{2}{\sqrt{2}}z \\ W_o &= W_m - \sqrt{2}z \end{aligned} \tag{3.2}$$

where W_m is the width of the mask opening, W_o is the estimated width of the membrane after etching and z is the thickness of the silicon wafer [29] [30]. For the desired IDT structure, a membrane dimension of **4** $\times$ **4 mm²** will be suitable. To achieve this dimension, the designed mask should have an opening of **4.740** $\times$ **4.740 mm²**, according to equation 3.2.

3.3.3 IDT Design parameters

The performance of the Lamb wave device is strongly depended on the design of the IDTs. The two-port structure, also known as the bidirectional IDT structure, consists of an input and output port, and will be used in this study. Figure 3.6 illustrates the standard bidirectional IDT structure, which encompasses four key factors: width, number of finger pairs, aperture (overlap of fingers), and the length of the delay line.

The feature size of IDTs is usually between 1 and 200 µm and is microfabricated using photolithography and the lift-off process. Straight IDTs are the simplest type of IDT, which are straight rectangular metal bars (IDT fingers) that connect alternately on either end. This pattern generates a series of electric fields with an alternating direction between the IDT finger pairs and, as a result, the alternating areas of tensile strain and compressive strain are created in the piezoelectric layer. A drawback of this standard design is that half of the generated wave energy is lost due to the signal being generated on both sides of the input IDT.

As the periodicity of IDT finger pairs determines the resulting wavelength (λ) of the Lamb wave, the distance between each IDT finger and the adjacent next one should be $\lambda/4$. Moreover, the surface wave velocity is determined by the material properties of the piezoelectric layer and also the thickness of IDTs. The resonant frequency ($f_0 = v/\lambda$) of a device depends on the substrate and design of the IDT [31].

Due to the fact that the chosen wavelength plays an essential role in the design configurations, it has been decided not to change the wavelength and parameters that are dependent on the wavelength, as this would lead to a modification of the IDT configuration. The only parameter that can be changed without affecting the IDT configuration is the length of the delay line. A delay line that is excessively large will result in significant attenuation of the wave. This will lead to a weak signal being received by the output IDT. However, for a bio-sensing device, a delay line of considerable size will expand the area where captured antibodies can influence the frequency of the wave. The designed Lamb wave devices will have three different delay line lengths, as the appropriate length for the delay line remains uncertain. The selected values of the IDT parameters are placed in table 3.4.

Since Au, which has a high density, has been chosen as the material for the IDTs, the IDTs should not be extremely thick as this will increase the mass load and the mechanical stress on the membrane. The increased mass load and mechanical stress will reduce the sensitivity of the device and will also lead to breakage of the membrane. However, having an ultra thin IDTs will result in cracks in the IDT structure due to the deterioration. As a result, the IDT will be unable to generate the desired signals. Therefore, it is decided to keep the thickness of the gold IDTs to 90 nm. A 10 nm layer of Cr is deposited prior to the deposition of gold to improve the adhesion of the gold to the AlN surface. This brings the total electrode thickness to 100 nm.

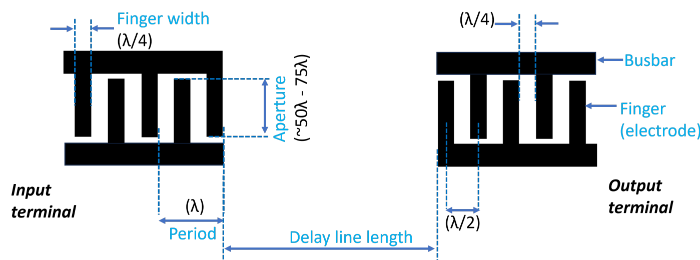

Figure 3.6: IDT design.

Table 3.4: IDT design parameters.

Device	Finger width (μm)	Wavelength (μm)	No of finger pairs	Aperture (λ)	Delay line (μm)	Thickness (Cr/Au) (nm)
1	5	20	30	75	750	100
2	5	20	30	75	1000	100
3	5	20	30	75	1500	100

An overview of the 3D design of the desired Lamb wave device is presented in figure 3.7 and figure

3.8. With this design, it is possible to include the liquid media needed for biosensors on the back side while also protecting the IDTs.

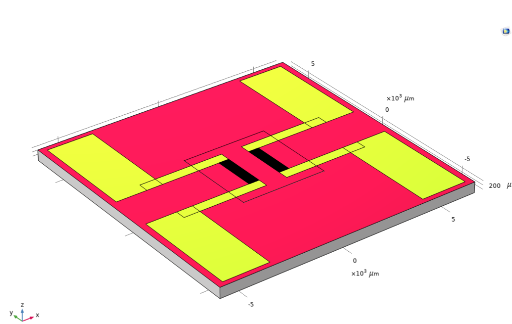

Figure 3.7: Top-side design view of the Lamb wave device.

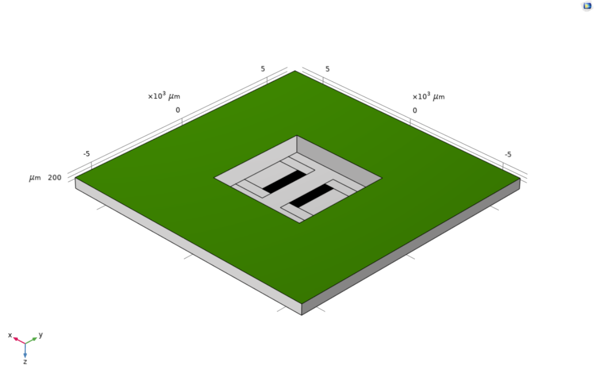

Figure 3.8: Back-side design view of the Lamb wave device.

Reflections from edges towards output IDT

When the waves of the Lamb wave device are generated by the left-side (input) IDT and received by the right-side (output) IDT, some of the wave energy will be reflected back from the silicon substrate to the output IDT, which can impact the results. In order to reduce the reflection from the edges towards the output, a $45°$ rotated bidirectional IDT design will be considered to see if the reflections can be reduced. The initial IDT design and the modified IDT design can be seen in figure 3.9 and figure 3.10, respectively. The blue square in the center represents the membrane plate, while the red pattern represents the IDT structure of the device. The arrows in the figures illustrate the directions of the reflected waves. By considering the designed IDT structure and the desired membrane dimension, the two-port Lamb wave device will have a size of **12.5** $\times$ **12.5 mm^2**.

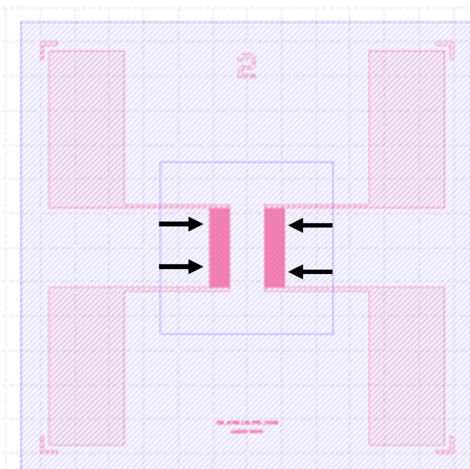

Figure 3.9: Design 1 - Normal.

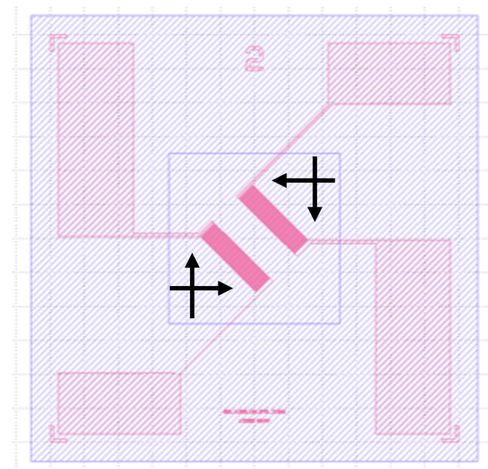

Figure 3.10: Design 2 - Rotated.

Chapter 4

COMSOL simulation

In this chapter, a finite element method (FEM) analyis will be performed using COMSOL multiphysics to analyze different design cases for the Lamb wave devices. This is done to get a better understanding of the acoustic interactions that happen on the piezo-electric material and also to get a better look at the behaviour of the IDTs. COMSOL multiphysics is a software package for engineering analysis that contains a wide range of physics modules. This software package is widely used in academia and is highly recommended for applications related to the study of MEMS structures. The main reason for the use of COMSOL in this project is the high-level optimization of the MEMS module, which is able to simulate piezoelectric phenomena with pre-defined piezo-electrical materials in the materials library [26].

4.1 Determining the resonant frequency

A 3D block study was performed with the desired membrane layers in order to find the resonant frequency of the device. The design as seen in figure 4.1 consists of 500 nm SiN as the bottom layer, $1\ \mu m$ AlN (piezoelectric layer) and on top 100 nm of Au electrodes (IDTs).

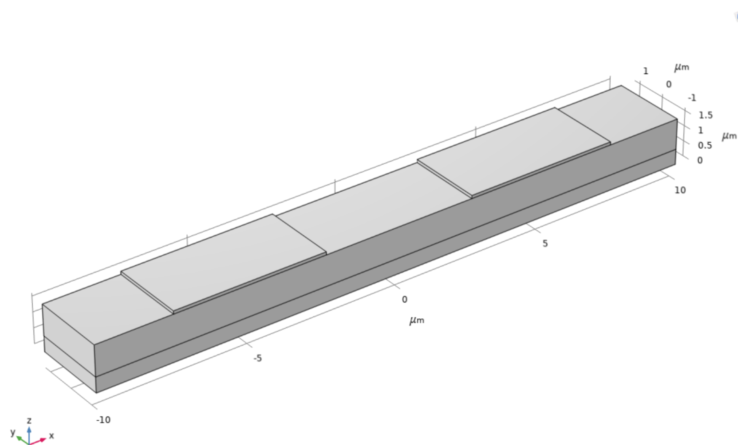

Figure 4.1: Unit cell representation of the Lamb wave device.

Eigenfrequency study

Figure 4.2 shows the result after performing an eigenfrequency study to find the resonant frequency of the device. Using figure 2.4 as the reference, a clear A0 mode was observed at around 63 MHz. The resonant frequency of the A0 Lamb wave device was also determined by utilizing equations 2.8 and 2.10. By adding the appropriate AlN parameter values in the equations, the calculated frequency matched the simulated frequency. This confirms that the resonant frequency of the designed A0 Lamb wave device is 63 MHz.

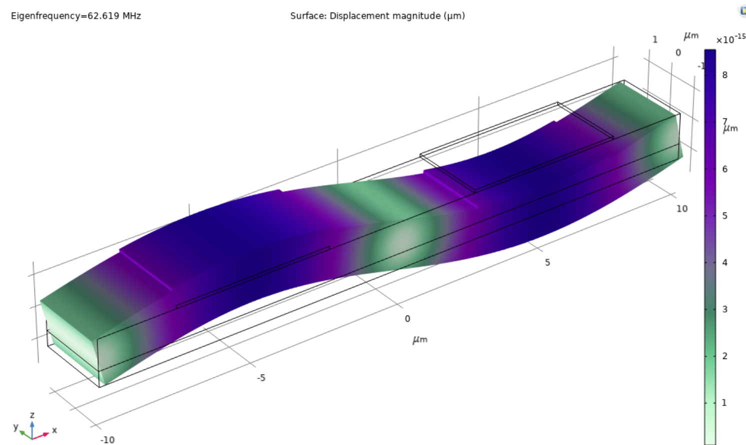

Figure 4.2: Eigenfrequency study.

4.2 Propagation of the signal

Due to the limited space available on the computer and the limited time available, it was not feasible to replicate the entire design. A small 3D version of the membrane was designed on COMSOL to predict the propagation of the signals. With a resonant frequency of 63 MHz, a passband signal, ranging from 33 MHz - 93 MHz, was applied to the input IDT. Upon examining the 3D simulations depicted in figure 4.3 of the Lamb wave device with the normal design, it became apparent that the waves generated by the input IDTs are reflected back by the edges of the membrane, as previously stated. The presence of wave reflections from the edges will pose a problem for the sensors as these reflections are received by the output sensing electrodes. However, in the 3D simulation of the second design shown in figure 4.4, where the IDT design is rotated by $45°$, the reflections from the edges were successfully redirected, leading to a decrease in reflections towards the output IDT.

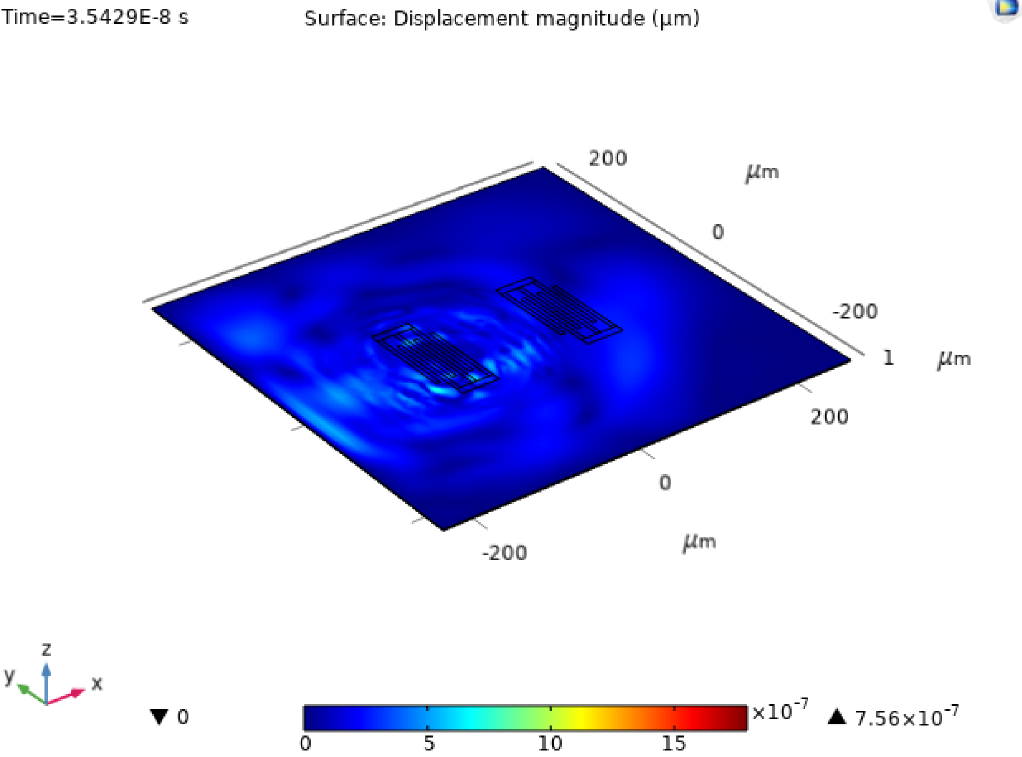

Figure 4.3: Normal IDT design.

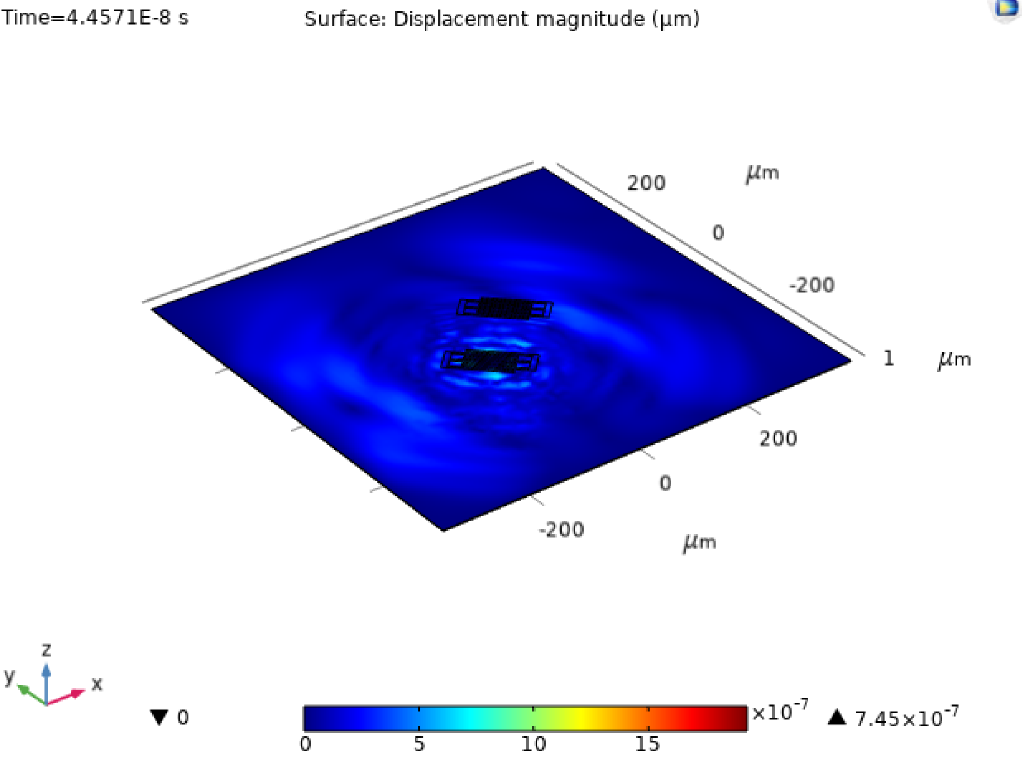

Figure 4.4: Rotated IDT design.

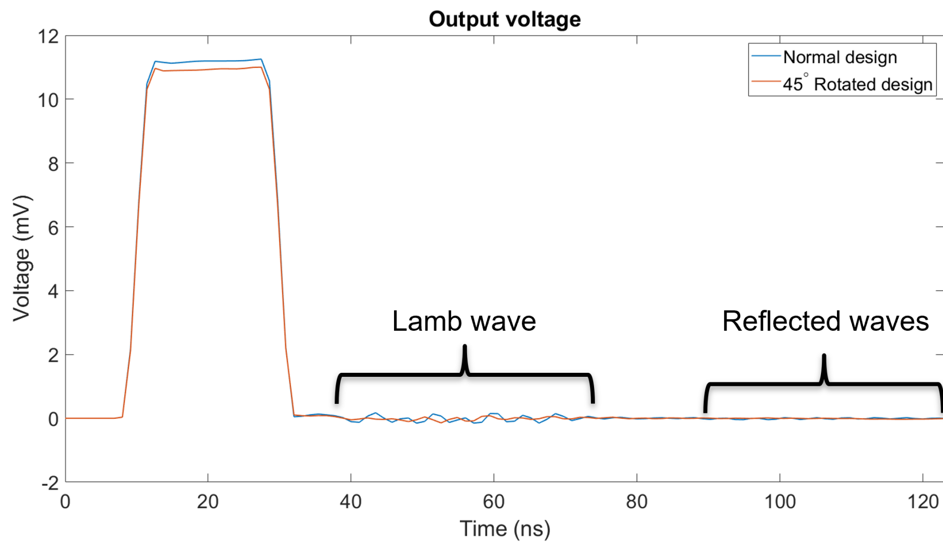

Figure 4.5: Output voltage (normal vs rotated design).

In figure 4.5, the voltages at the output IDTs of both the designs are presented. Based on the analysis of the simulated models, it appears that the reflection starts after 80 ns. Additionally, when examining the specific section where the reflection commences, as depicted in figure 4.6, there seems to be a reduction of 10 dB in edge reflections towards the output. This makes the rotated design more suitable for sensing applications. Now, it has to be seen whether this is also the case when performing the measurements practically. Therefore, these two designs will be considered for the final fabrication of the Lamb wave device.

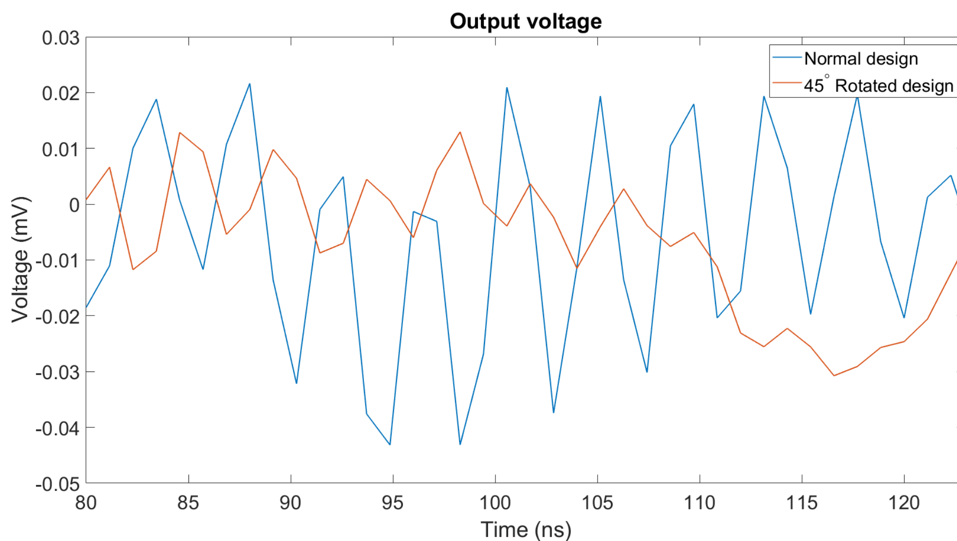

Figure 4.6: Edge reflections towards the output IDTs (normal vs rotated design).

While there is an observable difference in voltage from the reflection towards the output IDT between the rotated and normal designs, the gain difference between these two designs is minimal, as shown in figure 4.7. This could be a consequence of employing a smaller version of the design instead of the full-scale device for the simulation, leading to similar levels of loss and gain in both configurations. Furthermore, the simulated version has a much shorter delay line length compared to the actual device.

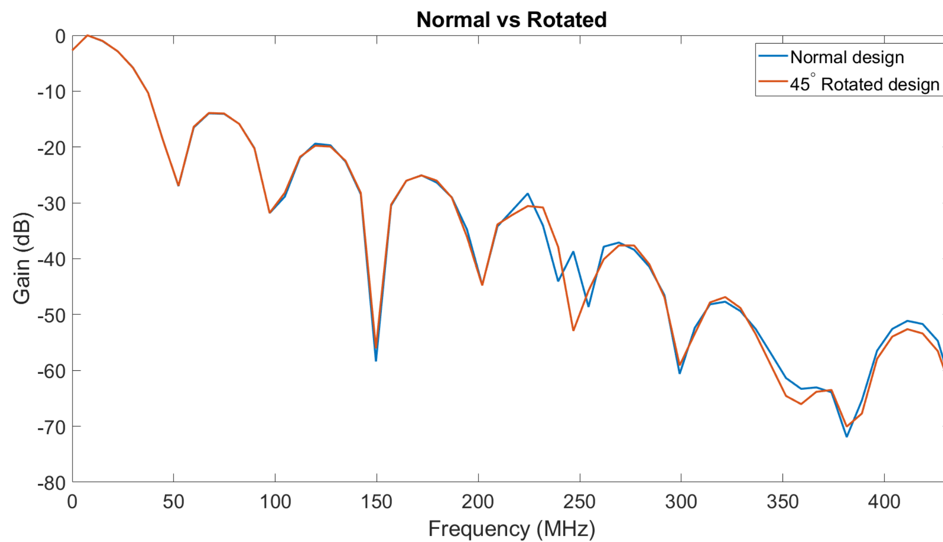

Figure 4.7: Gain in dB (normal vs rotated design).

4.3 Performance of the Lamb wave device

The performance of the device was studied by using a 500 nm polymer layer (PMMA) as the ”added liquid” at the backside of the device. The impact of the PMMA's density change on the phase shift of the device was investigated to imitate the gravimetric change that takes place when different liquids are placed in the sensing area. A 2D model was made for this as it was not feasible to do a 3D simulation of the whole design owing to the time and the space available in the computer. The 2D model is presented in figure 4.8 and the excitation and the propagation of the Lamb waves can be seen in figure 4.9.

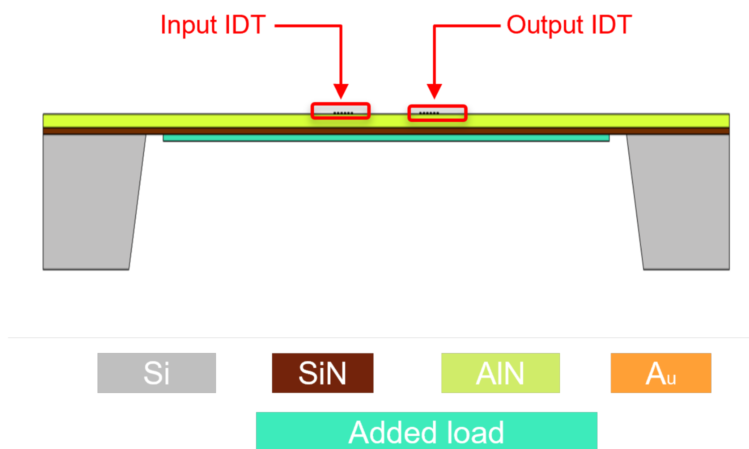

Figure 4.8: 2D Lamb wave device design with the added load.

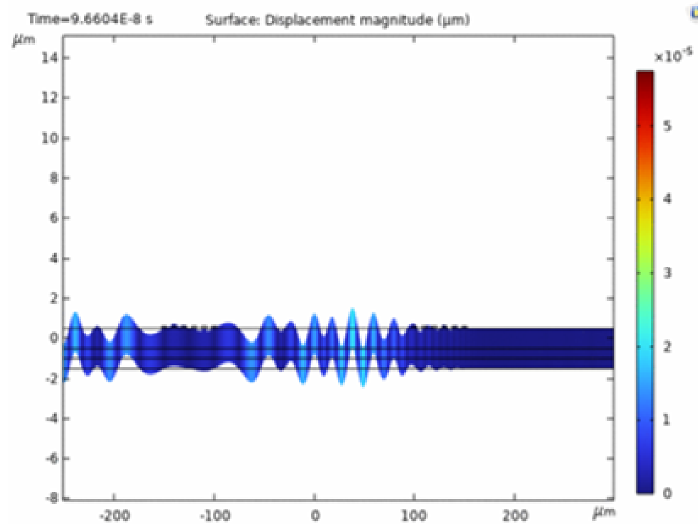

Figure 4.9: 2D propagation of the Lamb wave device with added load.

By changing the density of the added PMMA layer, a phase shift is expected. Figure 4.10 shows the result of the output voltage of varying densities of the load. As the liquid density increases, the time it takes for the signal to travel to the output electrodes also increases. This ensures a shift in the phase when the density of the added load is altered.

The impact of altering liquid densities on the phase spectrum is illustrated in figure 4.11. Each modification in density leads to a distinct phase, which is in line with the anticipated behavior of a functional Lamb wave device. Figure 4.12 further presents a plot showcasing the correlation between the phase shift and liquid density at 62.25 MHz, providing a clearer understanding between these two parameters. The sensitivity of the designed device to density changes is evident through the observed phase shift, despite the PMMA thickness being as thin as 500 nm.

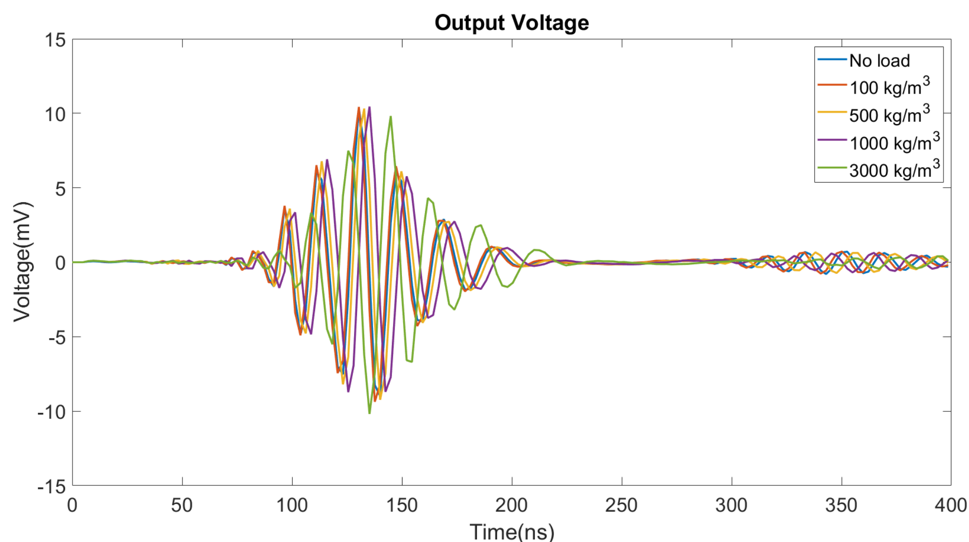

Figure 4.10: Output voltage of different densities.

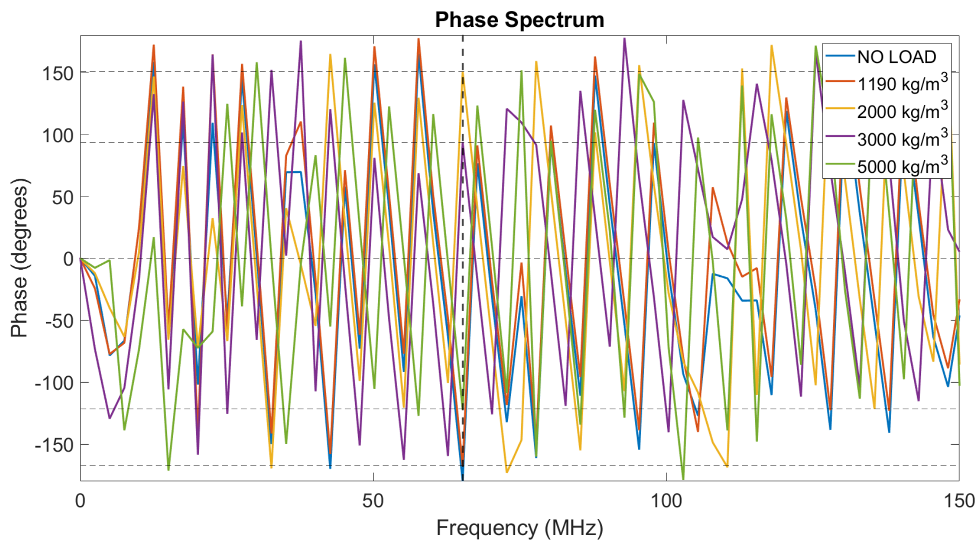

Figure 4.11: Phase vs Frequency.

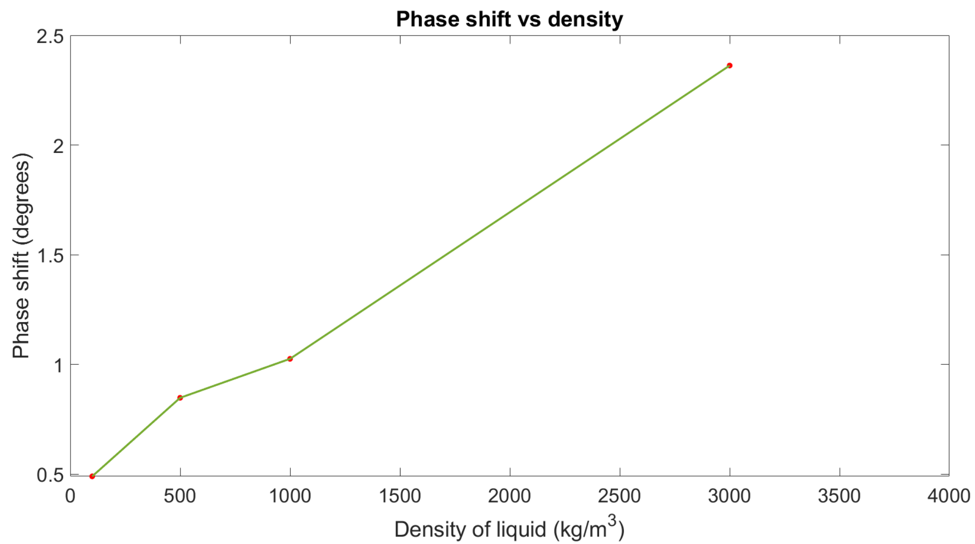

Figure 4.12: Phase shift vs liquid density at 62.25 MHz.

Based on the results from the COMSOL simulations, a functional Lamb wave device can be fabricated that can be used for sensing applications. However, it is important to acknowledge that the performance of the designed model is primarily for evaluation purposes. The model designed on COMSOL is smaller in size compared to the physical device, and not all parameters could be incorporated into the model. Therefore, these results are not suitable for making accurate comparisons with the fabricated devices. The next step would be to fabricate such a device to demonstrate that these ideas work in practice.

Chapter 5

Device fabrication

This chapter provides an overview of the main manufacturing steps, the manufacturing techniques employed and also the difficulties encountered during the fabrication of the Lamb wave device.

The following are the techniques used at various stages of the manufacturing process:

- **Low Pressure Chemical Vapour Deposition (LPCVD)** is a type of chemical vapor deposition where heat is used to create a reaction between a precursor gas and a solid surface. This reaction creates a solid phase material on the surface. LPCVD uses low pressure to reduce any potential gas phase reactions and also helps to make the substrate more uniform.
- **Plasma-enhanced chemical vapor deposition (PECVD)** is another type of chemical vapor deposition that uses plasma rather than heat to react with a source gas or vapor, allowing depositions at lower temperatures.
- **Sputtering** is a physical vapor deposition method also known as thin film deposition and is a popular way of depositing thin films onto substrates. It works by using ion bombardment to create a vapor from the source material, which is the target material. The vapor is created by a purely physical process called sputtering.
- **Evaporation**: is another type of physical vapor deposition method in which the substrate is put in a vacuum chamber at a room temperature and a crucible is filled with the material to be deposited (target material). The crucible is heated by a heating source, resulting in evaporation and condensation of the material on all exposed cold surfaces of the vacuum chamber and substrate.
- **Lithography** is the process of using light to transfer a pattern onto a photosensitive material.
- **Wet etching**, also called chemical etching, is the most basic type of etching. It involves removing a chemical from a material with a liquid reactant.
- **Dry etching**, also known as Plasma etching, is the process of ion bombardment of semiconductor material to remove a masked pattern. Two of the dry etching techniques are the RIE (reactive-ion etching) and the DRIE (deep reactive-ion etching). For RIE, the etch depth is limited to about 10 um at an etch rate of 1 um/min. DRIE, on the other hand, has an etch depth of 600 um or higher with a rate of 20 um/min [33].

Creating an acoustic wave device that contains membrane structures is challenging due its fragility and the stress produced by the composite plate. The primary cause of this stress is the in-plane compressive stress generated by the AlN film during the fabrication process as explained in section 3.2.2. Therefore, it is better to do some membrane dimension tests before starting the official fabrication of the Lamb wave device in order to determine which membrane dimension is most appropriate for this project. Furthermore, in the test fabrication, the available best quality AlN recipes will be tried in order to determine the AlN recipe that possesses the desired orientation and minimal stress. Subsequently, the stress levels of all the deposited layers will be measured.

5.1 Test fabrication

In this test fabrication, various membrane dimensions will be created (without the electrodes) on a wafer to evaluate the quality of the membranes. The flowchart of the test fabrication can be found at appendix A. The main processing steps for the test fabrication are shown in the figures below, as follows:

- **Step 1:** A 4” (100) p-type, double side polished Si wafer with 500 μm of thickness was chosen as the substrate. Afterwards, the wafer was cleaned with HNO_3 99% and 69.5%.
- **Step 2:** 500 nm of LPCVD SiN was deposited on the wafer.
- **Step 3:** A 1 μm thick AlN was deposited to function as the piezoelectric layer. This was done with the Trikon Sigma 204 equipment. For the best piezoelectric properties, a high-quality c-axis known as the (002) orientation was preferred for this project. For the deposition, two available recipes were tried to determine which of them had the (002) orientation. More details about this can be found in section 5.1.1. After the AlN deposition was completed and the required measurements were done, this wafer was then taken to kavli to do the rest of the fabrication process. Before doing the next deposition, it has to be known which orientation the deposited AlN layer has. The measurements were done with the Bruker XRD equipement and the results of these measurement are placed in section 5.1.1.
- **Step 4:** A 300 nm of PECVD SiN was deposited on top of the AlN layer. The purpose of this layer is to protect the IDTs and also the AlN layer against the KOH wet etching that will be performed later on.
- **Step 5-6:** In order to release the membrane, the bulk silicon layer below the deposited layers has to be removed. This will be done through wet etching from the backside with KOH (40% by weight and @80°C). For this, the backside has to be patterned first to create the SiN mask windows. This begins with first coating the backside of the wafer with resist. After the coating, the exposure and development of the designed patterns are performed to create the SiN mask patterns. For this project, a maskless lithography equipment called the laserwriter had been used. Further information regarding the Maskless Lithography process is provided in section 5.1.2.
- **Step 7:** The 500 nm of SiN on the backside is patterned with RIE to make the SiN mask openings for the wet etching process.
- **Step 8:** After stripping the photo-resist, the bulk silicon layer is then removed through the SiN windows with KOH (40% by weight and @80°C) and the SiN/AlN/SiN membrane will be released. The steps for the KOH wet etching process are described in section 5.1.4.

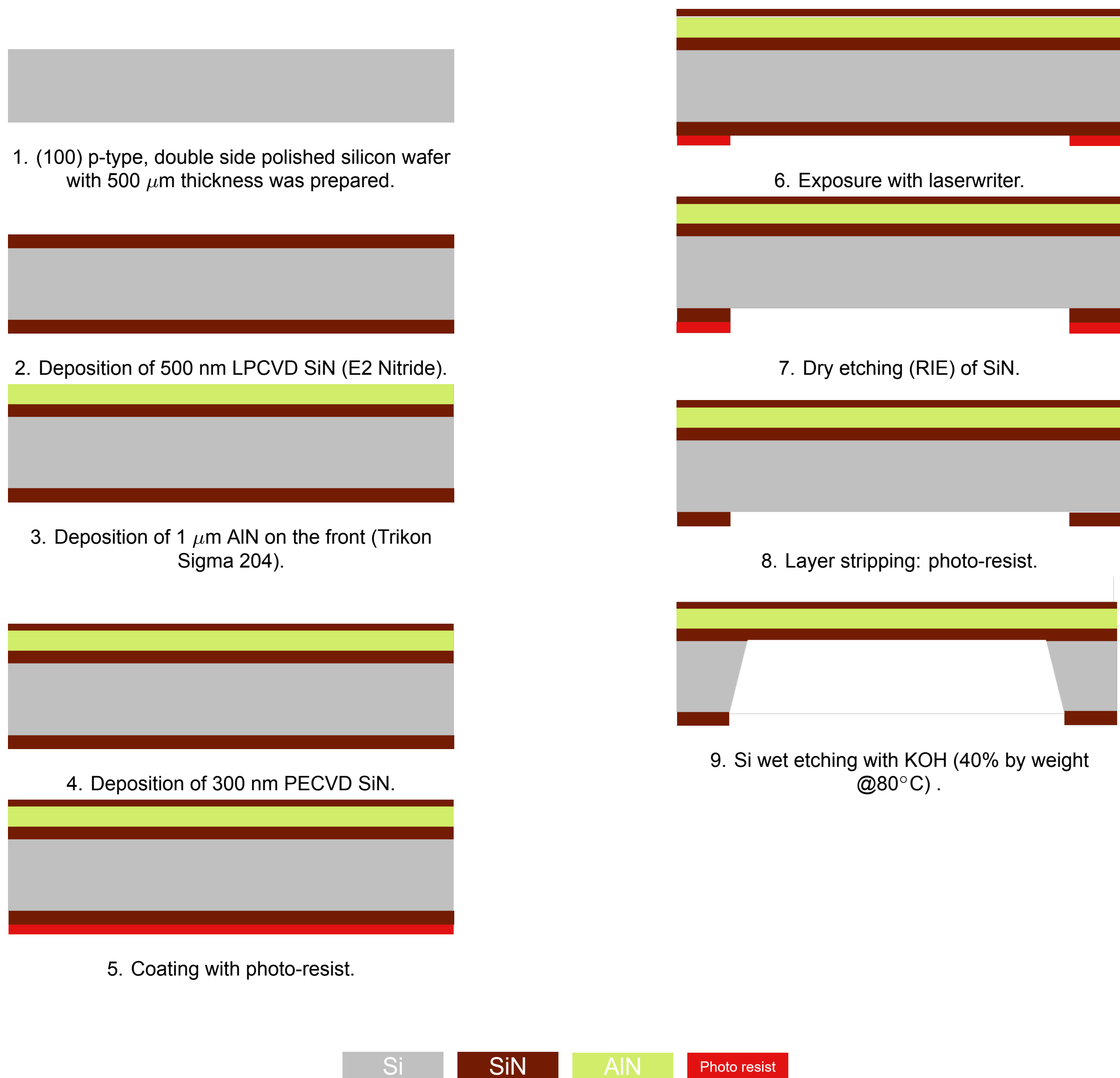

5.1.1 Sputtering of 1um AlN

AlN recipes at EKL

The AlN will be deposited through sputtering on the wafer with the Trikon Sigma 204 equipment. The desired thickness for the AlN layer is $1\ \mu m$. Two different AlN recipes are available at EKL, however, no information about the material properties such as the film stress, crystallographic orientation was known as these recipes were not used for a long time. For this reason, both recipes will be used for the test fabrication and the best recipe will be chosen for the final fabrication of the Lamb wave devices. The choice will be made primarily on the basis of prefered orientation (002) and subsequently on stress level.
The two recipes which were chosen at EKL were:

- Recipe 1: **AlN_1um_400C_LS**.
- Recipe 2: **AlN_1mu_ESLEE_50C**.

The process conditions for these two recipes are placed in table 5.1.

Table 5.1: Process conditions 1 um AlN (recipe 1 and 2).

Module recipe	Target	Electrode temp.	Gasses & flows	Target power	Time
1. AlN_1um_400C_LS	Al	400 °C	Ar/N2 = 20/80 sccm	3 kW	2700 $\pm$ $600\ s$
2. AlN_1mu_ESLEE_50C	Al	50 °C	Ar/N2 = 19/38	2 kW	3600 $\pm$ $900\ s$

Thin film stress measurement

Thin film stress is an important parameter to consider when manufacturing devices as mentioned in section 3.2.2. A very high film stress can lead to delamination and poor adhesion. For devices that release beams or membranes, the stress of the film or stack that is being released is really important. In the case of beams (cantilevers), the gradients of stress through the film thickness will curve the beam. For membranes, the stress must be slightly tensile in order to prevent membrane buckling due to compressive stress.

The **Flexus FLX 2320-S** stressmeter measures the stress applied to the wafer after depositing the thin film by measuring the surface curvature of the wafer. This tool uses scanning laser detectors to measure the wafer's surface position over its diameter. The local stress can be determined from the local curve of the sample by comparing the before and after measurement of the sample.

Thin film stress measurement is the measurement of the change in the radius of curvature (ROC) of a substrate due to the deposition of a thin film on it. The thin film should only be deposited on one side (front) of the substrate, as depositing it on both sides will equalize the stress. This is achieved by measuring the original substrate curvature radius and then measuring the curvature radius after depositing the film of interest on the front of the substrate (single side). If the deposition happens on both sides of the substrate (such as LPCVD), the film must be removed from the back of the substrate in order to measure the stress.

It is imperative for the membrane to have low stress levels in its layers and to exhibit tensile stress rather than compressive stress in order to be stable. The stress in this project is measured by a thin film stress measurement system (Flexus (FLX 2320-S)). A positive measurement value indicates a tensile stress, while a negative value indicates a compressive stress.

Stress measurement LPCVD SiN

The stress of LPCVD SiN was measured with the following steps:

- Measure the stress of a bare Double Side Polished wafer on which the LPCVD SiN stress will be measured. Select ”no film (first measurement)” to do the pre-deposition measurement and save this data afterwards.
- Deposit the 500 nm of LPCVD SiN on the measured wafer.
- Measure the thickness of the SiN layer with the ellipsometer.
- Remove the SiN from the backside of the wafer through dry etching (RIE). As LPCVD does the deposition at both sides of the wafer, the backside deposition have to be removed first to be able to measure the actual stress of the LPCVD SiN film. The RIE was done with the Trikon Omega 201 equipment.
- Measure the stress of the SiN and fill in the measured SiN thickness to get the actual stress value.

Stress measurement AlN

After the LPCVD SiN deposition, the next film that had to be deposited was AlN. For measuring the thickness of a layer on top of another layer, the best method is to add a monitor wafer (bare Si wafer) during the deposition and to measure the thickness of the deposited layer on the monitor wafer. As a monitor wafer will be used, it is also nice to measure the stress of AlN on this monitor wafer in addition to the stress measurement of AlN on the LPCVD SiN wafer. Two recipes were available for depositing 1 um of AlN with the Trikon Sigma 204 sputter as mentioned before. Both these recipes were used to see which one offered better stress results.

For the stress measurement of the ALN, the following steps were taken:

- Measure the stress of the wafer(s) on which the AlN will be deposited as ”no film” and save the data.
- Deposit 1 um of AlN with the Sigma sputter.
- Measure the thickness of the AlN layer with the ellipsometer.
- Measure the stress of the AlN layer with the measured AlN thickness.

At KN lab, the PECVD SiN was deposited and also the stress of this layer was measured at the KN with the same type of equipment. The stress measurements of all the three deposited layers are placed in table 5.2. While it is important to know the exact stress of each deposited layer so that some changes can be made in future fabrication if the current stress is not suitable for the creation of membranes, it is even more critical to know the total stress of the deposited layers on the wafer. Table 5.2 shows that the total stress from the deposited layers with the first AlN recipe was compressive, while the total stress from the layers with the second recipe was tensile. Although tensile stress is preferred for the membrane creation and only the second recipe fulfilled this criteria, the compressive stress from the first ALN recipe is still acceptable as it was low. Moreover, the absence of the electrodes did definitely have an effect on the actual stress and a more accurate conclusion can be made during the final fabrication of the Lamb wave device with the presence of the IDTs.

Table 5.2: Stress measurement results.

LAYER	SUBSTRATE	THICKNESS (Angstrom)	STRESS (MPa)
LPCVD SiN	on bare DSP Si wafer	4995 $\pm$ 50	125 $\pm$ 5
AlN_recipe_1	on LPCVD SiN deposited Si wafer	9680 $\pm$ 500	230 $\pm$ 5
	on bare Si wafer	9680 $\pm$ 500	480 $\pm$ 5
AlN_recipe_2	on LPCVD SiN deposited Si wafer	11470 $\pm$ 500	145 $\pm$ 5
	on bare Si wafer	11470 $\pm$ 500	205 $\pm$ 5
PECVD SiN	on AlN_recipe_1	3000 $\pm$ 500	500 $\pm$ 5
	on AlN_recipe_2	3000 $\pm$ 500	1210 $\pm$ 5
PECVD_SiN/AlN_recipe_1/LPCVD_SiN	on bare DSP Si wafer	17500 $\pm$ 500	-34 $\pm$ 6 (compressive)
PECVD_SiN/AlN_recipe_2/LPCVD_SiN	on bare DSP Si wafer	19470 $\pm$ 500	18 $\pm$ 5

XRD Measurement

The **Bruker XRD (X-ray Diffractometer)** equipment was used to examine the crystalline structure and orientation of the AlN film. The preferred orientation of AlN for this project is (002) as this orientation had the best piezoelectric properties. The AlN film is considered to be of a highly c-axis oriented piezoelectric film when there is a high peak at $36°$ for 2θ [23]. The XRD pattern of the AlN film can be seen in figure 5.1. In this figure, it can be seen that the AlN from the first recipe has a nice peak at $36°$ and can therefore be considered as a (002) oriented AlN film. On the other hand, the AlN film from the second recipe has a small peak at around $38°$. According to [34] the peak at $38°$ indicates the (101) orientation. As the (002) is preffered for the AlN, the first recipe will be used for the final Lamb wave device fabrication.

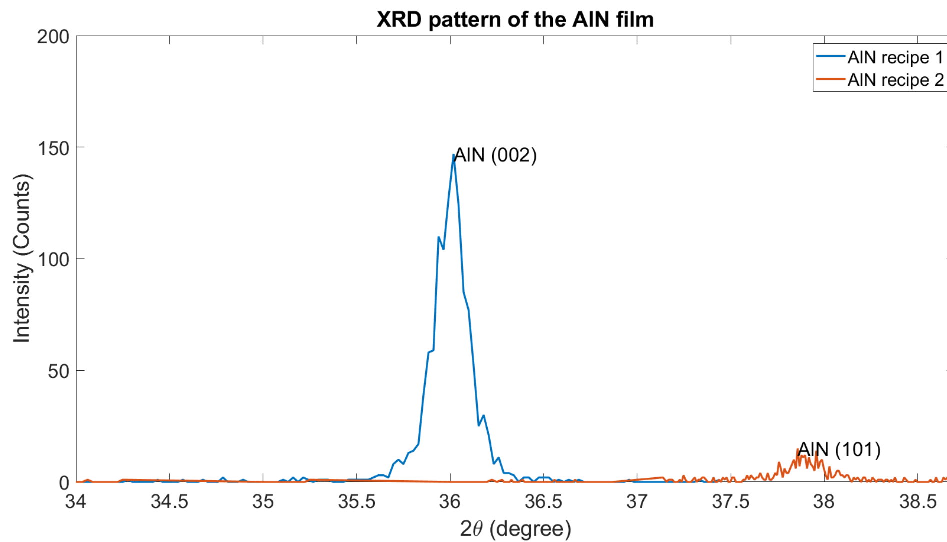

Figure 5.1: XRD pattern of the two different AlN film recipes.

5.1.2 Maskless lithography

Lithography process is an important sub-process of the process flow for the fabrication of devices. It is a process that is used before the etching or deposition process so that the desired pattern is etched or deposited. In traditional photolithography process, a photomask has to be fabricated or purchased first to transfer the CAD pattern onto a resist-coated wafer or plate using a stepper or mask aligner. In this project, a laserwriter will be used. This is a maskless photo lithography equipment that can transfer the design directly onto the wafer without the need for a photomask [35]. The steps of the lithography process are provided below:

1. Coat the substrate with photo-resist.
2. Expose the pattern design onto the photo-resist using the laserwriter with the correct dose and defocus settings.
3. Do the development to complete the lithography process.

The design of the test membrane, which consists of various dimensions of the membrane, can be seen in figure 5.2. As the thickness of the SiN on the backside is 500 nm, the resist coating has to be much thicker than this to ensure that only the SiN below the pattern is etched. Furthermore, it is also not clear which dose and defocus value is needed for a particular resist type and thickness, so it is thus better to have a dose test done with the laserwriter to inspect which dose value can give the best result for a particular resist type and thickness. Dose and defoc tests are tests where different levels of energy and dose are tried for a design in a series.

Once the optimal dose and defoc values are determined, the membrane design exposure can be performed. After the completion of the exposure, the resist has to be developed. This is done by putting the wafer in a beaker filled with **MF21A** developer for approximately 2 minutes and then rinse it with DI water to complete the development.

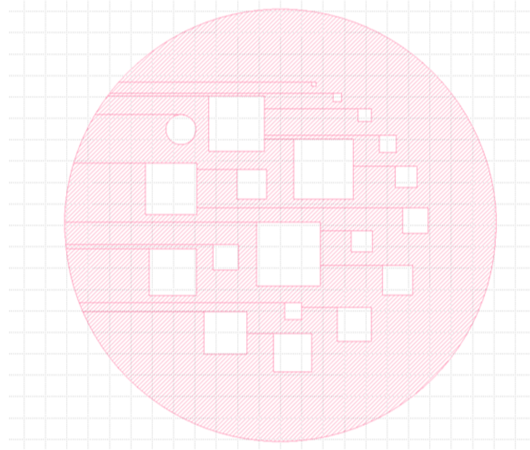

Figure 5.2: Design of the test membrane.

5.1.3 RIE

To create windows for the backside etching of silicon, the RIE technique was utilized to pattern the backside of the SiN layer. The Sentech F2 equipment was employed for the RIE process. After 35 minutes of RIE, the etching of the SiN layer was successfully accomplished, and the process was stopped to prevent overetching. The visual representation of this outcome can be found in figure 5.3.

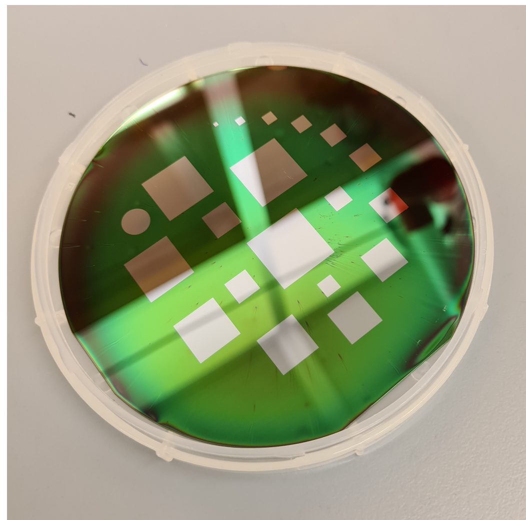

Figure 5.3: RIE result.

5.1.4 KOH wet etching

After the backside SiN was patterned, the final step of the membrane test fabrication is the removal of the bulk silicon through the opened windows by wet etching. This is done by putting the processed wafer in a KOH solution (40% by weight at $80°C$). The wafer has a thickness of approximately 525 um and the etch rate of KOH (40%) is between 0.6-1 μm/min at a temperature of $80°C$. The bulk silicon will be wet etched up to the SiN etch-stop layer to provide the release of the suspended membrane.

After a wet etching period of approximately 9 hours, when all the silicon had been removed and the transparent layers around the cavity could be seen, the wafer was carefully removed from the KOH vessel and placed into a beaker containing DI water. Afterwards the wafer was submerged in a beaker of H_20/HCL (4:1) solution for a period of 5 minutes. This solution was used for stopping the KOH reaction. After this, the wafer was again put in a beaker with DI water for two more times. Due to the presence of the membranes on the wafer, it was not possible to dry it using either the nitrogen gun or

spin dryer. An appropriate solution was to rinse the wafer in acetone and IPA, and subsequently placed on a sheet of paper to air dry. The results of the wafer after the KOH wet etching process can be seen in figure 5.4 and figure 5.5.

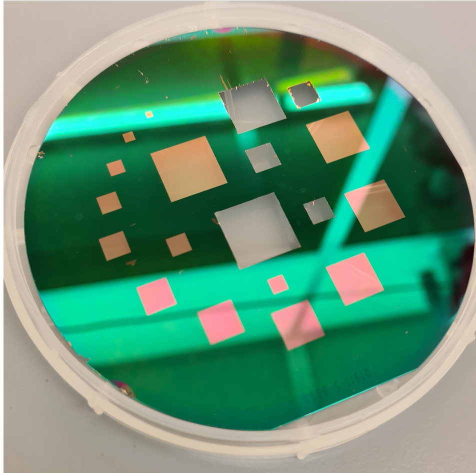

Figure 5.4: Top-side view of wafer with SiN/AlN/SiN membranes.

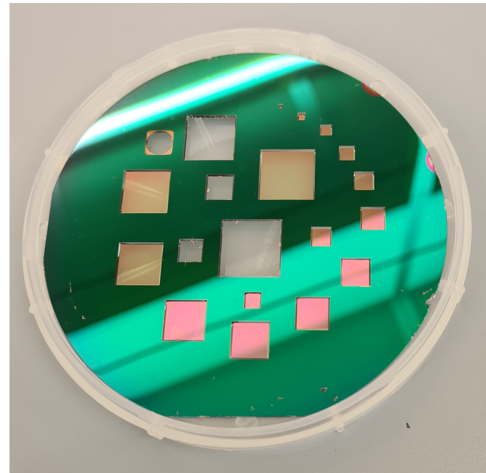

Figure 5.5: Back-side view of wafer with SiN/AlN/SiN membranes.

The aim of this test fabrication was to determine the membrane dimension that is suited for liquid sensing for this thesis project. Multiple membrane dimensions were designed starting from **1** $\times$ **1 mm^2** to **15** $\times$ **15 mm^2**. From the results it can be seen that even the bigger membranes were able to withstand the wet etching process. However, after careful observation, it appears that only the LPCVD SiN (green color) remained unaffected after the completion of the KOH wet etching process, while the other layers, namely the 300 nm PECVD SiN and 1 um AlN, were completely removed. This clearly indicates that the PECVD SiN layer failed to provide long-term protection to the top layer of the device. The reason behind this is the poor quality of the PECVD SiN, which made it susceptible to easy etching during the KOH wet etching process. A potential solution to rectify this issue will be discussed in the following section.

To assess the quality of the membrane, which consists of a 500 nm LPCVD SiN layer, a liquid drop test was conducted on the remaining membranes. The purpose of this test was to determine if the membranes could withstand the impact of liquid droplets. Using a pipette filled with DI water, multiple drops were placed on each membrane. Surprisingly, all the remaining membranes proved to be capable of tolerating these liquid drops, indicating their suitability for the project.

Based on these findings, it can be confirmed that the LPCVD SiN with a thickness of 500 nm possesses the necessary stability to endure multiple liquid drops, even when utilized on a membrane with a dimension of **14** $\times$ **14 mm^2**. The reason for the breakage of the other membranes located in the center of the wafer remains uncertain. Therefore, it is advisable to opt for a membrane dimension design of up to **12** $\times$ **12 mm^2** when designing and fabricating Lamb wave devices with membranes made of 500 nm LPCVD SiN.

However, it is important to consider the mass loading effect caused by the presence of the IDTs, as it can lead to the breakage of larger membranes. Therefore, it is recommended to select an appropriate membrane dimension that is compatible with the designed IDT structure. Additionally, it should be noted that the actual size of the membrane will be smaller than its designed dimensions as a result of anisotropic etching. More information about this matter can be found in chapter 3.3.2.

5.2 Final device fabrication process

The completion of the membrane dimension test fabrication allows for the selection of the appropriate membrane dimension. The test results indicate that a membrane dimension of **4** $\times$ **4 mm^2** is not only suitable for the IDT design but also meets the required standards.

Following the selection of the membrane dimension for the Lamb wave device, the final fabrication of the Lamb wave device can begin. The flowchart of the final Lamb wave device fabrication can be found at appendix A.

The key processing steps of the chosen strategy are shown in the figures below and are as follows:

- **Step 1:** A 4" (100) p-type, double side polished Si wafer with 500 μm of thickness was chosen as the substrate. Afterwards, the wafer was cleaned with HNO_3 99% and 69.5%.
- **Step 2:** 500 nm of LPCVD SiN was deposited on the wafer.
- **Step 3:** Deposition of 1 μm thick c-axis oriented AlN through sputtering to function as the piezoelectric layer. This was done with the Trikon Sigma 204 equipment.
- **Step 4-8:** illustrates the lift-off process to create the IDTs. The IDTs consist of 10 nm of Cr and 90 nm of Au that were deposited through evaporation.
- **Step 9:** A 500 nm of PECVD SiN was deposited on top of the AlN layer and the IDTs. The purpose of this layer is to protect the IDTs and also the AlN layer against the KOH wet etching that will be performed later on.
- **Step 10-11:** Making the SiN mask patterns on the backside of the samples. With the chosen IDT design, a membrane with a dimension of **4** $\times$ **4 mm^2** was preferred. To get a membrane of this dimension, the membrane mask opening has to be **4**.**740** $\times$ **4**.**740 mm^2** according to equation 3.2 due to the anisotropic etching process of the KOH wet etching. Furthermore, as the laserwriter does not have the double side alignment possibility, it has to be made sure manually that the backside patterns are well aligned with the front side patterns. Especially the membrane should be in the center of the IDT structure.
- **Step 12-13:** The SiN is dry etched with the RIE equipment(Sentech F2) and the patterned SiN mask openings are made. Afterwards, the photo-resist is removed with acetone and rinsed with IPA.
- **Step 14:** The wafer is coated with a protective layer (AR-PC 5040) to prevent any leakage of KOH on the front side. The combination of PECVD SiN and AR-PC 5040 provides a double layer of protection.
- **Step 15:** The bulk silicon layer is then removed through the SiN windows with KOH (40% by weight and @80°C) and the SiN/AlN/SiN membrane will be released.
- **Step 16:** Upon the completion of the wet etching process, the AR-PC 5040 used for KOH protection can be removed using acetone.
- **Step 17:** In order to establish connections with the contact pads, it is necessary to remove the 500 nm of PECVD SiN layer that is currently covering the IDTs. This is done through dry etching with the RIE equipment (Sentech F2).

1. (100) p-type, double side polished silicon wafer with 500 μm thickness was prepared.

2. Deposition of 500 nm LPCVD SiN (E2 Nitride).

3. Deposition of 1 μm AlN on the front (Trikon Sigma 204).

4. Coating with photo-resist.

5. IDT patterning with laserwriter.

6. 10 nm Cr deposition (evaporation).

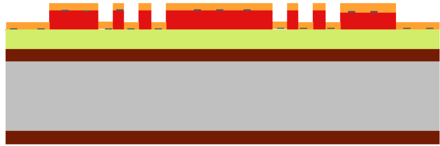

7. 90 nm Au deposition (evaporation).

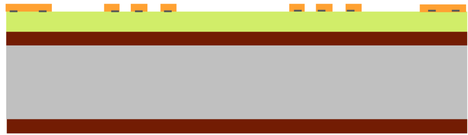

8. Lift-off process.

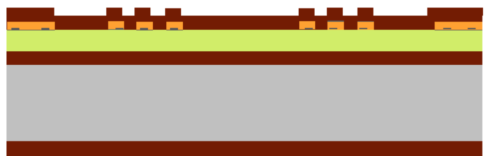

9. 500 nm PECVD SiN deposition.

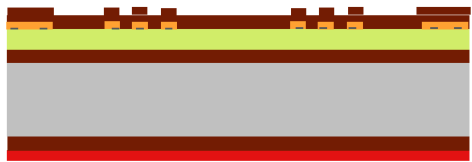

10. Coating backside with photo-resist.

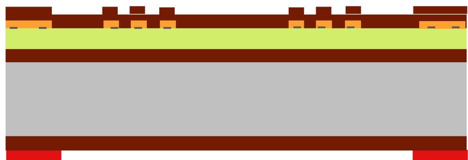

11. Window patterning.

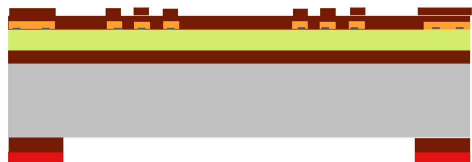

12. Dry etching of SiN (RIE).

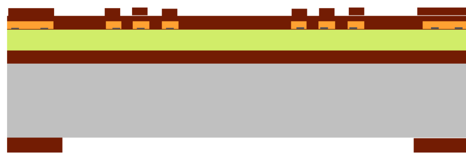

13. Layer stripping: photo-resist.

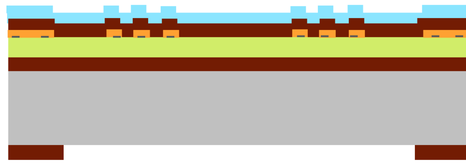

14. Add KOH protective coating on the front side (AR-PC 5040).

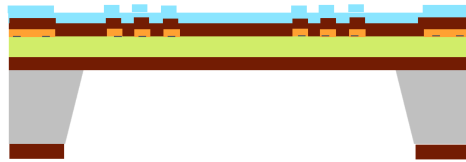

15. Si wet etching with KOH (40% by weight @80°C).

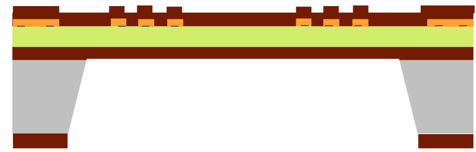

16. Layer stripping: KOH protective coating.

17. Dry etching of SiN (RIE).

5.2.1 Fabrication Result

The total stress of the deposited layers on the wafer is measured to be 300 MPa (tensile stress), which deemed to be appropriate for the fabrication of the Lamb wave devices. Figure 5.6 and figure 5.7 illustrate the results achieved following the completion of the wet etching process for the two designs. The main fabrication outcomes and any failures encountered during the process are documented in appendix B. Fortunately, all of the devices successfully withstood the wet etching process and are now ready for further utilization. Due to the appropriate backside design, the wafers could be easily cleaved into the Lamb wave devices. The subsequent step involves removing the protection layers from the devices to facilitate wirebonding of the contact pads. The final results of some of the fabricated Lamb wave devices are presented in figure 5.8 and figure 5.9.

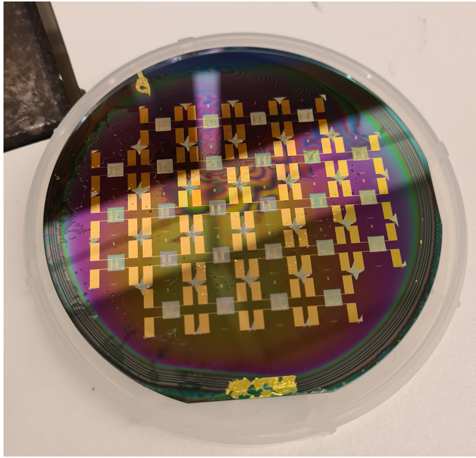

Figure 5.6: After the completion of KOH wet etching process Design 1.

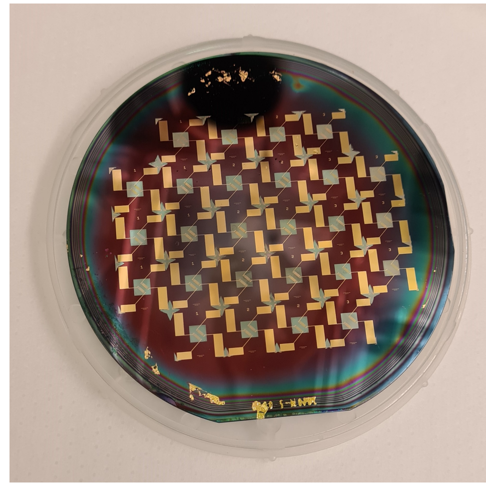

Figure 5.7: After the completion of KOH wet etching process Design 2).

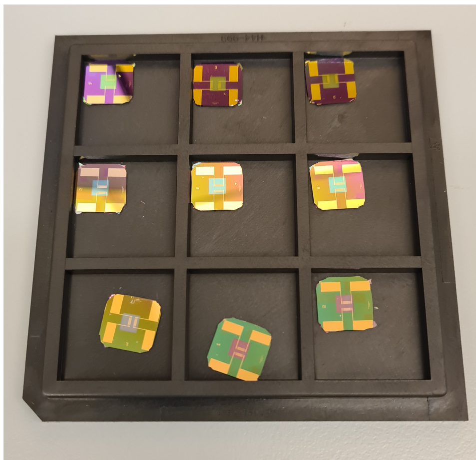

Figure 5.8: Lamb wave device - Design 1.

Figure 5.9: Lamb wave device - Design 2.

5.3 Problems encountered during fabrication process

The challenges encountered during the fabrication of the Lamb wave devices and the chosen solution are discussed in this section.

5.3.1 Finding suitable resist and developer for AlN layer

A lift-off process requires a suitable resist to perform lift-off without any issues. A negative resist is usually preferred for this process. The layer on which the IDTS structure will be placed is AlN. This makes it difficult to use the available resist in the laboratory. This is due to the fact that the developers used to develop the resist contain TMAH (Tetramethylammonium Hydroxide), which is an etchant chemical. This chemical etches Al and will thus also etch the AlN layer. This was observed while performing an exposure test on a chip that had an AlN layer on top. After the chip was put in a developer for a minute, the whole exposed AlN was removed. Therefore, another resist had to be found that had could be developed by a developer that does not contain the TMAH chemical. The resist should also be suitable for lifting off processes. The resist that meets all these criteria is AR-P 5350, a positive resist specially designed for lifting-off due to its undercut structure as seen in figure 5.10. This resist should be developed using a solution of developer AR 300-35 and water (DI) (1:2) [36].

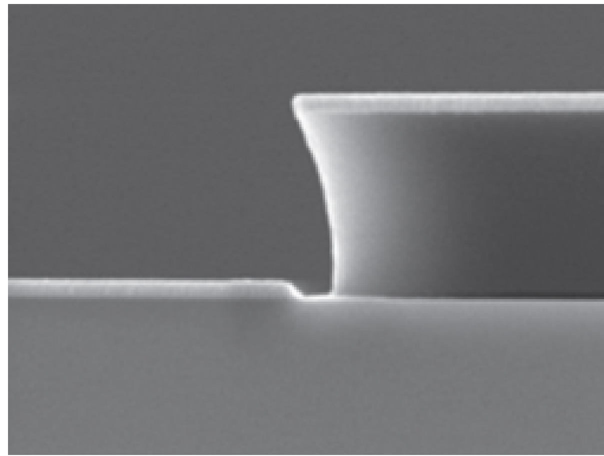

Figure 5.10: AR-P 5350 Lift-off resist structure after metal evaporation [36].

5.3.2 KOH wet etching

The initial plan was to dice the wafer to ensure perfect alignment of the patterned front and back sides, followed by the wet etching process. However, it became evident during the wet etching process that the PECVD SiN was not capable of enduring the KOH solution for a long period of time. To achieve deep wet etching of the silicon, it was crucial to utilize a high-quality SiN film, such as LPCVD SiN. A low-quality SiN film is less dense and can easily be removed by the KOH, which is what happened in this project. Therefore, a different approach for the fabrication of the Lamb wave device was needed.

Different strategies that were considered to address this issue, were:

1. Increasing the thickness of PECVD SiN, so that it takes longer for the KOH to remove this SiN layer and get to AlN layer.
2. Use alternative protective coating against KOH such as AR-PC 5040 on the diced samples. The problem with this coating was that the protective coating layer was stripped away after some hours of etching.
3. Deposit LPCVD SiN instead of PECVD since the gold electrodes can withstand the deposition temperature of $850°$ C. The quality of LPCVD is higher than that of PECVD and will therefore be able to withstand KOH etching for a longer time than PECVD. Unfortunately, because of the gold IDT structures, the deposition of LPCVD SiN was not allowed due to the risk of contamination of the equipment. Therefore, this option was not considered.
4. A combination of DRIE and Wet etching. Remove 400-450 um of Si layer with DRIE etching and afterwards the remaining Si layer will be removed with the KOH wet etching process. This will reduce the wet etch time and membranes can be released before the KOH will be able to reach the AlN layer through the protection layer.
5. Use the dedicated 4” KOH etching chuck to protect the front side of the devices. As the KN only has a 4” KOH etching chuck, this method cannot be used for diced samples. Additionally, after the KOH process is completed, the wafer cannot be diced due to the presence of the membranes. The vacuum pressure and the water rinsing during the dicing of the wafer with the disco dicer equipment will certainly break all the membranes on the wafer. The issue of not using the dicer can be solved by designing the posterior mask in such a way that the wafers can be broken into smaller squared samples after the wet etching process is completed. Furthermore, the laserwriter does not have a double alignment option and thus the alignment has to be done manually. For this, it is better to have a symmetric design for both sides during the fabrication process, to ensure good alignment of the designs.

   After testing the 4” holder setup with a dummy AlN wafer, it seemed that after some hours of wet etching, the KOH had reached the protected side of the wafer and etched the AlN layer away. The reason of this was unknown. In order to still use the 4” holder, the addition of a protection layer would be ideal. A protection layer is mandatory, to prevent KOH from penetrating a broken

membrane and destroying the other devices. For this, a different PECVD SiN recipe will be tried to obtain a better quality SiN layer. In addition, a KOH protective coating will be applied. In the past, this coating was stripped away after some hours of etching during the wet etching of the diced samples. However, this time, the O-ring of the 4” holder will ensure that the coating does not come off. After the wet etching process is completed, the protective layers can be removed. This approach proved to be the most effective for the project, as it guaranteed the successful fabrication of the Lamb wave devices.

Chapter 6

Experimental setup

6.1 Fabricated Lamb wave devices

Table 6.1 gives an overview of the fabricated Lamb wave devices that will be used for the experiments is placed below. Further details regarding the design parameters of these devices can be obtained from table 3.4.

Table 6.1: Overview of the fabricated Lamb wave devices.

D1: Delay line length = 750 um	Device 1 - NORMAL design
	Device 1 - ROTATED design
D2: Delay line length = 1000 um	Device 2 - NORMAL design
	Device 2 - ROTATED design
D3: Delay line length = 1500 um	Device 3 - NORMAL design
	Device 3 - ROTATED design

6.2 PCB design

The fabricated Lamb wave devices can be mounted on a printed circuit board (PCB) for ease of connection to the measuring equipment and portability. The design of the PCB was created with the Altium designer. The front- and back-side of the final design can be seen in figure 6.1 and figure 6.2, respectively.

Holes were made on the designed PCB with a diameter of 5 mm and the fabricated devices will be attached to it. This will expose the backside of the membrane to the environment. The liquid that will be used for testing can easily be put on the backside of the devices through the holes.

On the PCB, there will be two devices attached: one with the normal IDT design and one with the rotated IDT design. This will make it easier to compare the results of the two IDT designs. The contact pads of the devices will be wire-bonded to the dedicated pads on the PCB to make the connections. Furthermore, SMA connectors were used to connect the PCBs to the measurement equipment. Figure 6.3 shows the overview of the Lamb wave devices attached on a PCB and ready for measurements.

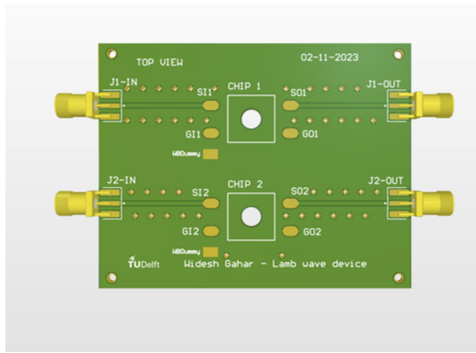

Figure 6.1: Top-side view of the PCB design.

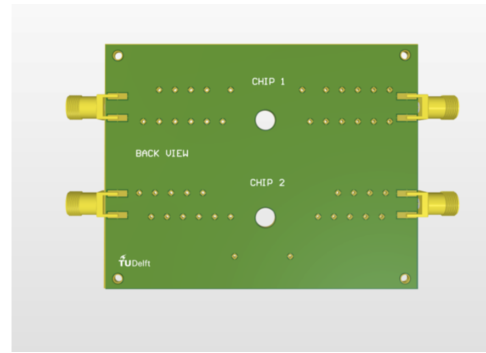

Figure 6.2: Back-side view of the PCB design.

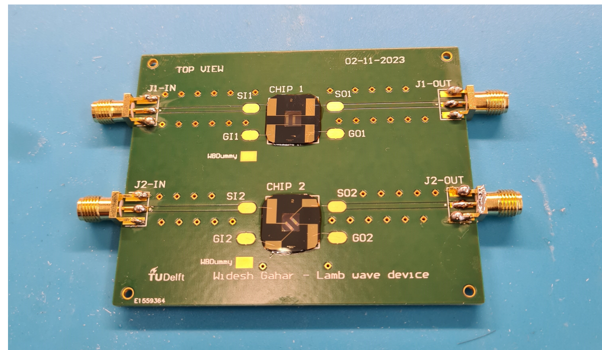

Figure 6.3: Lamb wave devices attached and wirebonded on a PCB with the SMA connectors.

6.3 Vector Network Analyzer

After the wirebonding and soldering of the components are completed, the measurement will be performed with a Nano Vector Network Analyzer. The NanoVNA-H is a portable vector network analyzer that operates in the frequency range of 10 kHz to 1.5 GHz. It is specifically designed to measure the reflection and transmission coefficients without requiring a large analyzer. Equipped with a 2.8” touchscreen, it can display measurements at 101 different points. Additionally, the NanoVNA-H comes with a built-in 650 mAh battery and can be effortlessly connected to an android phone or PC using a USB-C connection, enabling efficient data transfer and analysis [37]. The input-output relationships between ports in an electrical system are described by scattering (S) parameters. A Vector Network Analyzer can measure the following S parameters:

- $\mathbf{S_{11}}$ is the reflection coefficient of the input port voltage.
- $\mathbf{S_{12}}$ is the gain of the reverse voltage.
- $\mathbf{S_{21}}$ is the gain of the forward voltage.
- $\mathbf{S_{22}}$ is the reflection coefficient of the output port voltage [38].

Before starting with the measurements, a calibration of the VNA is needed. This is necessary due to the presence of numerous non-linearities within the VNA itself. Additionally, the measurements also depend on the location of the placed DUT (Device Under Test). The frequency range for the measurement has to be chosen according to the DUT and the calibration will be done for that frequency range. Once the calibration of the equipment is completed, the PCB containing the attached devices will be connected to the NanoVNA-H, and the resulting data will be saved on the computer. The measurement setup can be seen in figure 6.4.

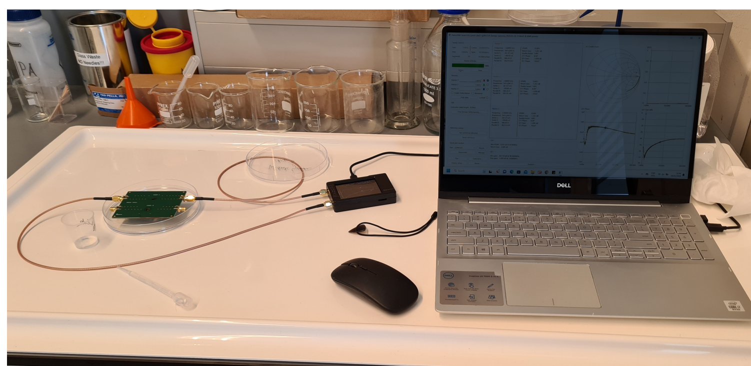

Figure 6.4: Measurement setup for the liquid tests.

As previously stated, every design will consist of three devices, each equipped with delay line lengths that vary among the three. The initial test will be conducted without any load on the sensing area (dry test) and the S21 data will be recorded. Following the dry test, the liquid test can be performed by introducing the liquid through dedicated holes on the backside of the PCBs. This ensures direct placement of the liquid on the membrane while safeguarding the other side of the devices.

6.4 Liquid tests

The intention was to employ a wide range of liquids in order to conduct comprehensive liquid sensing tests. However, the fabricated Lamb wave devices can only be re-used when there are no residues left on the sensing area to get more accurate and reliable results. Therefore, it is crucial to choose a liquid that does not leave many traces behind after it is dried. Another constraint is that the devices are attached to the PCB using photo-resist as a form of adhesive. The reason for selecting this method is the ease of replacing the devices in case their membrane breaks. This can be accomplished by removing the photo-resist using acetone. Consequently, liquids that possess the capability to effortlessly remove photo-resist will be avoided during the testing process.

The liquids that are available in the EWI measurement room and will be used for the liquid testing experiments are: **IPA (Isopropyl alcohol)**, **DI water** and **D-PBS (Dulbecco's Phosphate-Buffered Saline)**. This experiment will involve placing a volume of **40 µL** of the selected liquids on the sensing area of the device. D-PBS is a salt water solution, which means that it may leave behind residues such as sodium and chloride ions when the water evaporates. To ensure accurate results, the D-PBS liquid test will be conducted only after all the other liquid tests have been completed. Furthermore, to eliminate the residues on the sensing area from the D-PBS liquid testing experiment, the cavity will be carefully rinsed with DI water drops for at least three times. The densities of the selected liquids are: **IPA (786 kg/m^3)**, **DI water (1000 kg/m^3)** and **D-PBS (1,190 kg/m^3)**. The S21 data obtained from each experiment will be recorded and subsequently analyzed using MATLAB.

Chapter 7

(Experimental) Results and Discussions

7.1 VNA measurements

A frequency range of 10 kHz - 100 MHz was entered in the nano-VNA for the Lamb wave devices, as it is anticipated that the resonant frequency of the A0 mode will fall within this range. The initial step involves measuring the S21 parameters of the devices, without applying any load to the sensing area. Due to the use of separate wafers for each design, devices with the same design exhibited an identical resonant frequency. The results presented below indicate that the resonant frequency of the devices with the normal design is 52 MHz, while the resonant frequency of the rotated design is 60 MHz.

The resonant frequencies of the devices deviate from the resonant frequency of 63 MHz, which was determined using COMSOL and calculations. This difference in resonant frequency can be due to a failure to achieve the desired thicknesses for the deposited layers. The condition of the equipment plays a crucial role in determining the deposition rate of the materials, which consequently can affect the ability to achieve the desired thickness. Due to this, the actual thicknesses of the deposited layers may either surpass or fall below the intended thicknesses.

A decrease in the resonant frequency suggests that the thickness of the membrane may be less than the intended $1.5\ \mu m$. This is indeed the case as the deposited AlN layer was lower than the desired thickness of 1000 nm. The wafer containing the devices with the normal IDT design had an AlN layer of 900 nm, while the wafer that had the devices with the rotated IDT design had an AlN layer of 980 nm. The results of the measured thicknesses and stress of each layer can be found in appendix D. With a thinner membrane, the resonant frequency decreases and the mass sensitivity of the device will increase, as indicated in equation 2.14. Although the issue of not achieving the desired thicknesses can be disregarded, it is advisable to conduct experiments in the future to determine the actual deposition rates and adjust the recipes accordingly. This will help achieve thicknesses that closely match with the desired values, ensuring reliable results.

7.1.1 Liquid test

Once the results of the dry test were obtained, the liquid test could commence. Droplets of $40\ \mu L$ of the selected liquids were placed on the sensing area one by one with a micropipette and the results were measured. The liquid test was conducted thrice for each liquid, and the resulting average was determined. Unfortunately, the D-PBS test could not be carried out on Device 1 with the rotated design due to a broken membrane. Nevertheless, the data obtained from the other devices can be utilized to derive a conclusion. The phase and gain plots achieved from the S21 parameter measurements are presented in the figures below. Differences in frequency, phase and gain are observed across different liquids, implying that the produced devices exhibit sensitivity towards mass loading and can differentiate between various liquid substances. Furthermore, the length of the delay line does not significantly impact the outcome. These observations remain valid even for devices with the rotated design.

S21 Gain comparisons

- Normal IDT design

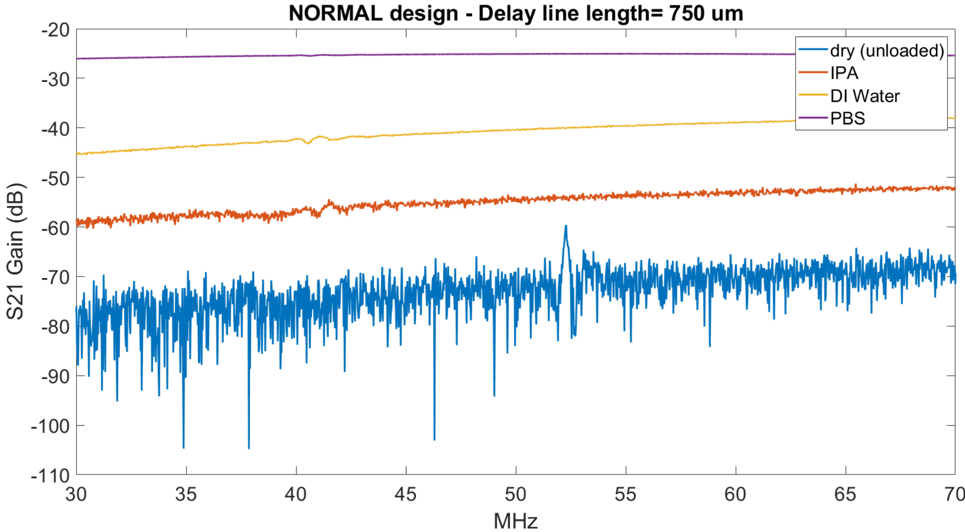

Figure 7.1: Device 1 Gain comparison - NORMAL design.

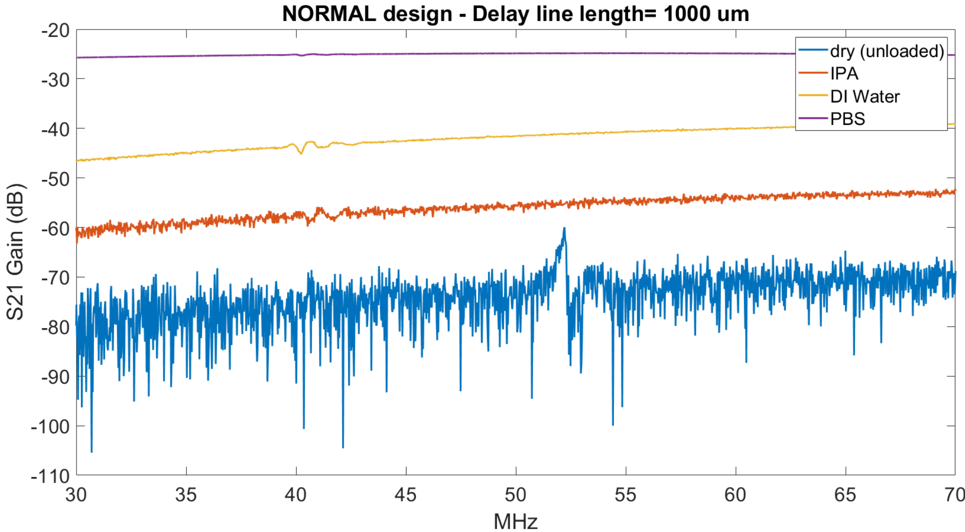

Figure 7.2: Device 2 Gain comparison - NORMAL design.

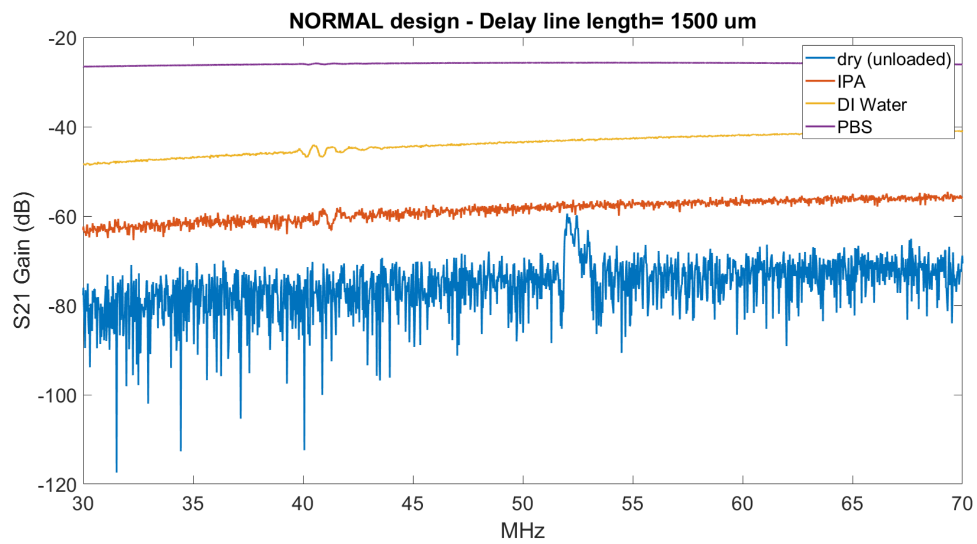

Figure 7.3: Device 3 Gain comparison - NORMAL design.

- Rotated IDT design

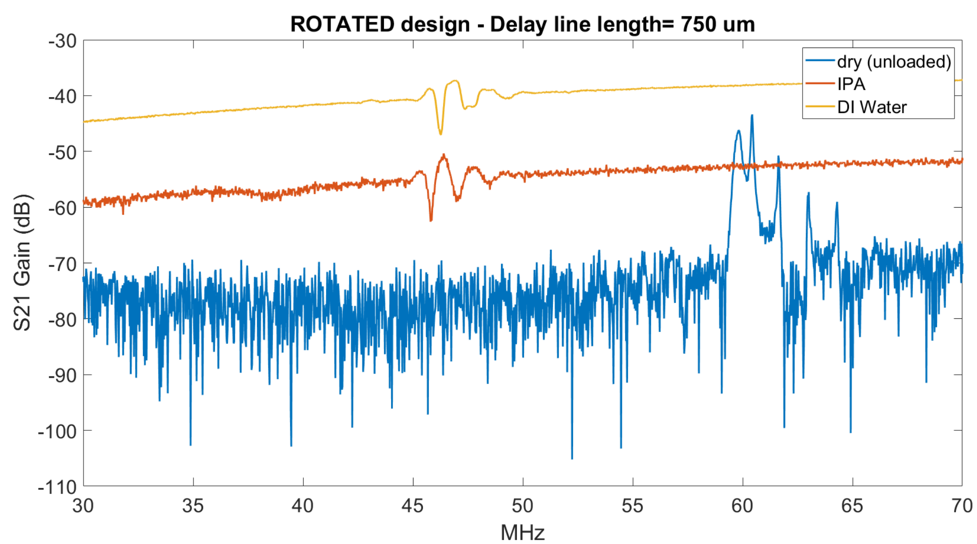

Figure 7.4: Device 1 Gain comparison - ROTATED design.

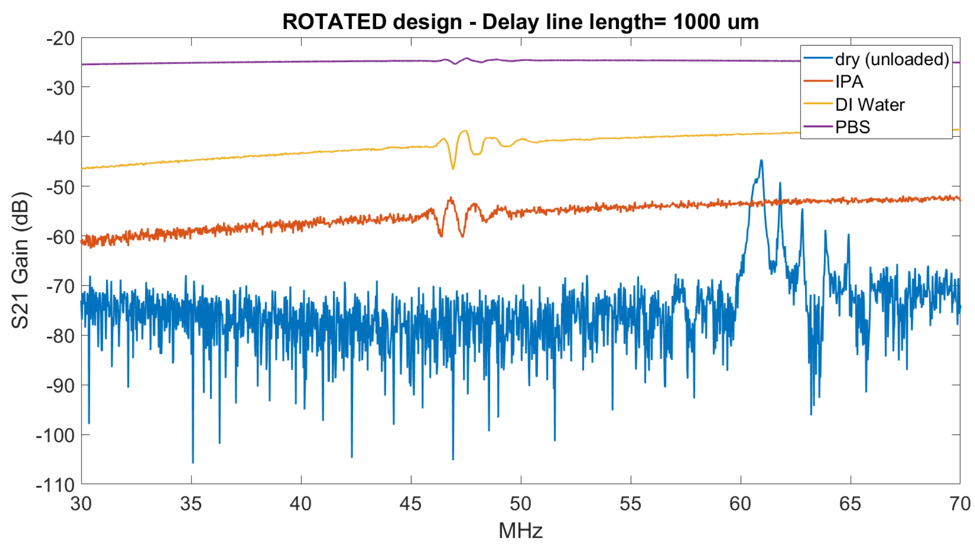

Figure 7.5: Device 2 Gain comparison - ROTATED design.

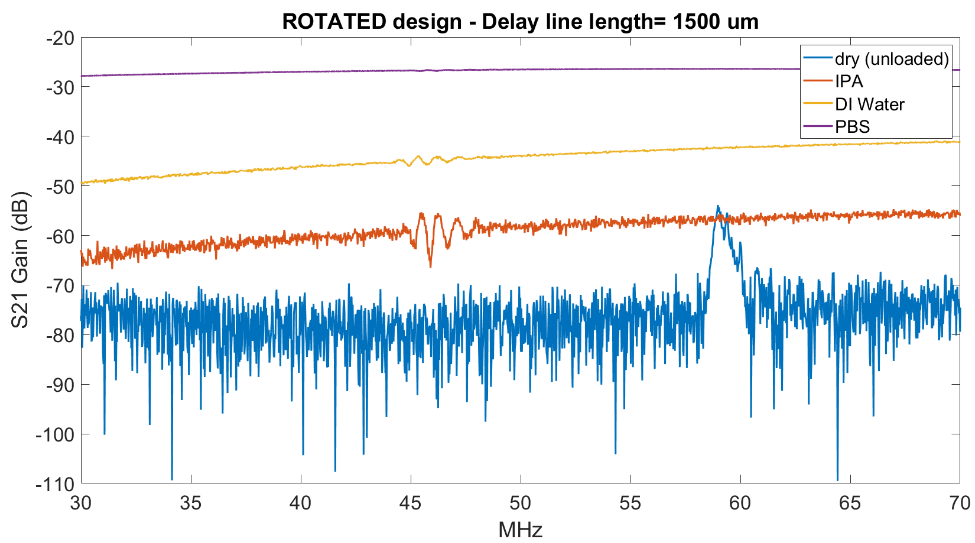

Figure 7.6: Device 3 Gain comparison - ROTATED design.

S21 Phase comparison

- NORMAL IDT design

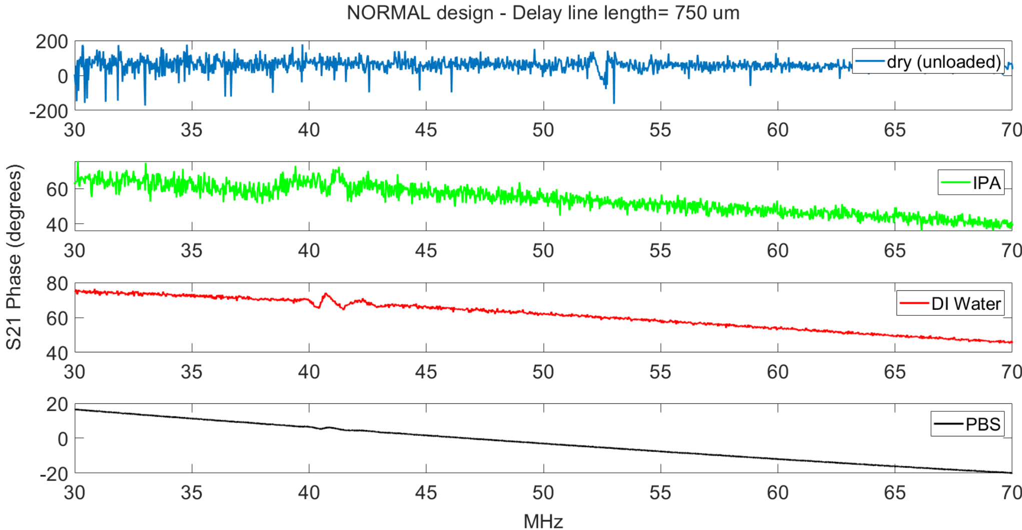

Figure 7.7: Device 1 Phase comparison - NORMAL design.

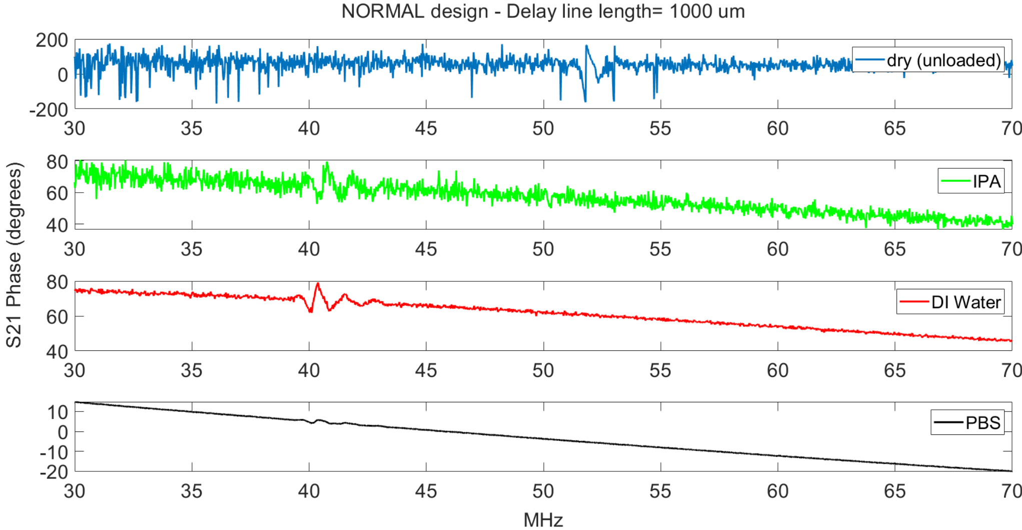

Figure 7.8: Device 2 Phase comparison - NORMAL design.

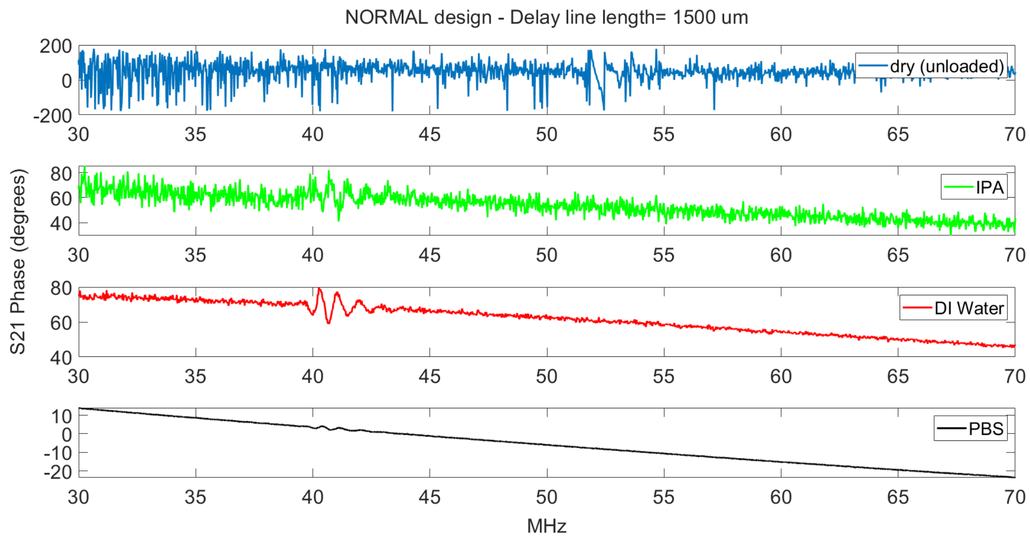

Figure 7.9: Device 3 Phase comparison - NORMAL design.

- Rotated IDT design

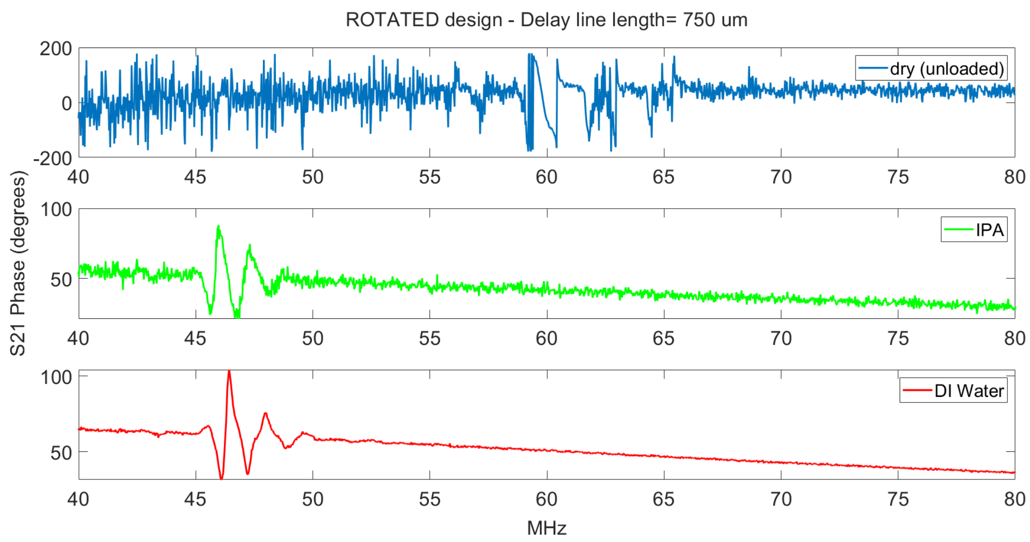

Figure 7.10: Device 1 Phase comparison - ROTATED design. The D-PBS liquid test could not be performed on Device 1 - rotated design as the membrane was broken.

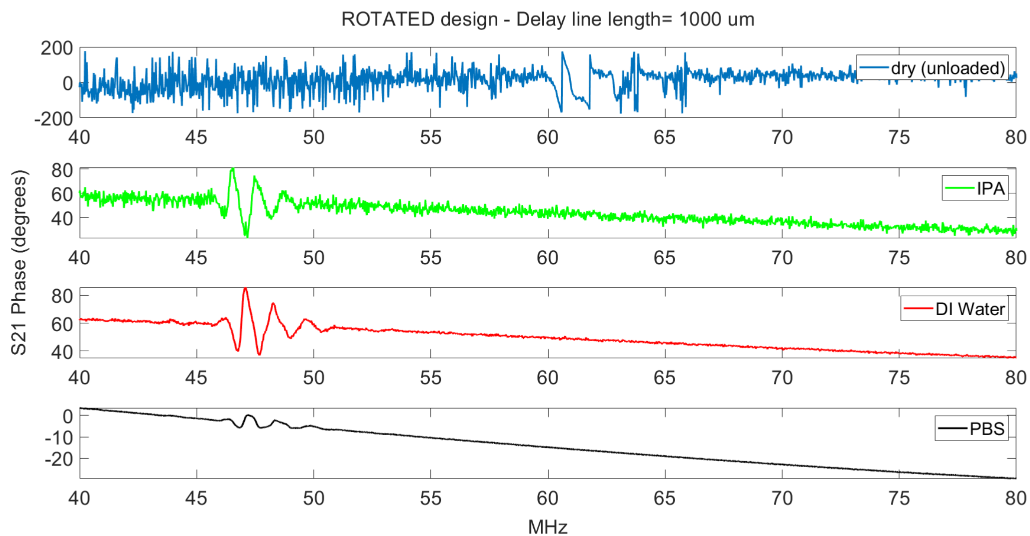

Figure 7.11: Device 2 Phase comparison - ROTATED design.

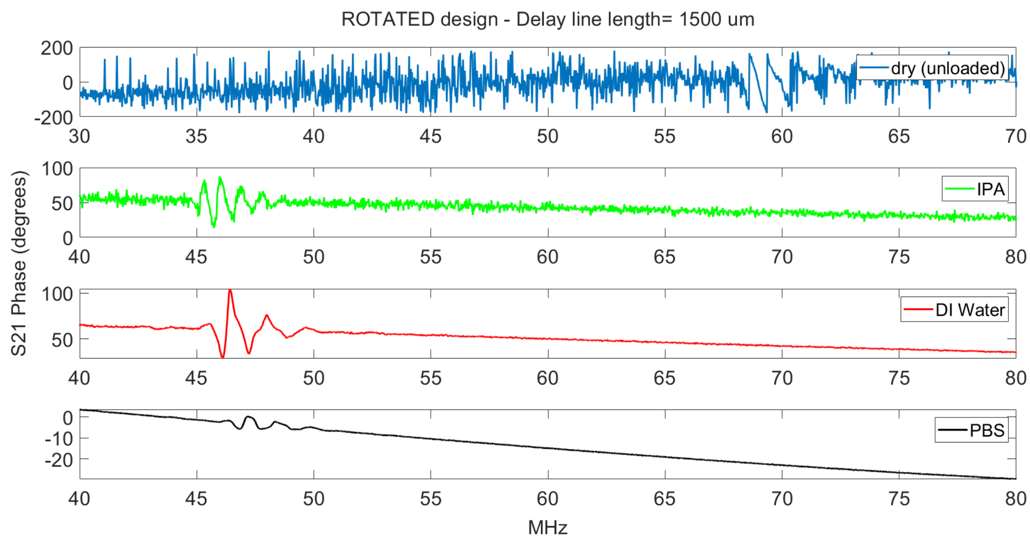

Figure 7.12: Device 3 Phase comparison - ROTATED design.

7.1.2 Phase shift vs density

The primary attention will be directed towards the phase shift rather than the frequency shift, as a noticeable change will be observed in the phase, whereas the frequency shift might not be apparent. The relationship between the phase shift and the density of the liquid for the devices with the normal and rotated design presented in figure 7.13 and figure 7.14, respectively.

The devices with the normal design exhibit an average phase shift of 80 degrees when IPA is applied to the sensing area. On the other hand, the devices with the rotated design show an average phase shift of 81 degrees under the same conditions. While there is a significant difference in density between IPA and DI water, the average phase shift between DI water and IPA is merely 2 degrees for the normal design devices, while it amounts to 13 degrees for the rotated design devices. Due to the faster evaporation rate of IPA in comparison to other liquids, the volume of IPA does not remain constant, thereby hindering accurate comparisons with the other liquids. Nonetheless, there are noticeable variations in the gain of IPA and DI water. Lastly, the average phase shift difference between D-PBS and DI water is 72 degrees for the normal design devices, whereas it is 92 degrees for the

rotated design devices. The rotated devices do show a better phase shift between the liquids, making this design the ideal choice for achieving superior performance and results.

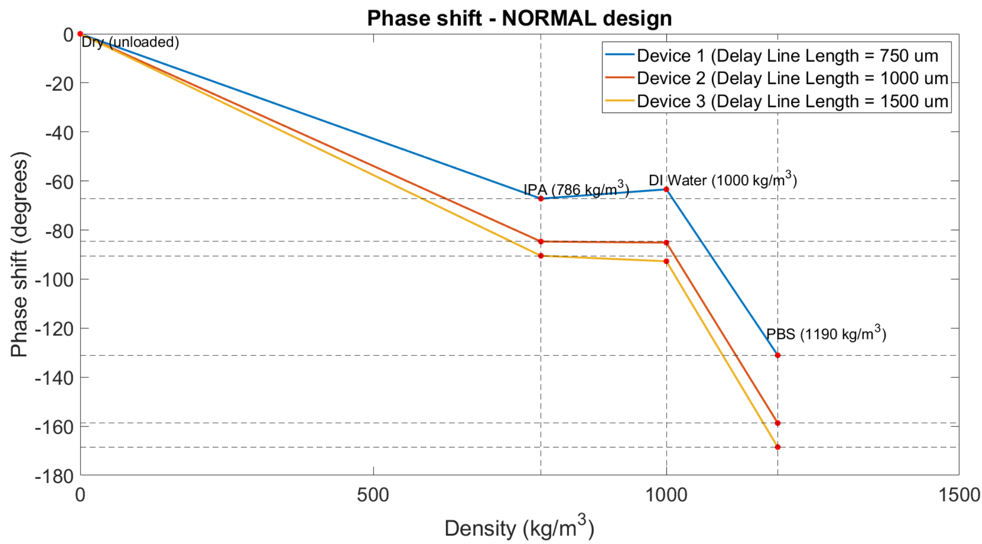

Figure 7.13: Phase shift vs liquid density of devices with NORMAL design.

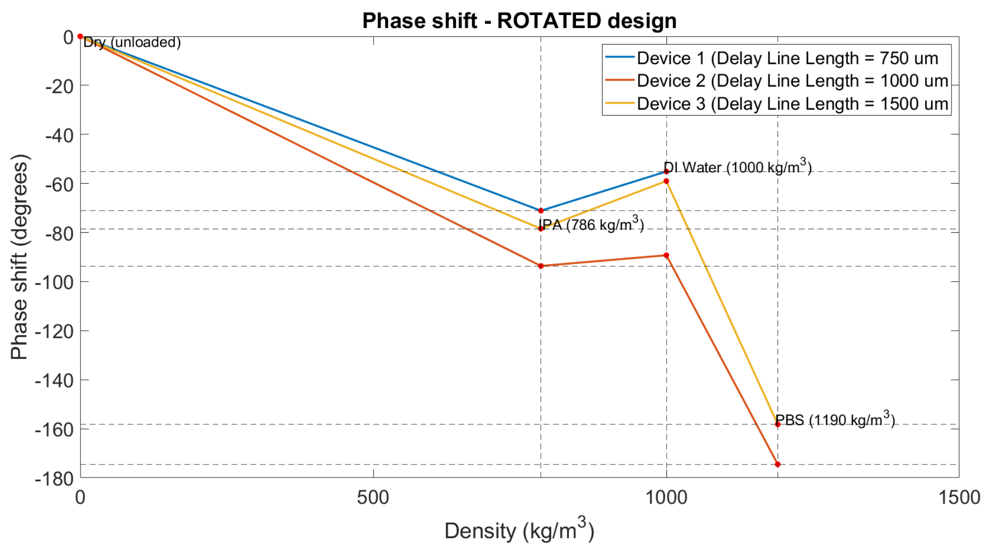

Figure 7.14: Phase shift vs liquid density of devices with ROTATED design.

7.1.3 Frequency shift vs density

Although the phase shift between IPA and DI water may not be substantial, there is an observable shift in frequency when switching between the two liquids. The graphs illustrating the relationship between frequency shift and density for both designs are provided below. Adding IPA to the sensing area results in an average frequency shift of 11 MHz for devices with the normal design, and an average frequency shift of 13 MHz for devices with the rotated design as seen in figure 7.15 and figure 7.16.

Additionally, figure 7.17 and figure 7.18 show the differences in frequency shift between the liquids only. Devices featuring the same design demonstrate consistent frequency shift behaviors. However,

there exists a conflicting shift between IPA and DI water for each design, which poses challenges in comprehending the relationship between density and frequency shift. The average frequency difference between IPA and DI water for the normal and rotated design devices is 430 kHz and 450 kHz, respectively. Furthermore, the average frequency difference between DI water and D-PBS is 90 kHz for normal design devices and 100 kHz for rotated design devices. Also here, the rotated devices do show a better shift between the liquids, indicating that they are more sensitive.

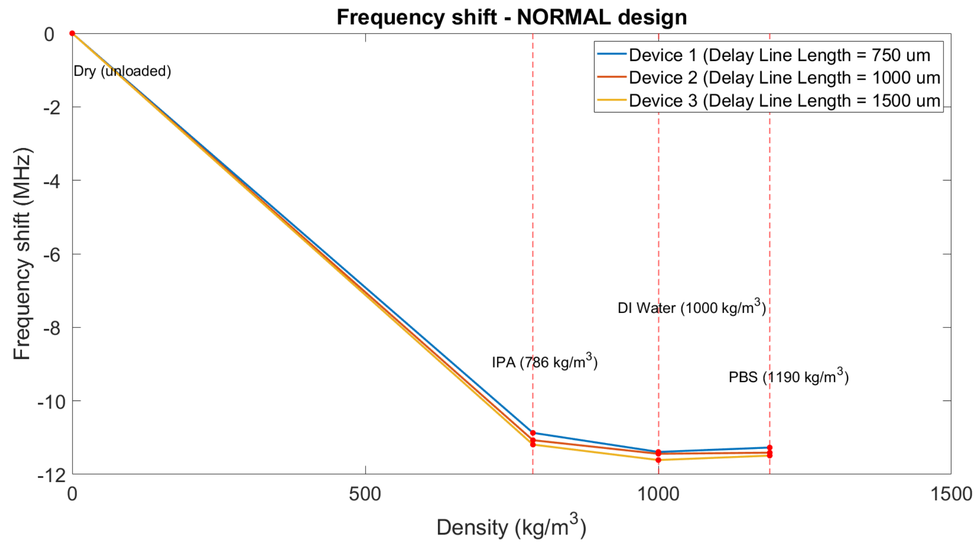

Figure 7.15: Frequency shift vs liquid density of devices with NORMAL design.

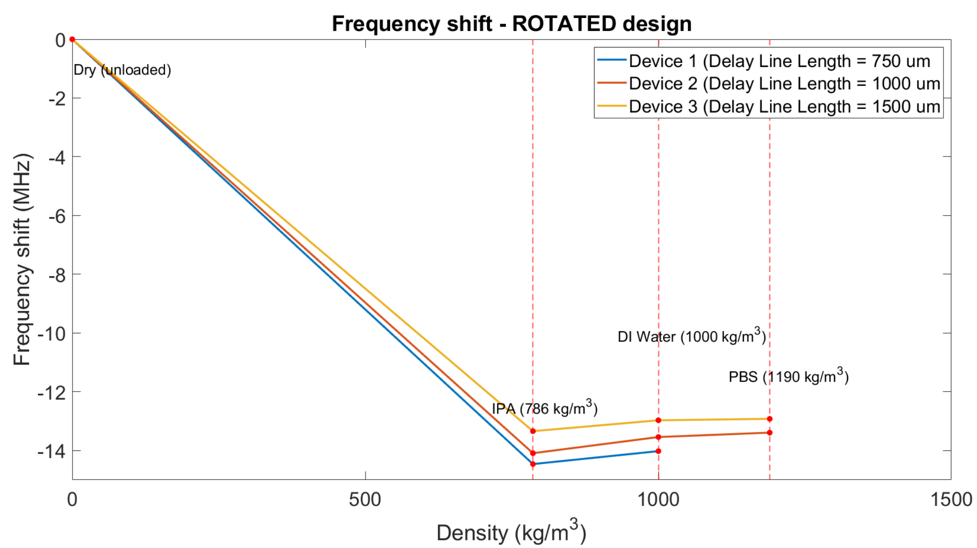

Figure 7.16: Frequency shift vs liquid density of devices with ROTATED design.

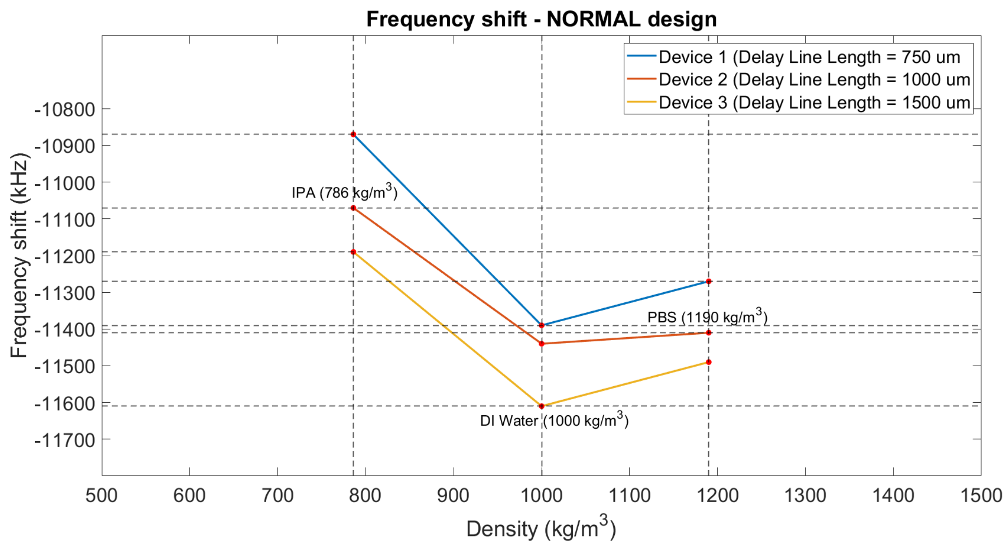

Figure 7.17: Frequency shift vs liquid density between liquids for devices with NORMAL design.

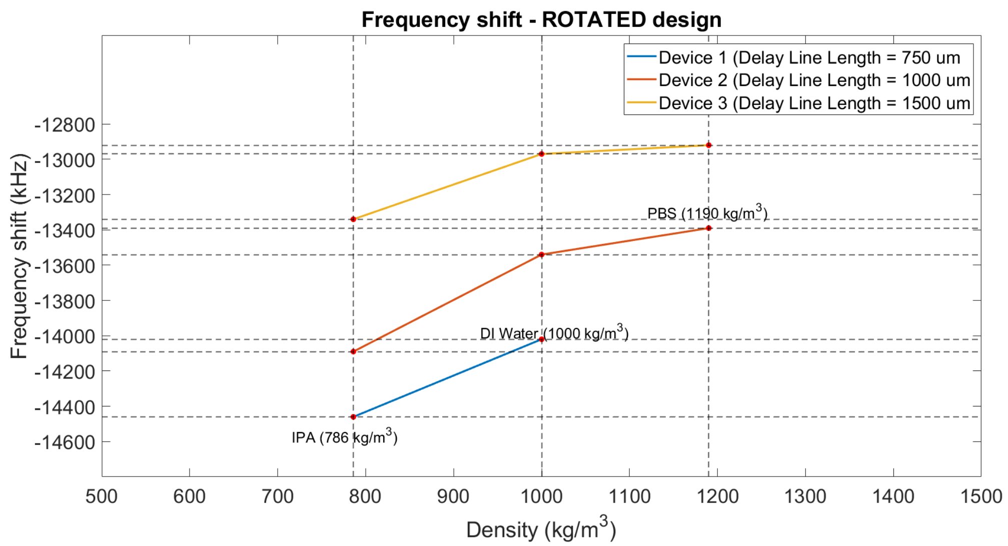

Figure 7.18: Frequency shift vs liquid density between liquids for devices with ROTATED design.

7.1.4 Impact of different liquid volume on the sensing area

The performance of the Lamb wave device was evaluated by investigating the consequences of adjusting the liquid volume on the sensing area. This was done by placing liquid drops of DI water and D-PBS, ranging from $20\ \mu L$ to $60\ \mu L$, on the sensing area. The majority of the outcomes, as illustrated in the figures below, indicate that the devices are sensitive to changes in liquid volume on the sensing area. While there was not a significant alteration in frequency, there was a noticeable change in the gain of the signal. The findings indicate that devices with a standard design are unaffected by variations in the volume of DI water, but are impacted by changes in the volume of D-PBS on the sensing area. On the other hand, devices with a rotated design are impacted by volume changes for both liquids on the sensing area. As a result, the rotated devices exhibit greater sensitivity to mass changes. Therefore, it is recommended to maintain a consistent liquid volume during testing for reliable comparisons, especially in biomedical applications.

DI water

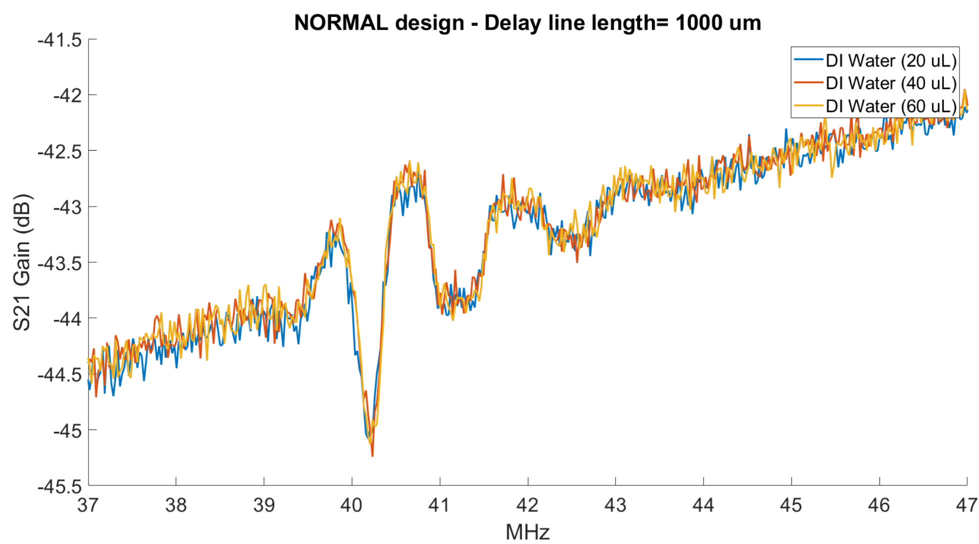

Figure 7.19: Gain of various volume levels of DI water - NORMAL design.

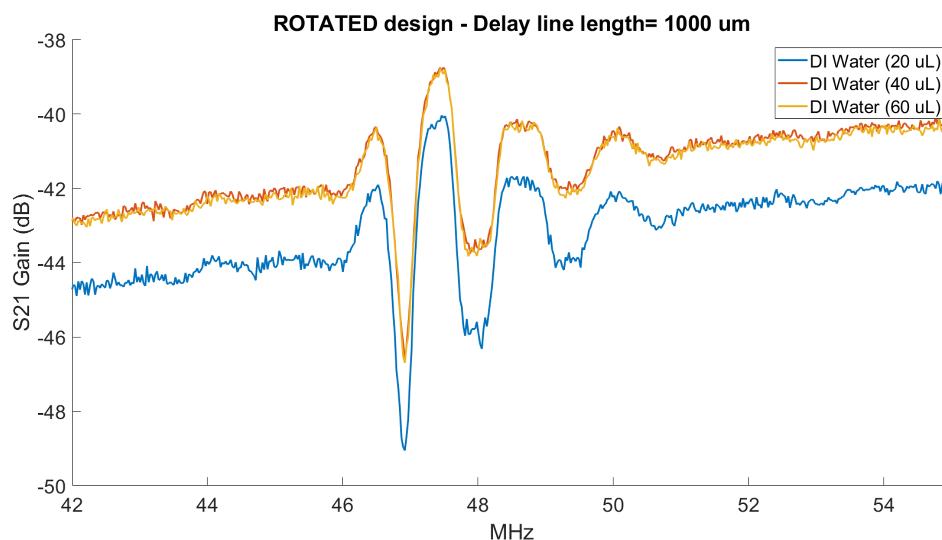

Figure 7.20: Gain of various volume levels of DI water - ROTATED design.

D-PBS

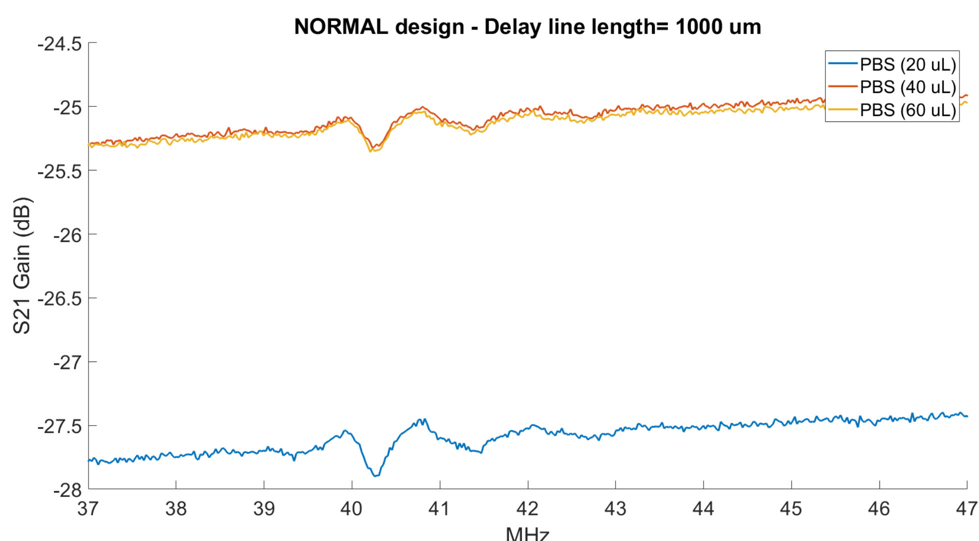

Figure 7.21: Gain of various volume levels of D-PBS - NORMAL design.

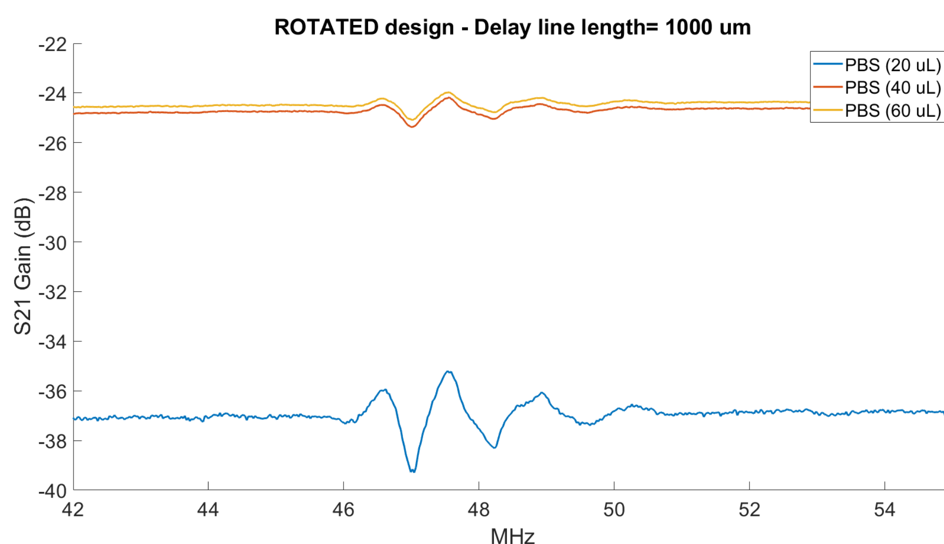

Figure 7.22: Gain of various volume levels of D-PBS - ROTATED design.

7.1.5 Evaluation of reproducibility

An evaluation of reproducibility was conducted on the fabricated devices to determine whether they can produce the same results after an experiment. First, the devices were measured without any liquid on the sensing area, referred to as Dry test 1. Afterwards, the liquid test experiment was carried out, followed by the drying of the devices. The measurements referred to as Dry Test 2 and Dry Test 3 were performed on the devices after the removal of the test liquid and allowing them to dry completely. It was crucial to ensure that the sensing area was completely dried for this experiment. It is possible for some residues to remain on the sensing area after a liquid test experiment, which could potentially alter the results. The results obtained from this experiment, as depicted in the figures below, indicate that the devices possess the capability to consistently produce the same results even after multiple tests. This is evident from the fact that their resonant frequency remained unchanged throughout several experiments, thereby confirming their reproducibility.

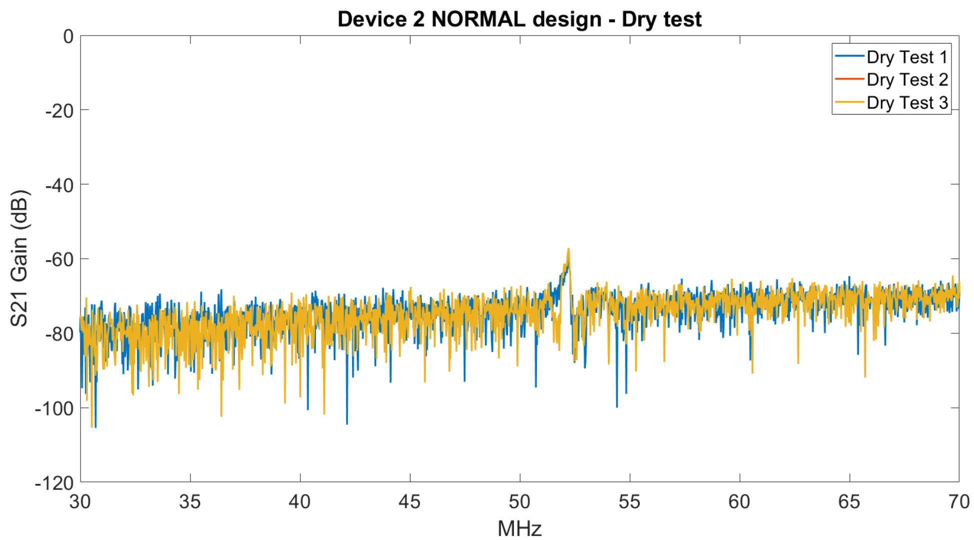

Figure 7.23: Repeating of dry test - NORMAL design.

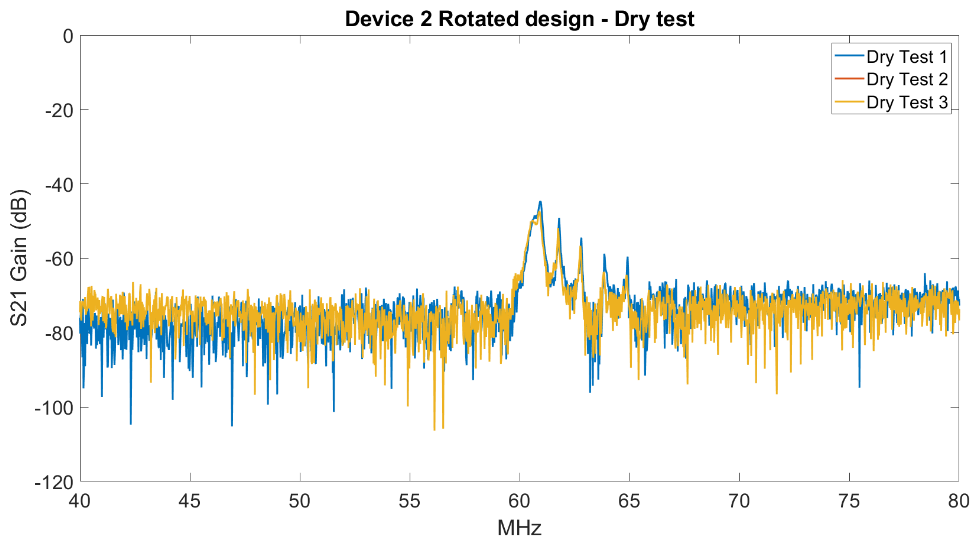

Figure 7.24: Repeating of dry test - ROTATED design.

7.1.6 Analyzing performance parameters for devices with Normal and Rotated designs.

The Q factor and the Insertion Loss parameters will be utilized to compare the performances of the normal and the rotated designs. The Q factor is commonly employed to assess the quality of an acoustic wave device, while the insertion loss quantifies the amount of signal loss during its propagation towards the output. These two factors will determine which of the devices demonstrate better performance.

Q factor

The Q factor is determined by employing equation 2.23. The devices with the normal design have an average Q factor of 450, while the devices with the rotated design have an average Q factor of 680. This indicates that the devices with the rotated design outperform those with the normal design.

Insertion Loss

The gain comparison between the normal and rotated IDT design for Device 2 is depicted in figure 7.25. A noticeable difference can be observed in the resonance of the device equipped with the rotated IDT design, which outperforms the device featuring the normal IDT design by 15 dB. This makes the devices with the rotated design more suitable for sensing applications as their insertion loss is less than the devices with the normal designs.

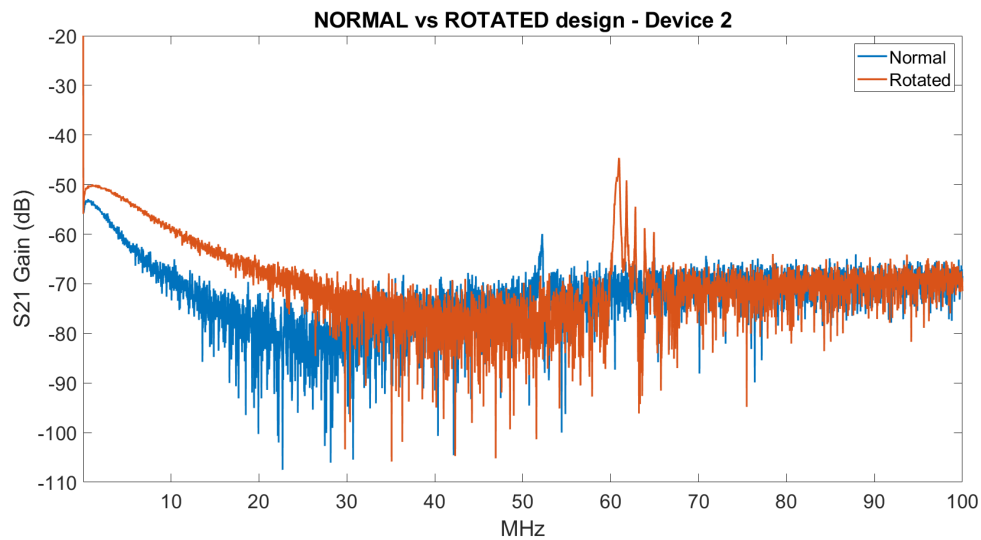

Figure 7.25: Gain comparison between Normal and Rotated design for Device 2.

Chapter 8

Conclusions and Future work

8.1 Conclusions

In conclusion, this study has presented the design, fabrication, and characterization of an AlN-based Lamb wave liquid sensing device for biomedical applications. The incorporation of a 1.5 μm composite membrane composed of LPCVD SiN and (002) oriented AlN layers, along with variations in the interdigital transducer (IDT) design, allowed for the exploration of device performance and sensitivity to liquid properties.

The fabrication of Lamb wave devices was met with notable difficulties, particularly during the wet etching process intended to remove bulk silicon without causing damage to the opposite side. However, through meticulous adjustments to the fabrication process, the successful production of Lamb wave devices was achieved.

Although the fabricated devices were capable of generating the A0 mode, discrepancies between expected and observed resonant frequencies underscore the need for further optimization in deposition techniques to achieve desired membrane thickness and resonant frequency.

Experimental results demonstrated the ability of the devices to differentiate between various liquid types based on phase, frequency, and gain characteristics. Notably, devices featuring the rotated IDT design exhibited enhanced sensitivity and resonance, with a substantial improvement in the quality factor (Q factor). This highlights the effectiveness of IDT design modifications in minimizing reflections and improving device performance.

In summary, the findings of this thesis project suggest that AlN-based Lamb wave devices hold significant potential for various biomedical applications, particularly in liquid sensing.

8.2 Future research and recommendations

Despite the successful fabrication and functionality of the Lamb wave devices in this project, there remains room for improvement and potential for further investigation. The following propositions have been made for future iterations:

- Enhance the functionality of the sensor to operate as a biosensor by implementing appropriate modifications. Additional details regarding the biosensor can be found in section 8.2.1.
- Investigate an alternative piezoelectric material for the desired application. The use of AlN as the piezoelectric material caused complications during the fabrication process. This was particularly noticeable when developing the IDT patterns on the AlN layer, given that most developers contain TMAH, which has the potential to cause damage to the AlN layer.
- Choose thinner DSP wafers, preferably $300\ \mu m$, to minimize the wet etching time.

8.2.1 Lamb wave device as biosensor

The fabricated Lamb wave devices can be converted into a biosensor by coating the sensing area on a delay line with a bio-sensitive film. Usually, the backside of the device is used as the sensing area as it protects the IDTs from the liquid.

A biosensor measures a biological or chemical reaction by producing signals that are proportional to an analyte's concentration in a reaction. A biosensor is used in a variety of applications, including disease tracking, drug identification, the detection of contaminants, disease-promoting microorganisms, and biomarkers (signs of a disease) in bodily fluids such as blood, urine, saliva and sweat.

The components of a typical biosensor are:

- **Analyte:** An analyte is a target substance that needs to be identified. For example, glucose is a target substance in a glucose-sensitive biosensor.
- **Bioreceptor:** A bioreceptor is a molecule that uniquely identifies the analyte. Examples of these include enzymes, cells, aminotrimers, DNA deoxynucleases and antibodies.
- **Transducer:** Transducer is the element that transforms one energy source into another. The role of a transducer in a biosensor is to transform the bio-identification occurrence into a quantifiable signal.
- **Electronics:** The electronics part of the biosensor is responsible for processing the sensor signal and preparing it for the display. It is made up of complex electronic devices that control the signal, such as amplifying and converting signals from analogue to digital.
- **Display:** The display is the user interpretation system, such as a computer's liquid crystal display (LCD) or a printer's direct printout, that interprets numbers or curves in a way that the user can understand. This part often is a combination of a biosensor's hardware and software, which interprets the biosensor results in an easy-to-understand way. Depending on the end user's needs, the output signal can be numerical, graphical, tabular, or an image [39].

Characteristics of a biosensor
Every biosensor has both static and dynamic properties. Optimising these properties will have an impact on the performance of the biosensor.

- **Selectivity**
  Selectivity refers to a bioreceptor's ability to identify a particular analyte in a mixture of admixtures and impurities. The best illustration of selectivity can be found in antigen-antibody interaction. Antibodies typically act as a bioreceptor and bind to the antigen on a surface between the IDTs (sensing area). The antibodies are then exposed to a solution (typically a buffer of salts) that contains the antigen, where antibodies bind only to the antigen. Selectivity is thus the most important factor to consider when constructing a biosensor [39].

- **Reproducibility**
  The capability of a biosensor to produce the same results for a replicate experimental set up. Reproducibility refers to the accuracy and precision of the sensor and its electronics. Precision refers to the sensor's ability to produce the same results each time the sample is measured, and accuracy refers to its ability to produce a mean value that is close to the actual value when the sample is measured multiple times.

- **Stability**
  The stability of the biosensor depends on how sensitive it is to environmental changes in and around the system. These changes can cause the output signals of the biosensor to fluctuate, which can lead to an inaccuracy in the concentration measured. This is especially important in applications where the biosensor needs to be incubated for a long time or monitored continuously.The response of the transducers and electronics can be temperature sensitive, which can affect the stability. Therefore, proper tuning of the electronics is necessary to ensure a stable sensor response. Furthermore, the stability is also affected by the degree to which a bioreceptor binds to the analyte. Biosensors with high affinities tend to have a strong electrostatic bond or

covalent bond with the analyte, which strengthens the stability of the biosensor over time. Additionally, the degradation of a biosensor over time can also have an impact on the stability of measurements.

- **Sensitivity**
  The amount of analytes a biosensor can detect is known as the limit of detection (LOD) or the sensitivity. In many medical and environment monitoring applications, the biosensor must detect analyte concentrations as low as a few nanograms per milliliter (ng/ml) or even fractions of a milliliter (fg/ml) in a sample to confirm the presence of analytes. That's why sensitivity is so important for a biosensor.

- **Linearity**
  Linearity is the characteristic that demonstrates the accuracy of the measured response to a straight line for a set of measurements with different analyte concentrations. The linearity is represented by the equation $y = m \cdot c$, where c is the analyte concentration, y is the output signal, and m is the sensitivity of the biosensor. The range of analyte concentrations being tested as well as the biosensor's resolution can both affect the sensor's linearity. The resolution is the smallest change in an analyte's concentration that is necessary to affect the response of the biosensor. A good resolution is necessary for many biosensor applications, as they require not only the detection of analytes, but also the measurement of their concentrations over a broad working range. Linear range is another term related to linearity, which is the extent to which a biosensor response is linearly related to the concentration for which the response changes [39].

References

[1] N. Gözde Durmuş et al. “Acoustic-Based Biosensors”. In: *Encyclopedia of Microfluidics and Nanofluidics*. Springer US, 2014, pp. 1–15. ISBN: 9783642277580. DOI: 10.1007/978-3-642-27758-0_10-2. URL: http://dx.doi.org/10.1007/978-3-642-27758-0_10-2.

[2] Y.Q. Fu et al. “Advances in piezoelectric thin films for acoustic biosensors, Acoustofluidics and lab-on-chip applications”. In: *Progress in Materials Science* 89 (2017), pp. 31–91. DOI: 10.1016/j.pmatsci.2017.04.006.

[3] Ioana Voiculescu and Anis N. “Acoustic Wave Based MEMS Devices, Development and Applications”. In: *Microelectromechanical Systems and Devices*. InTech, Mar. 2012. DOI: 10.5772/28214. URL: https://doi.org/10.5772/28214.

[4] H CHANG and J SHIH. “Surface acoustic wave immunosensors based on immobilized C60-proteins”. In: *Sensors and Actuators B: Chemical* 121.2 (Feb. 2007), pp. 522–529. ISSN: 0925-4005. DOI: 10.1016/j.snb.2006.04.078. URL: http://dx.doi.org/10.1016/j.snb.2006.04.078.

[5] Jingting Luo et al. “A new type of glucose biosensor based on surface acoustic wave resonator using Mn-doped ZnO multilayer structure”. In: *Biosensors and Bioelectronics* 49 (Nov. 2013), pp. 512–518. ISSN: 0956-5663. DOI: 10.1016/j.bios.2013.05.021. URL: http://dx.doi.org/10.1016/j.bios.2013.05.021.

[6] Shyam Trivedi and Harshal B. Nemade. “Finite element simulation of Love wave resonator for DNA detection”. In: *International Journal of Advances in Engineering Sciences and Applied Mathematics* 7.4 (Oct. 2015), pp. 210–218. ISSN: 0975-5616. DOI: 10.1007/s12572-015-0149-7. URL: http://dx.doi.org/10.1007/s12572-015-0149-7.

[7] Onur Tigli et al. “Fabrication and Characterization of a Surface-Acoustic-Wave Biosensor in CMOS Technology for Cancer Biomarker Detection”. In: *IEEE Transactions on Biomedical Circuits and Systems* 4.1 (Feb. 2010), pp. 62–73. ISSN: 1940-9990. DOI: 10.1109/tbcas.2009.2033662. URL: http://dx.doi.org/10.1109/TBCAS.2009.2033662.

[8] Fatemeh Gholami et al. “A study of optimizing lamb wave acoustic mass sensors’ performance through adjustment of the transduction electrode metallization ratio”. In: *Sensors* 22.17 (2022), p. 6428. DOI: 10.3390/s22176428.

[9] Mengwei Liu et al. “Design and fabrication of a MEMS Lamb wave device based on ZnO thin film”. In: *Journal of Semiconductors* 32.4 (Apr. 2011), p. 044006. DOI: 10.1088/1674-4926/32/4/044006. URL: https://doi.org/10.1088/1674-4926/32/4/044006.

[10] Zhongqing Su and Lin Ye. *Identification of Damage Using Lamb Waves*. Springer London, 2009. DOI: 10.1007/978-1-84882-784-4. URL: https://doi.org/10.1007/978-1-84882-784-4.

[11] URL: https://www.sciencelearn.org.nz/resources/340-seismic-waves.

[12] Nov. 2023. URL: https://en.wikipedia.org/wiki/Seismic_wave.

[13] Lokesh Rana et al. “Development of MEMS-based Lamb Wave Acoustic Devices”. In: *IEEE Transactions on Electron Devices* 65.4 (2018), pp. 1523–1528. DOI: 10.1109/ted.2018.2805698.

[14] Tiancheng Luo et al. “A High-Sensitivity Gravimetric Biosensor Based on S1 Mode Lamb Wave Resonator”. In: *Sensors* 22.15 (Aug. 2022), p. 5912. DOI: 10.3390/s22155912. URL: https://doi.org/10.3390/s22155912.

[15] M. Rucka, B. Zima, and R. Kędra. “Application Of Guided Wave Propagation In Diagnostics Of Steel Bridge Components”. In: *Archives of Civil Engineering* 60.4 (Dec. 2014), pp. 493–516. DOI: 10.2478/ace-2014-0033. URL: https://doi.org/10.2478/ace-2014-0033.

[16] Jie Zou. *EECS at UC Berkeley*. URL: http://www.eecs.berkeley.edu/Pubs/TechRpts/2015/EECS-2015-1.html.

[17] R. Duhamel et al. “Sensitivity of a Lamb wave sensor with 2μm AlN membrane”. In: *Ultrasonics* 44 (Dec. 2006), e893–e897. ISSN: 0041-624X. DOI: 10.1016/j.ultras.2006.05.206. URL: http://dx.doi.org/10.1016/j.ultras.2006.05.206.

[18] Feb. 2023. URL: https://www.flukenetworks.com/blog/cabling-chronicles/cable-testing-101-insertion-loss-matters-fiber-and-copper.

[19] Lixia Li et al. “Quality Factor Enhancement of Piezoelectric MEMS Resonator Using a Small Cross-Section Connection Phononic Crystal”. In: *Sensors* 22.20 (Oct. 2022), p. 7751. ISSN: 1424-8220. DOI: 10.3390/s22207751. URL: http://dx.doi.org/10.3390/s22207751.

[20] Samaher Al-Janabi, Ihab Al-Janabi, and Noora Al-Janabi. “Analysis the structural, electronic and effect of light on PIN photodiode achievement through SILVACO software: a case study”. In: *Data Science for Genomics*. Elsevier, 2023, pp. 165–178. ISBN: 9780323983525. DOI: 10.1016/b978-0-323-98352-5.00003-3. URL: http://dx.doi.org/10.1016/B978-0-323-98352-5.00003-3.

[21] July 2023. URL: https://www.nanomotion.com/nanomotion-technology/the-piezoelectric-effect/.

[22] Ajit Behera. “Piezoelectric Materials”. In: *Advanced Materials*. Springer International Publishing, Nov. 2021, pp. 43–76. ISBN: 9783030803599. DOI: 10.1007/978-3-030-80359-9_2. URL: http://dx.doi.org/10.1007/978-3-030-80359-9_2.

[23] A. S. Bakri et al. “Electrical and structural comparison of (100) and (002) oriented aln thin films deposited by RF Magnetron Sputtering”. In: *Journal of Materials Science: Materials in Electronics* 33.15 (2022), pp. 12271–12280. DOI: 10.1007/s10854-022-08186-w.

[24] Liping Fang et al. “Substrate Temperature Dependent Properties of Sputtered AlN:Er Thin Film for In-Situ Luminescence Sensing of Al/AlN Multilayer Coating Health”. In: *Materials* 11.11 (Nov. 2018), p. 2196. ISSN: 1996-1944. DOI: 10.3390/ma11112196. URL: http://dx.doi.org/10.3390/ma11112196.

[25] Abid Iqbal and Faisal Mohd-Yasin. “Reactive Sputtering of Aluminum Nitride (002) Thin Films for Piezoelectric Applications: A Review”. In: *Sensors* 18.6 (June 2018), p. 1797. ISSN: 1424-8220. DOI: 10.3390/s18061797. URL: http://dx.doi.org/10.3390/s18061797.

[26] Volga Yavuz. In: *Finite element analysis and fabrication studies of mems saw device employing manipulable phase velocity* (2015).

[27] J. G. Gardeniers, H. A. Tilmans, and C. C. Visser. “LPCVD silicon-rich silicon nitride films for applications in micromechanics, studied with statistical experimental design*”. In: *Journal of Vacuum Science amp;amp; Technology A: Vacuum, Surfaces, and Films* 14.5 (1996), pp. 2879–2892. DOI: 10.1116/1.580239.

[28] Erhard Kohn. “Harsh Environment Materials”. In: *Comprehensive Microsystems*. Elsevier, 2008, pp. 131–181. DOI: 10.1016/b978-044452190-3.00005-7. URL: https://doi.org/10.1016/b978-044452190-3.00005-7.

[29] Ummikalsom Abidin, Burhanuddin Yeop Majlis, and Jumril Yunas. “Fabrication of pyramidal cavity structure with micron-sized tip using anisotropic koh etching of silicon (100)”. In: *Jurnal Teknologi* 74.10 (June 2015). DOI: 10.11113/jt.v74.4846. URL: https://doi.org/10.11113/jt.v74.4846.

[30] Prem Pal and Kazuo Sato. “Fabrication methods based on wet etching process for the realization of silicon MEMS structures with new shapes”. In: *Microsystem Technologies* 16.7 (Feb. 2010), pp. 1165–1174. DOI: 10.1007/s00542-009-0956-5. URL: https://doi.org/10.1007/s00542-009-0956-5.

[31] Zhenzhen Chen et al. “Acoustic microreactors for chemical engineering”. In: *Chemical Engineering Journal* 433 (Apr. 2022), p. 133258. ISSN: 1385-8947. DOI: 10.1016/j.cej.2021.133258. URL: http://dx.doi.org/10.1016/j.cej.2021.133258.

[32] Xing Lu et al. "GAN-based s_0-wave sensors on silicon for chemical and biological sensing in liquid environments". In: *IEEE Sensors Journal* 13.4 (2013), pp. 1245–1251. DOI: 10.1109/jsen.2012.2231958.

[33] Bryan Janaskie and Shuk Yin Chuk. URL: http://classweb.ece.umd.edu/enee416.F2007/GroupActivities/Report6.pdf.

[34] Pravuram Panda et al. "A study on erosive wear analysis of glass fiber–epoxy–AlN hybrid composites". In: *Journal of Composite Materials* 48.1 (Dec. 2012), pp. 107–118. DOI: 10.1177/0021998312469239. URL: https://doi.org/10.1177/0021998312469239.

[35] URL: https://heidelberg-instruments.com/core-technologies/maskless-laser-lithography/.

[36] Jan. 2017. URL: https://www.allresist.com/wp-content/uploads/sites/2/2020/03/AR-P5300_english_Allresist_product_information.pdf.

[37] URL: https://eleshop.eu/nanovna-h.html.

[38] Mohit Garade, Andreas Henkel, and Editorial Team. *Everything RF*. Nov. 2018. URL: https://www.everythingrf.com/community/what-are-s-parameters#:~:text=For%20a%20two%20port%20network,output%20port%20voltage%20reflection%20coefficient.

[39] Nikhil Bhalla et al. "Introduction to biosensors". In: *Essays in Biochemistry* 60.1 (June 2016). Ed. by Pedro Estrela, pp. 1–8. DOI: 10.1042/ebc20150001. URL: https://doi.org/10.1042/ebc20150001.

Appendix A

Flow chart

FLOWCHART TEST FABRICATION: MEMBRANE DIMENSION

STARTING MATERIAL
Use **DOUBLE SIDE** polished **LOW RESISTIVITY (**L_{RES}**)** wafers, with the following specifications:

Type:	*p / phosphorus*
Orientation:	*(100)*
Resistivity:	*1-5* Ωcm
Thickness:	*525* $\pm$ *15 um*
Diameter:	*100 mm*

NOTE DOWN THE WAFER NUMBER WITH ITS ID
Wafer 1 DSP = 201911-5-0120 (*this wafer will be used for SiN stress measurement)
Wafer 2 DSP = 201911-5-0008 (*this wafer will be used for AlN LS stress measurement)
Wafer 3 DSP = 201911-5-0132
Wafer 4 DSP = 201911-5-0125 (*this wafer will be used for AlN 2 stress measurement)
Wafer 5 DSP = 201911-5-0038
Wafer 6 SSP = 201911-2-0859 (*this wafer will be used for LS AlN thickness)
Wafer 7 SSP = 201911-2-0858 (*this wafer will be used for AlN thickness)

STRESS MEASUREMENT FOR WAFERS 1, 6 AN 7
Use the Flexus Stress Meter to do the first ”no film” measurement to measure (pre- LPCVD SiN measurement).

CLEANING: HNO3 99% AND 69.5%
Clean

- 10 minutes in fuming nitric acid at ambient temperature. This will dissolve organic materials. Use wet bench ”HNO_3 99% (Si)” and the carrier with the white dot.

Rinse

- Rinse in the Quick Dump Rinser with the standard program until the resistivity is 5 $M\Omega$.

Clean

- 10 minutes in concentrated nitric acid at 110 °C. This will dissolve metal particles. Use wet bench ”HNO_3 69.5 5% 110C” and the carrier with the white dot.

Rinse

- Rinse in the Quick Dump Rinser with the standard program until the resistivity is 5 $M\Omega$.

Dry

- Use the ”Avenger Ultra-Pure 6” rinser/dryer with the standard program, and the white carrier with a red dot.

Note

- The next step must be performed immediately after drying.

LPCVD DEPOSITION: 500 NM LOW-STRESS SILICON NITRIDE ON WAFERS 1, 2, 3, 4 AND 5
Furnace tube: E2 Program name: 4INCHST (waits for operator)
Follow the instructions for the LPCVD furnace when using this equipment.

Process conditions:			
Gasses & flows	**Pressure**	**Temperature**	**Time**
SiH_2Cl_2/NH_3 = 315 / 85 sccm	150 mTorr	850 °C	variable command

Note:

- The layer thickness depends on the deposition time, which can be calculated from the average deposition rate during recent recipe usage. This can be found in the logbook of the system.
- An extra test wafer can be deposited for measurements and etch tests.

MEASUREMENT: SILICON NITRIDE THICKNESS FOR WAFERS 1, 2, 3 AND 4
Use the Woollam Ellipsometer measurement system for layer thickness measurements. Follow the operating instructions from the manual when using this equipment.

- Use program: DIMES lpcvd losin (0-1.5 um)
- Expected layer thickness: 500 nm

STRESS MEASUREMENT: PRE-ALN DEPOSITION STRESS MEASUREMENT FOR WAFERS 2, 4
Use the Flexus Stress Meter to do measure the deposited film stress.

SPUTTER DEPOSITION: 1 UM ALUMINUM NITRIDE AT 50°C ON WAFERS 4, 5 AND 7.
Use the TRIKON SIGMA 204 sputter coater for the deposition of an aluminium nitride layer on the wafers. It is not allowed to change the process conditions and time from a sputtering recipe!

Use recipe **AIN_1mu_ESLEE_50C** to obtain a 1 um thick low stress AlN layer.

Process conditions from module recipe AIN_1mu_ESLEE_50C:					
Module recipe	**Target**	**Electrode temp.**	**Gasses & flows**	**Target power**	**Time**
1. AIN_1mu_Eslee_50C	Al	50°C	Ar/N2 = 19/38 sccm	2 kW	??s

Note:

- The layer thickness depends on the deposition time, which can be calculated from the average deposition rate during recent recipe usage. This can be found in the logbook of the system.
- An extra test wafer can be deposited for measurements and etch tests.

SPUTTER DEPOSITION: 1 UM LOW-STRESS ALUMINUM NITRIDE AT 400°C ON WAFERS 1,2,3,4 AND 5

Use the TRIKON SIGMA 204 sputter coater for the deposition of an aluminium nitride layer on the wafers. It is not allowed to change the process conditions and time from a sputtering recipe!

Use recipe **AlN_1um_400C_LS** to obtain a 1 um thick low stress AlN layer.

Process conditions from module recipe AlN_1mu_ESLEE_50C:					
Module recipe	**Target**	**Electrode temp.**	**Gasses & flows**	**Target power**	**Time**
1. AlN_1um_400C_LS	Al	400°C	Ar/N2 = 20/80 sccm	3 kW	??s

Note:

- The layer thickness depends on the deposition time, which can be calculated from the average deposition rate during recent recipe usage. This can be found in the logbook of the system.
- An extra test wafer can be deposited for measurements and etch tests.

MEASUREMENT: ALUMINUM NITRIDE THICKNESS FOR WAFERS 6 AND 7.
Use the Woollam Ellipsometer measurement system for layer thickness measurements. Follow the operating instructions from the manual when using this equipment.

- Use program: 1um AlN on Si
- Expected layer thickness: 1083 nm

STRESS MEASUREMENT: STRESS OF ALN FOR WAFERS 2, 4, 6 AND 7
Use the Flexus Stress Meter to do measure the deposited film stress.

XRD MEASUREMENT FOR WAFERS 2 AND 4
Use the XRD equipment to describe the orientation of the crystals for AlN.

STRESS MEASUREMENT: PRE-SIN (PECVD) DEPOSITION STRESS MEASUREMENT FOR WAFERS 2, 4

FINAL FABRICATION: LAMB WAVE DEVICE

STARTING MATERIAL

Use **DOUBLE SIDE** polished **LOW RESISTIVITY (**L_{RES}**)** wafers, with the following specifications:

Type:	*p / phosphorus*
Orientation:	*(100)*
Resistivity:	*1-5* Ωcm
Thickness:	*525* $\pm$ *15 um*
Diameter:	*100 mm*

NOTE DOWN THE WAFER NUMBER WITH ITS ID

STRESS MEASUREMENT FOR WAFERS.

Use the Flexus Stress Meter to do the first ”no film” measurement to measure (pre- LPCVD SiN measurement).

CLEANING: HNO3 99% AND 69.5%

Clean

- 10 minutes in fuming nitric acid at ambient temperature. This will dissolve organic materials. Use wet bench ”HNO_3 99% (Si)” and the carrier with the white dot.

Rinse

- Rinse in the Quick Dump Rinser with the standard program until the resistivity is 5 $M\Omega$.

Clean

- 10 minutes in concentrated nitric acid at 110 °C. This will dissolve metal particles.
  Use wet bench ”HNO_3 69.5 5% 110C” and the carrier with the white dot.

Rinse

- Rinse in the Quick Dump Rinser with the standard program until the resistivity is 5 $M\Omega$.

Dry

- Use the ”Avenger Ultra-Pure 6” rinser/dryer with the standard program, and the white carrier with a red dot.

Note

- The next step must be performed immediately after drying.

LPCVD DEPOSITION: 500 NM LOW-STRESS SILICON NITRIDE ON WAFERS.

Furnace tube: E2 Program name: 4INCHST (waits for operator)

Follow the instructions for the LPCVD furnace when using this equipment.

Process conditions:			
Gasses & flows	**Pressure**	**Temperature**	**Time**
SiH_2Cl_2/NH_3 = 315 / 85 sccm	150 mTorr	850 °C	variable command

Note:

- The layer thickness depends on the deposition time, which can be calculated from the average deposition rate during recent recipe usage. This can be found in the logbook of the system.

- An extra test wafer can be deposited for measurements and etch tests.

MEASUREMENT: SILICON NITRIDE THICKNESS FOR WAFERS.

Use the Woollam Ellipsometer measurement system for layer thickness measurements. Follow the operating instructions from the manual when using this equipment.

- Use program: DIMES lpcvd losin (0-1.5 um)

- Expected layer thickness: 500 nm

STRESS MEASUREMENT: PRE-ALN DEPOSITION STRESS MEASUREMENT FOR WAFERS 2, 4

Use the Flexus Stress Meter to do measure the deposited film stress.

SPUTTER DEPOSITION: 1 UM LOW-STRESS ALUMINUM NITRIDE AT 400°C.

Use the TRIKON SIGMA 204 sputter coater for the deposition of an aluminium nitride layer on the wafers. It is not allowed to change the process conditions and time from a sputtering recipe!

Use recipe **AlN_1um_400C_LS** to obtain a 1 um thick low stress AlN layer.

Process conditions from module recipe AlN_1mu_ESLEE_50C:					
Module recipe	**Target**	**Electrode temp.**	**Gasses & flows**	**Target power**	**Time**
1. AlN_1um_400C_LS	Al	400°C	Ar/N2 = 20/80 sccm	3 kW	??s

Note:

- The layer thickness depends on the deposition time, which can be calculated from the average deposition rate during recent recipe usage. This can be found in the logbook of the system.
- An extra test wafer can be deposited for measurements and etch tests.

MEASUREMENT: ALUMINUM NITRIDE THICKNESS.

Use the Woollam Ellipsometer measurement system for layer thickness measurements. Follow the operating instructions from the manual when using this equipment.

- Use program: 1um AlN on Si
- Expected layer thickness: 1083 nm

STRESS MEASUREMENT: STRESS OF ALN FOR WAFERS.

Use the Flexus Stress Meter to do measure the deposited film stress.

COATING

Resist: AR-P5350
Spinspeed: 4000rpm (1 minute)
Bake in hotplate @105°C for 4 minutes.

EXPOSURE

Processing will be performed on the Heidelberg Instruments Laserwriter (µMLA) for Maskless Photo Lithography.
HBG_uMLA: Dose = 250 mJ/cm² (pneumatic focussing, defoc +2)

DEVELOPING

Development: 2 minutes in AR 300-35 (1:2) solution Rinse in DI water for 30 seconds.

INSPECTION

Visually inspect the wafers through a microscope:

- No resist residues are allowed.
- Check the linewidth of the structures.
- Check the overlay of the exposed pattern if the mask was aligned to a previous pattern on the wafer.

DEPOSITION: 10 NM CHROMIUM (EVAPORATION)

Use the AJA QT equipment to deposit 10 nm of Cr. **DEPOSITION: 90 NM GOLD (EVAPORATION)**

Use the AJA QT equipment to deposit 90 nm of Au.

LIFT-OFF PROCEDURE

Put wafer in a beaker filled with AR 600-71 (used for the All resist removal).

INSPECTION

Visually inspect the wafers through a microscope:

- No resist residues are allowed.
- Check the linewidth of the structures.
- Check the overlay of the exposed pattern if the mask was aligned to a previous pattern on the wafer.

PECVD SIN

Deposit 500 nm of PECVD SiN with the plasmba 80+ equipment. Use the recipe with temperature of $400°$ instead of $300°$ as the former is more dense. The deposition rate is approximately 13.5 nm/s.

COATING ON THE BACK

Use the coater station of the Delta RC80 system to coat the wafers with photoresist. The selected resist is: S1813 , which has a positive tone. The coating process consists of:

- HMDS as underlayer
- Spin HMDS @ 3000rpm
- Bake on hotplate @200°C for 2 minutes, gives a monolayer
- Spin S1813 @ 4000rpm 1 um.
- Bake on hotplate @ 115°C for 1 minutes.

EXPOSURE

Processing will be performed on the Heidelberg Instruments Laserwriter (μMLA) for Maskless Photo Lithography.
HBG_uMLA: Dose = 250 mJ/cm² (pneumatic focussing, defoc +2)

DEVELOPER

Development will be done in MF21A for 2 minutes Rinse in DI water

INSPECTION

Visually inspect the wafers through a microscope:

- No resist residues are allowed.
- Check the linewidth of the structures.
- Check the overlay of the exposed pattern if the mask was aligned to a previous pattern on the wafer.

DRY ETCHING: > 500NM SIN FROM THE BACKSIDE

Use the Sentech F2 to etch the SiN from the BACKSIDE of the wafers.
Will take approximately 35 minutes to remove the SiN layer **INSPECTION**

Visually inspect the wafers through a microscope:

- No resist residues are allowed.
- Check the linewidth of the structures.
- Check the overlay of the exposed pattern if the mask was aligned to a previous pattern on the wafer.

LAYER STRIPPING: PHOTORESIST)

1. Put the wafer in Acetone + Powersonic (10 minutes, 25C and 9 (power)).
2. Put the wafer in afterwards in IPA (5 minutes) and pour IPA from bottle when pulling the wafer out of the IPA beaker.
3. Put the wafer in the dryer.

(OPTIONAL): ADD KOH PROTECTIVE COATING

Pre-coating: AR 300-80 @ 4000 rpm (15 nm). Bake @ 180° for 2 min
Coating: AR-PC 5040 spinspeed: 1000 rpm Bake @ 190°

WET ETCHING: SI ETCHING WITH KOH(40% BY WEIGHT @80°C)

Etch rate = 0.6-1 um/min
Thickness Si wafer = 525 um
Etch time for 0.6um/min = 525/0.6 = 875 min = 15 hours
Etch time for 1um/min = 525/1 = 525 min = 9 hours
Total expected etch time in hours = 9 – 15 hours

LAYER STRIPPING

Remote the KOH protective coating by putting the wafer in acetone or AR 600-71 (rinse with DI water afterwards).

CLEAVING

Carefully cleave the wafer into squared samples. Reference line is made through wet etching. **DRY**

ETCHING

Remove the PECVD SiN from the top of the device with the Sentech F2 equipment. This is required in order to make the connections with the contact pads.

END OF FABRICATION PROCESS

Appendix B

FABRICATION RESULTS

After 500nm LPCVD SiN

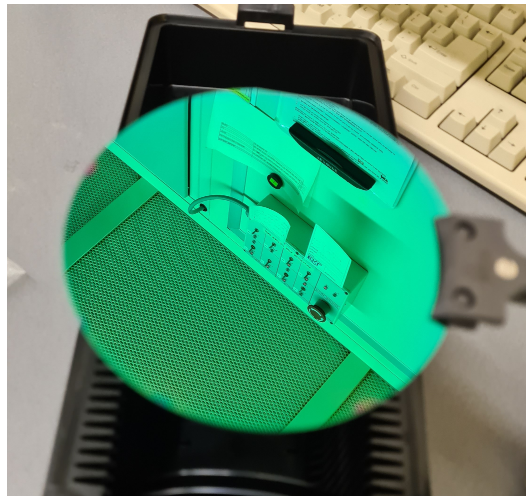

Figure B.1: After deposition of 500 nm LPCVD SiN on a bare DSP wafer

After 1 um AlN deposition

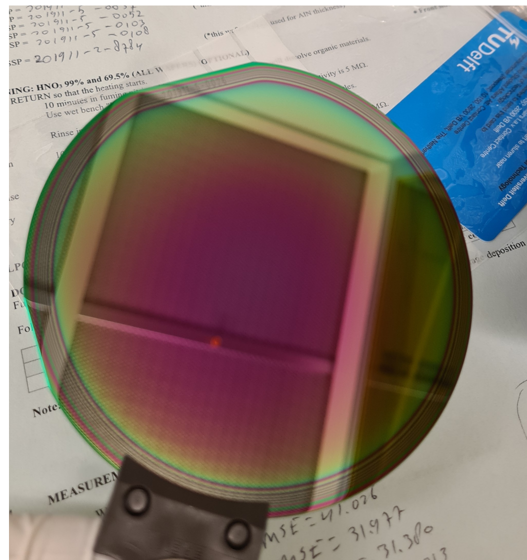

Figure B.2: After deposition of 1 um AlN

A problem had arisen as a result of contamination within the chamber, causing flakes to fall onto the wafer during the AlN deposition process. This has consequently resulted in an undesirable outcome for the AlN deposition, as as depicted in figure B.3. To overcome this issue, it is advisable to include a cleaning step after each wafer deposition.

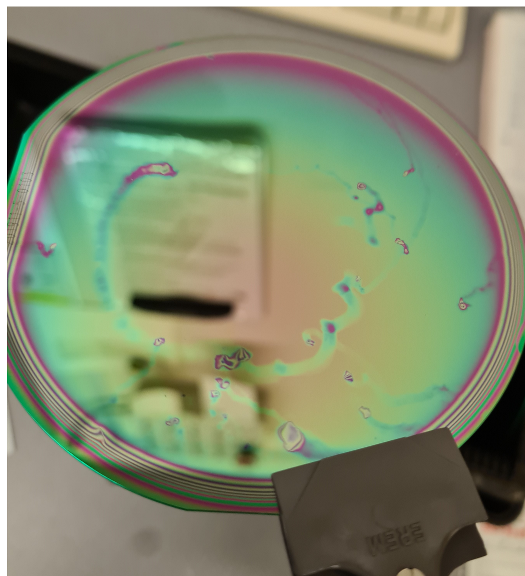

Figure B.3: Bad AlN deposition due to contamination. Therefore it is essential to include a cleaning step after each wafer deposition.

EXPOSURE RESULTS

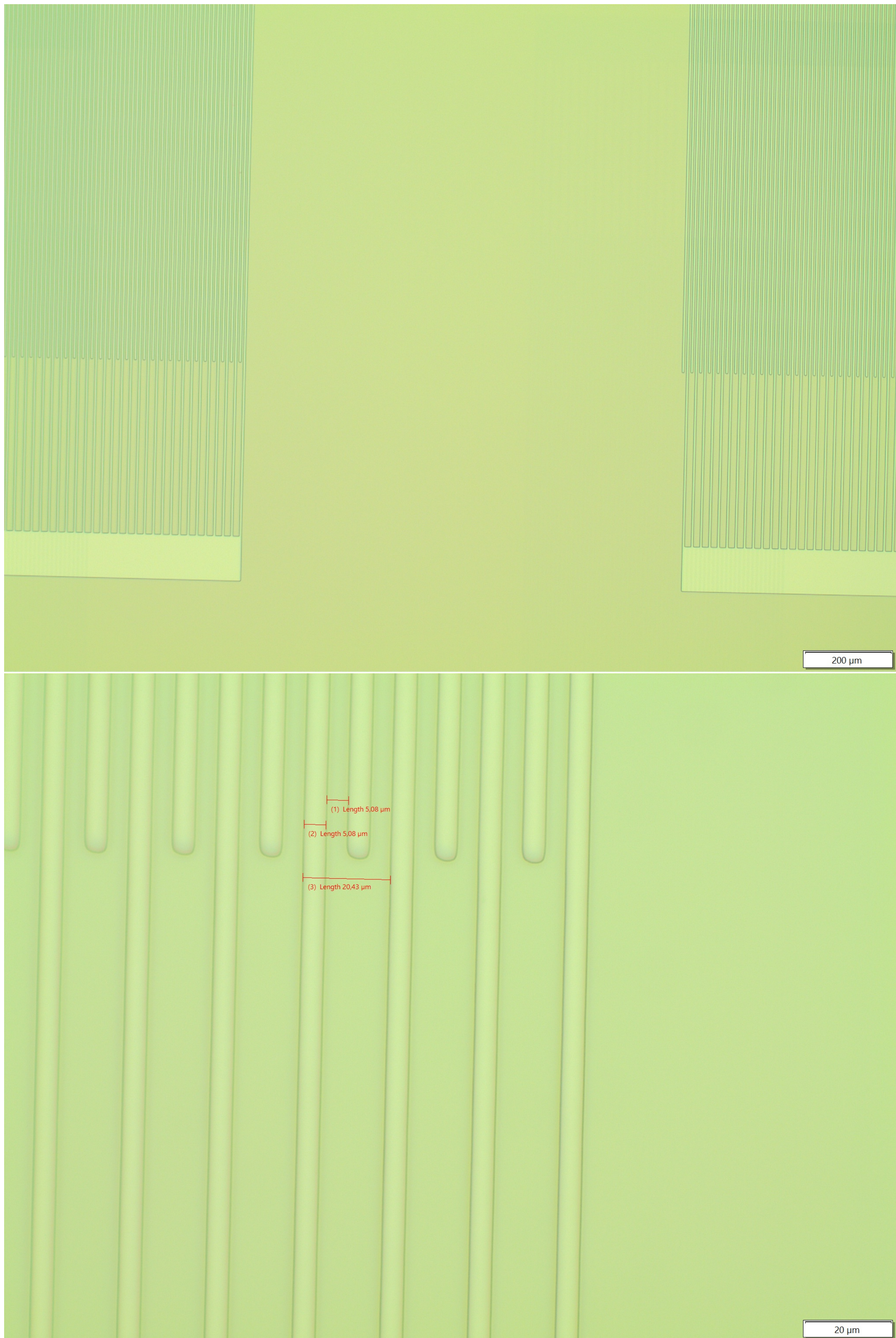

Figure B.4: Exposure result Design 1 (Normal Design)

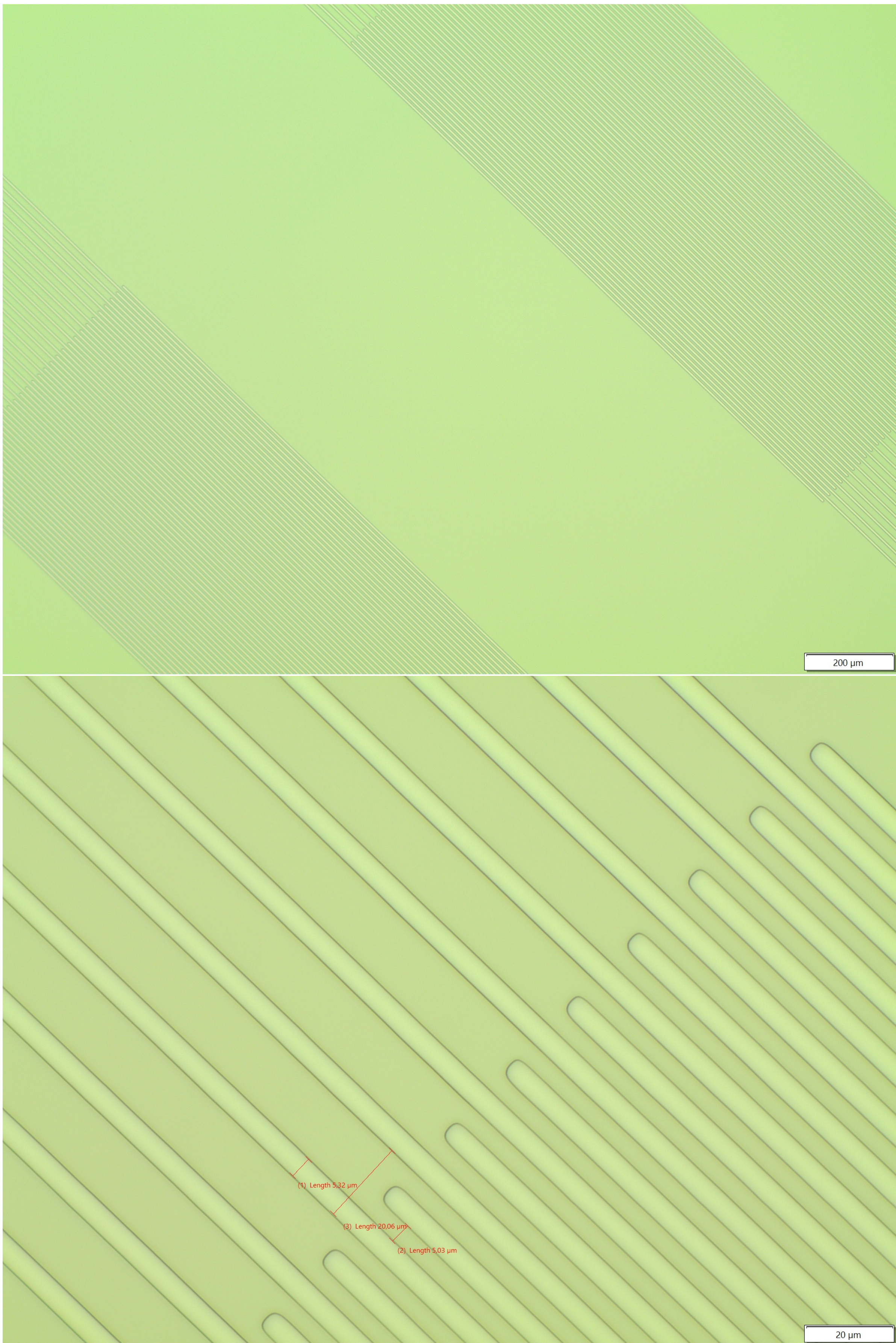

Figure B.5: Exposure result Design 2 (Rotated Design)

After Lift-off process

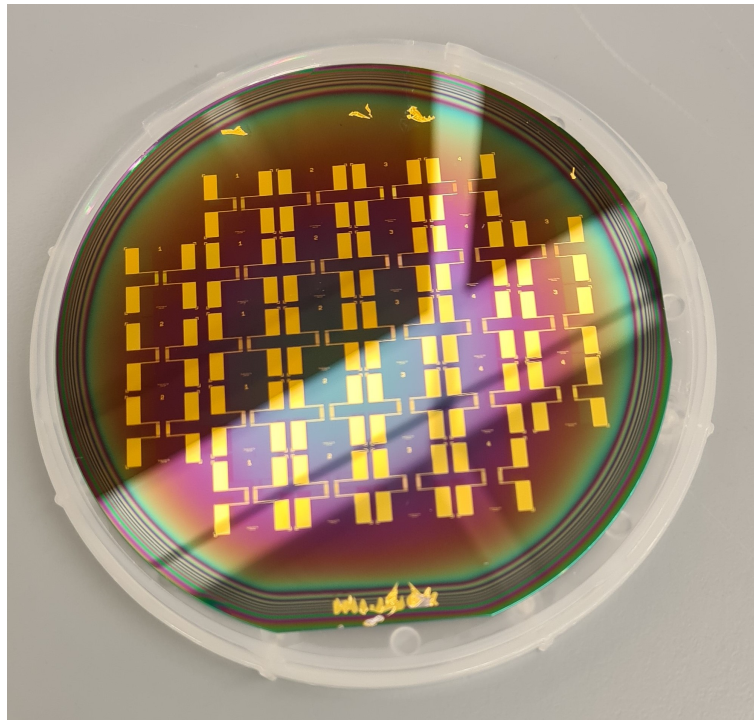

Figure B.6: Post Lift-off process normal design

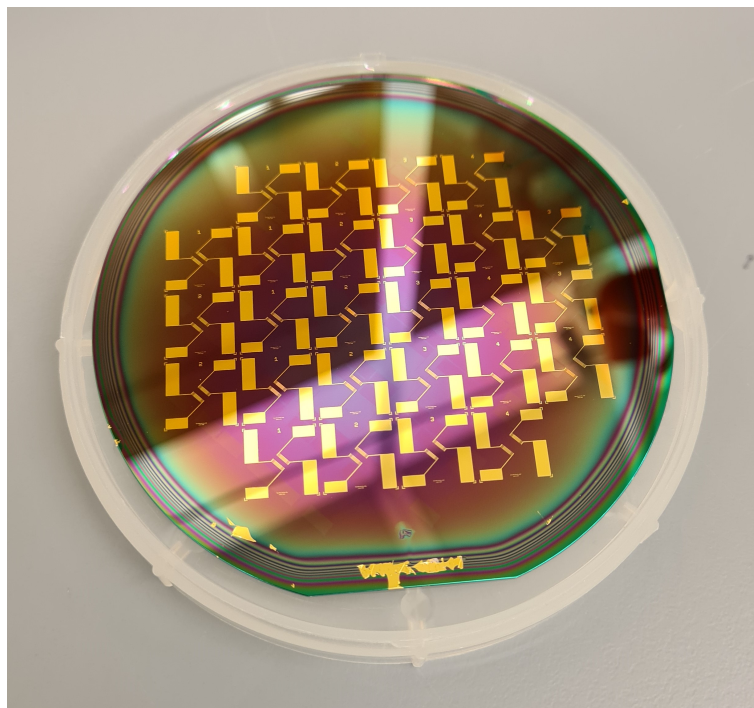

Figure B.7: Post Lift-off process rotated design

After KOH wet etching process

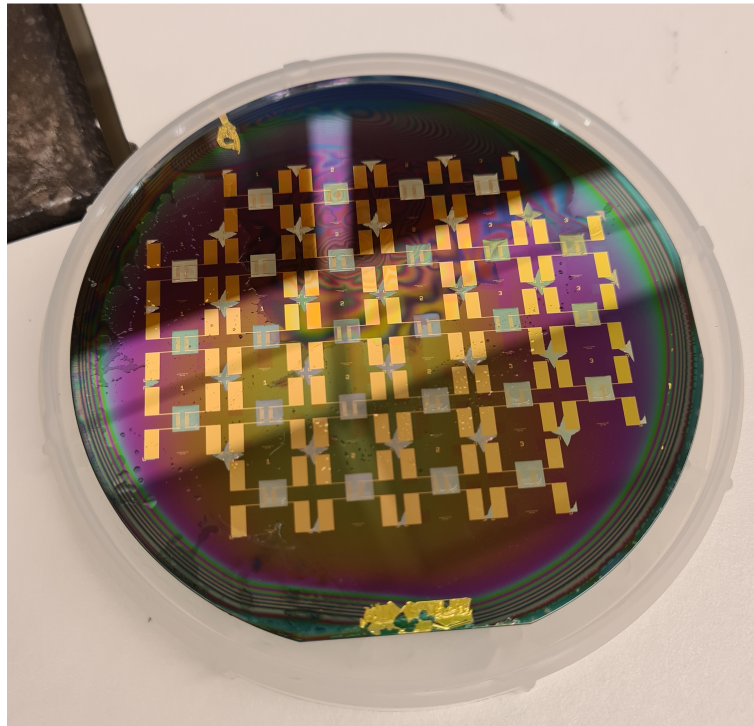

Figure B.8: After the completion of KOH wet etching process Design 1 (Front-side)

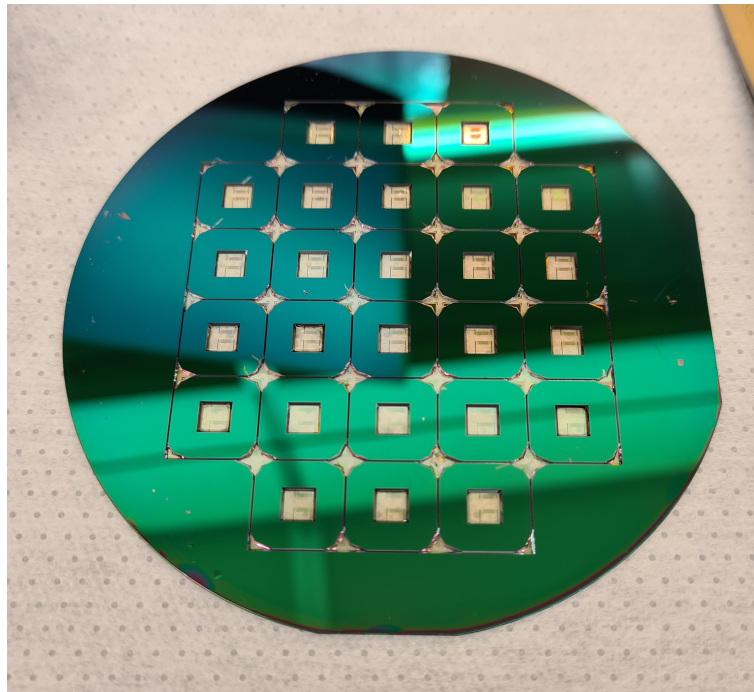

Figure B.9: After the completion of KOH wet etching process Design 1 (Back-side)

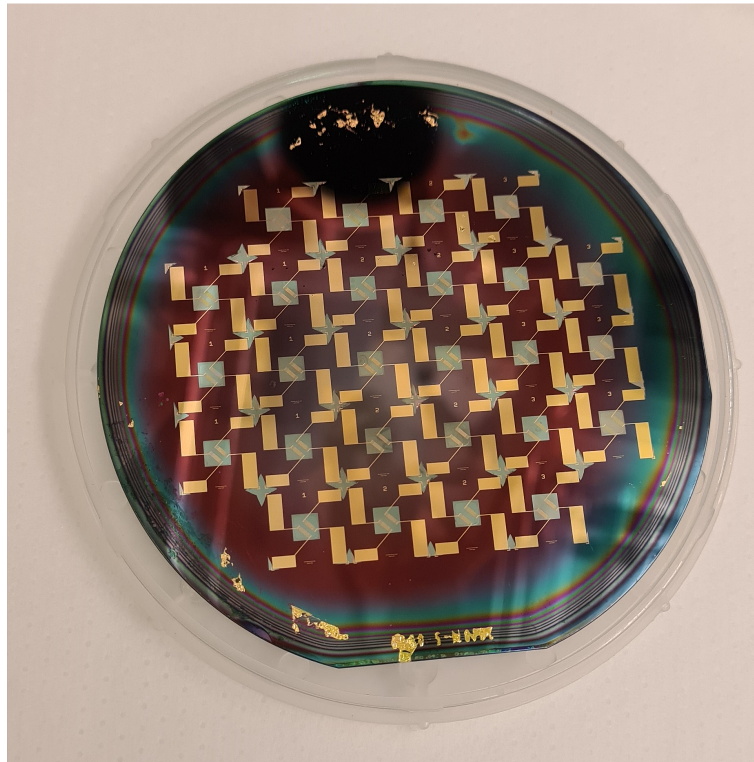

Figure B.10: After the completion of KOH wet etching process Design 2 (Front-side)

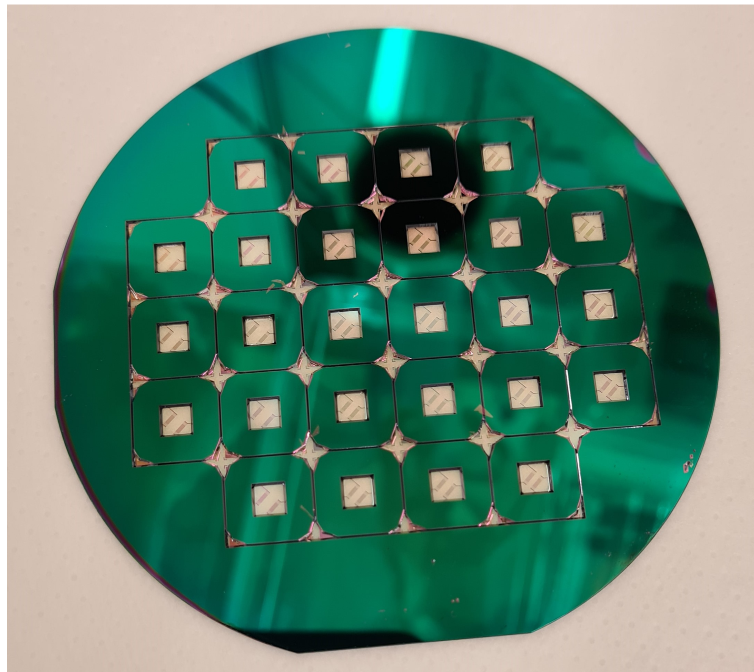

Figure B.11: After the completion of KOH wet etching process Design 2 (Back-side)

Appendix C

MASK DESIGNS

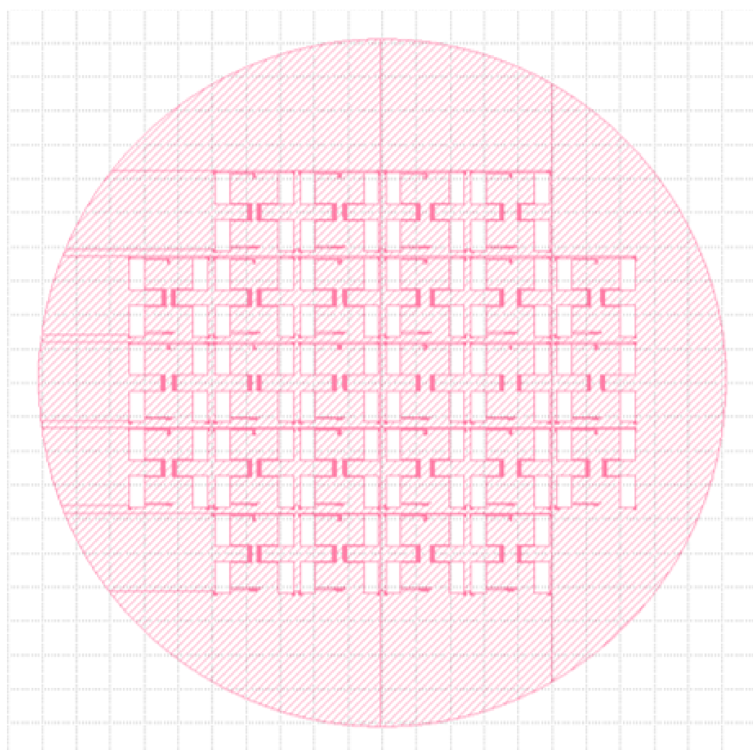

Figure C.1: Mask design of the normal structure

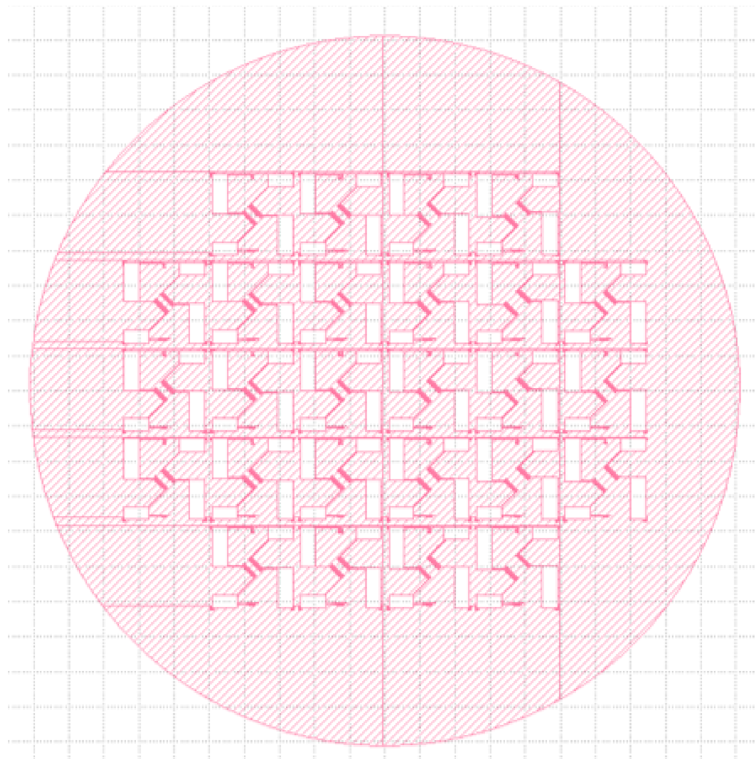

Figure C.2: Mask design of the rotated structure

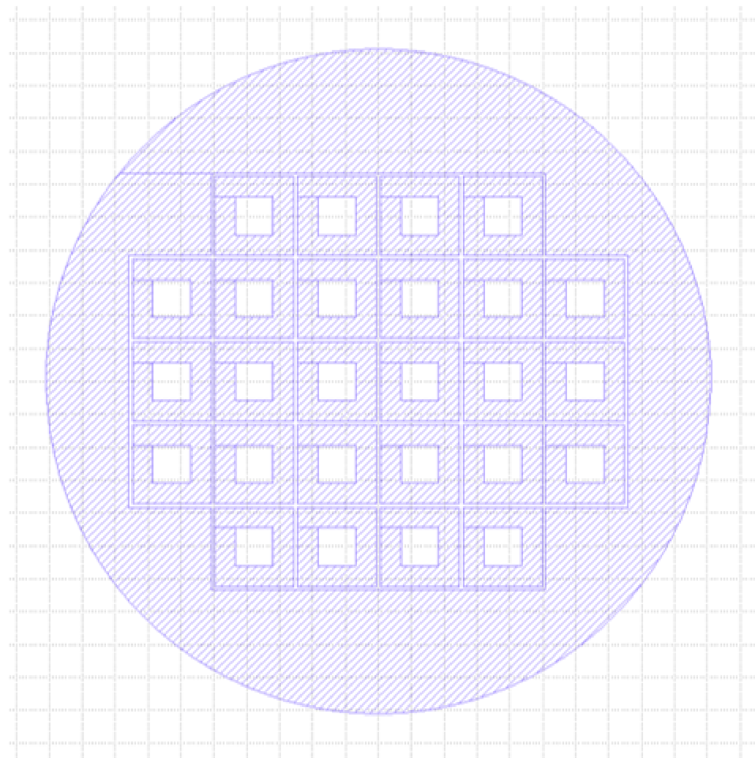

Figure C.3: Mask design of the backside pattern

Appendix D

DEPOSITION MEASUREMENTS

Table D.1: Results of SiN thickness measurement - Batch 2

TEST 2		ID	SiN thickness (nm)	MSE
DSP	Wafer 1	201911-5-0026	498.1 ± 5	40
DSP	Wafer 2	201911-5-0058	500.3 ± 5	30
DSP	Wafer 3	201911-5-0037	500.4±5	30
DSP	Wafer 4	201911-5-0052	500.5±5	30
DSP	Wafer 5	201911-5-0103	500.3±5	30
DSP	Wafer 6	201911-5-0108	500.2±5	30
SP	Wafer 7	201911-2-0784	NA	

Table D.2: Results of AlN stress and thickness measurement - Batch 3

TEST 2		ID	Substrate	Thickness (Angstrom)	Stress (MPA)
DSP	Wafer 1	201911-5-0026	LPCVD SiN/Si wafer	9070 ± 500	537 ± 5
DSP	Wafer 2	201911-5-0058	LPCVD SiN/Si wafer	9070 ± 500	590 ± 5
DSP	Wafer 3	201911-5-0037	LPCVD SiN/Si wafer	9070 ± 500	553 ± 5
DSP	Wafer 4	201911-5-0052	LPCVD SiN/Si wafer	9070 ± 500	554 ± 5
DSP	Wafer 5	201911-5-0103	LPCVD SiN/Si wafer	9070 ± 500	548 ± 5
DSP	Wafer 6	201911-5-0108	LPCVD SiN/Si wafer	9070 ± 500	537 ± 5
SP	Wafer 7	201911-2-0784	bare Si wafer	9070 ± 500	246 ± 5

Table D.3: Results of SiN thickness measurement - Batch 3

TEST 3		ID	SiN thickness (nm)	MSE
DSP	Wafer 8	201911-5-0022	500.12 ± 5	30
DSP	Wafer 9	201911-5-0029		
DSP	Wafer 10	201911-5-0069	500.38 ± 5	30
DSP	Wafer 11	201911-5-0051		
DSP	Wafer 12	201911-5-0014	500.24 ± 5	30
SP	Wafer 13	201911-2-0776	NA	
SP	Wafer 14	201911-2-0766	NA	

Table D.4: Results of AlN stress and thickness measurement - Batch 3

TEST 3		**ID**	**Substrate**	**Thickness (Angstrom)**	**Stress (MPA)**
DSP	Wafer 8	201911-5-0022	LPCVD SiN/Si wafer	9848 $\pm$ 500	315 $\pm$ 5
DSP	Wafer 10	201911-5-0069	LPCVD SiN/Si wafer	9848 $\pm$ 500	578 $\pm$ 5
DSP	Wafer 12	201911-5-0014	LPCVD SiN/Si wafer	9848 $\pm$ 500	535 $\pm$ 5
SP	Wafer 13	201911-2-0776	bare Si wafer	9848 $\pm$ 500	511 $\pm$ 5

Appendix E

EXTRA MEASUREMENT RESULTS

Normal IDT design

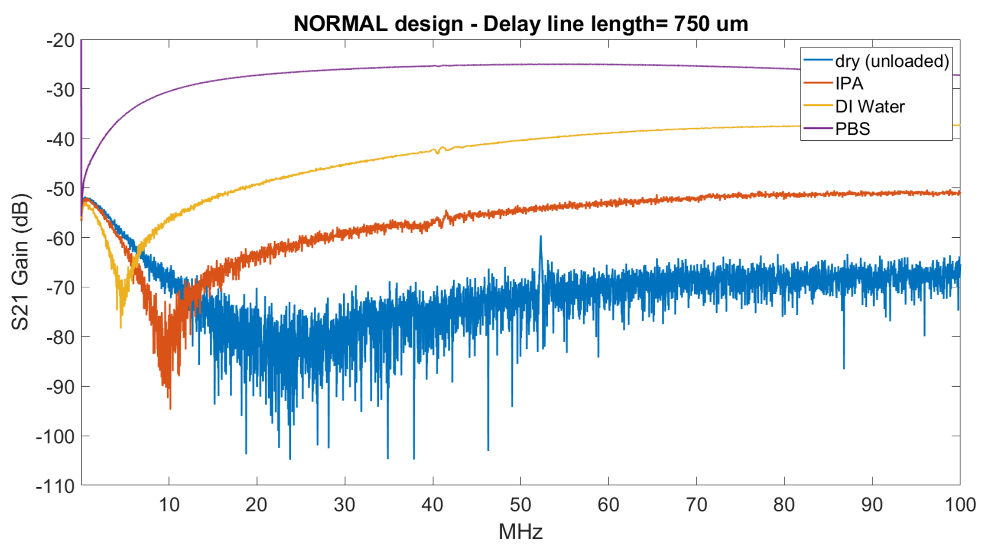

Figure E.1: Device 1 Gain comparison - NORMAL design.

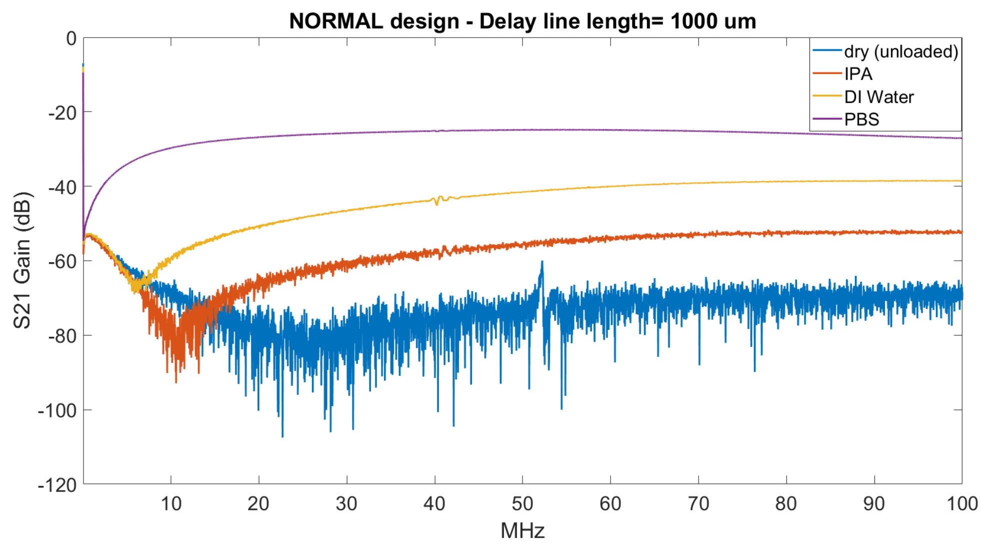

Figure E.2: Device 2 Gain comparison - NORMAL design.

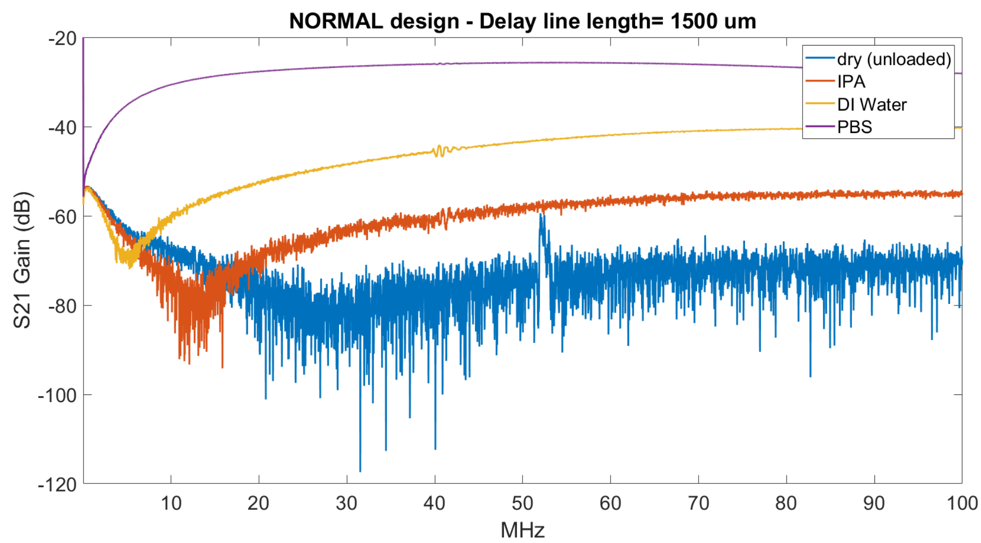

Figure E.3: Device 3 Gain comparison - NORMAL design.

Rotated IDT design

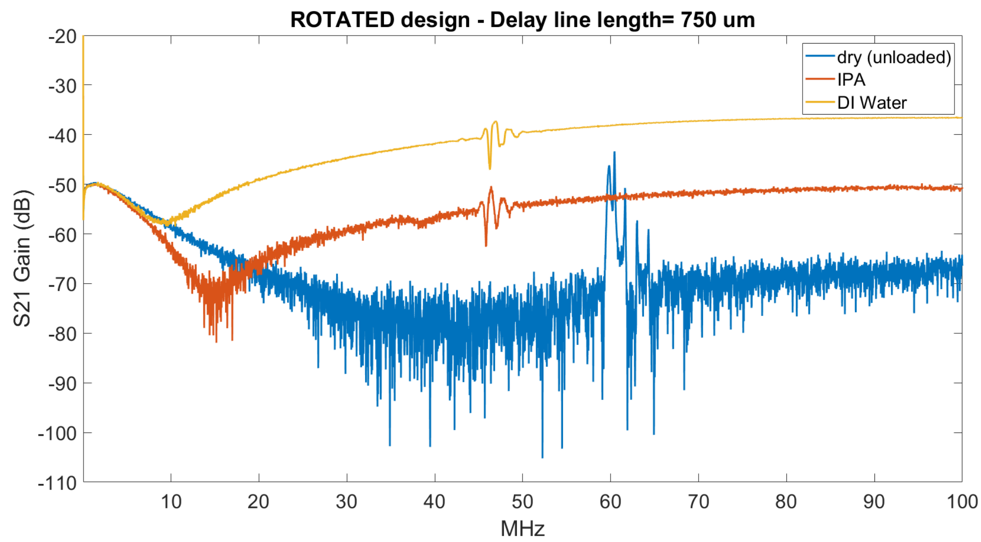

Figure E.4: Device 1 Gain comparison - ROTATED design.

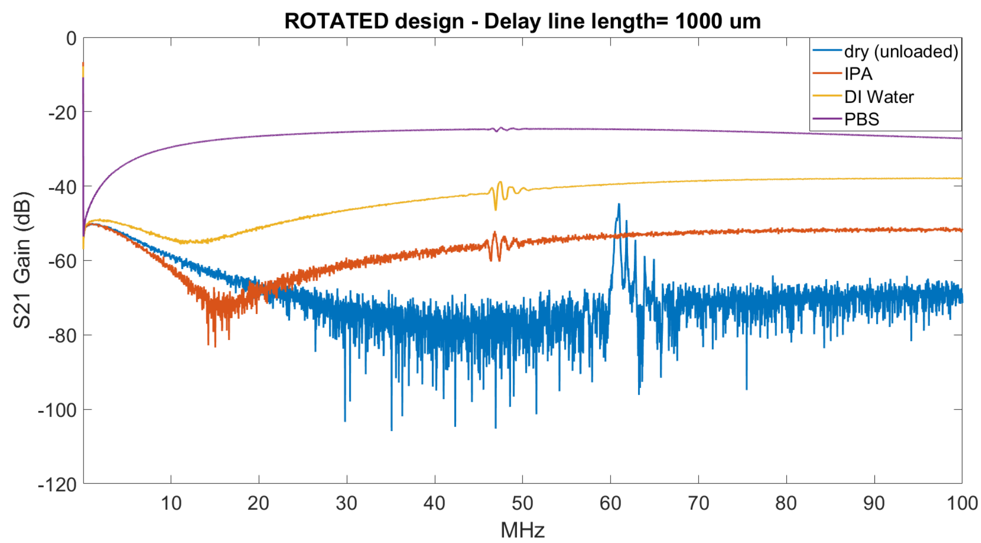

Figure E.5: Device 2 Gain comparison - ROTATED design.

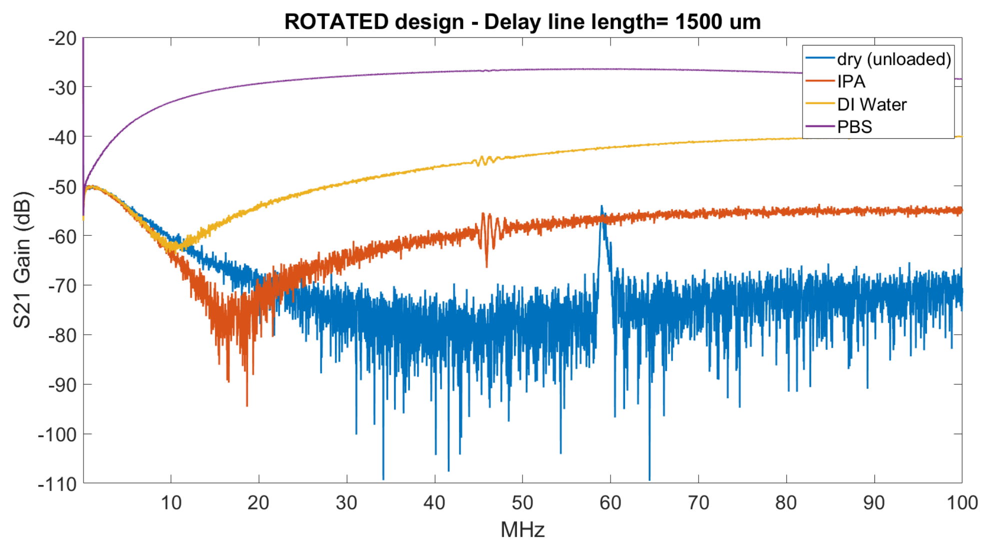

Figure E.6: Device 3 Gain comparison - ROTATED design.